Polycyclic Aromatic Hydrocarbon (PAH)

Redistribution in Extreme Dust Storms and Processing in Clouds

by

Jershon Eagar

A Dissertation Presented in Partial Fulfillment
of the Requirements for the Degree
Doctor of Philosophy

Approved July 2016 by the
Graduate Supervisory Committee:

Pierre Herckes, Chair
Mark Hayes
Everett Shock

ARIZONA STATE UNIVERSITY

August 2016

ABSTRACT

Dust storms known as 'haboobs' occur in the City of Tempe, AZ during the North American monsoon season. A haboob classification method based on meteorological and air quality measurements is described. There were from 3 to 20 haboob events per year over the period from 2005 to 2014. The calculated annual TSP (total suspended particulate) dry deposition during haboobs is estimated to contribute 74% of the total particulate mass deposited in Tempe, AZ.

Dry deposition is compared with the aqueous chemistry of Tempe Town Lake. Water management and other factors may have a stronger impact on Tempe Town Lake chemistry than haboob dry-deposition. Haboobs alter the Polycyclic Aromatic Hydrocarbon (PAH) concentrations and distributions in Tempe, AZ. PAH isomer ratios suggest $PM_{2.5}$ (particulate matter with aerodynamic diameters less than or equal to 2.5 μm) sources consistent with approximate thunderstorm outflow paths.

The importance of the atmospheric aqueous phase, fogs and clouds, for the processing and removal of PAHs is not well known. A multiphase model was developed to determine the fate and lifetime of PAHs in fogs and clouds. The model employed literature values that describe the partitioning between three phases (aqueous, liquid organic, and gas), in situ PAH measurements, and experimental and estimated (photo)oxidation rates. At 25 °C, PAHs with two, three and four rings were predicted to be primarily gas phase (fraction in the gas phase $x_g > 90$ %) while five- and six-ring PAHs partitioned significantly into droplets ($x_g < 60$ %) with aqueous phase fractions of 1 to 6 % and liquid organic phase fractions of 31 to 91 %. The predicted atmospheric lifetimes of PAHs in the presence of fog or cloud droplets (< 5 hours) were significantly

shorter than literature predictions of PAH wet and dry deposition lifetimes (1 to 14 days and 5 to 15 months respectively) and shorter than or equal to predicted PAH gas phase / particle phase atmospheric lifetimes (1 to 300 hours). The aqueous phase cannot be neglected as a PAH sink due to the large aqueous volume (*vs*. organic volume) and the relatively fast aqueous reactions.

DEDICATION

To all those who mentored and propelled me on my pathway to be a scientist. To my parents who instilled in me a hunger for learning and trying new things. To my wife who has supported me in my education. To my siblings for their good-natured encouragement. To my peers who have positively impacted me.

To historical figures for their example and optimism:

“Around here, however, we don’t look backwards for very long. We keep moving forward, opening up new doors and doing new things… and curiosity keeps leading us down new paths.” — Walt Disney

"You never fail until you stop trying." — Albert Einstein

"You have not failed until you quit trying." — Gordon B. Hinckley

ACKNOWLEDGMENTS

I first acknowledge my advisor, Pierre Herckes who has coached and guided me to this point and prepared me for what lies ahead. I acknowledge the help and direction I received from the members of my supervisory committee, Mark Hayes and Everett Shock. I additionally acknowledge the assistance and guidance I received from Hiliary Hartnett and Barbara Ervens in my research endeavors.

I would like to acknowledge my labmates at ASU: Jim Hutchings, Youliang Wang, Aurelie Marcotte, Jinwei Zhang, Sarah Frey, Christy Rose, Micah Wimmer, Denise Napolitano, Taka Nosaka, Alyssa Sherry, Samantha Donovan, Kevin Shaffer, Kirk Reed, Joana Sipe, Blanca Rodriguez, Yasmany Mancilla, and Gerardo Medina.

I would also like to acknowledge the training I received from Sean MacMillan, David Wehmeyer, Gary Thompson, and Walter Clifford.

I acknowledge sources of research funding: the School of Molecular Sciences Dissertation Fellowship, the CAP-LTER 2014, 2015, and 2016 Graduate Grants, the National Science Foundation (BCS-1026865, AGS0907261 and AGS0847710), and SRP.

TABLE OF CONTENTS

Page

CHAPTER Page

LIST OF TABLES

LIST OF FIGURES

Figure Page

GLOSSARY OF ABBREVIATIONS AND TERMS

τ_{dep}^{PM} ..... Typical Lifetime of Aerosol Particles in the Atmosphere

τ_{drydep} ..... Lifetime due to Dry Deposition (Gas and Particulate Phases)

τ_{rxn}^{fog} ..... Chemical Lifetime in Fogs and Clouds

$\tau_{rxn}^{g,PM}$ ..... Chemical Lifetime in Gas and Particulate Phases

τ_{wetdep} ..... Lifetime due to Wet Deposition

µg .....Microgram

µm .....Micrometer

$^{\bullet}NO_3$ .....Nitrate Radical

$^{\bullet}OH$.....Hydroxyl Radical

ACY .....Acenaphthylene

ADEQ .....Arizona Department of Environmental Quality

A^{fog}.....Total Fog Droplet Surface Area

ANT .....Anthracene

A^{PAH}.....Total PAH Surface Area

AQS.....United States Environmental Protection Agency's Air Quality System

B2.....Probable Carcinogen, Sufficient Evidence in Animals

BAA .....Benz[a]anthracene

BAP.....Benzo[a]pyrene

BAU .....Benzo[a]fluorene

BBF .....Benzo[b]fluoranthene

BBU .....Benzo[b]fluorene

BEP .....Benzo[e]pyrene

BGP.....Benzo[*g*,*h*,*i*]perylene

BKF.....Benzo[*k*]fluoranthene

BLDU.....Blowing Dust

BR .....Mist

$c(PM_{10})$.....Atmospheric Mass Concentration of PM_{10}

$c(PM_{2.5})$.....Atmospheric Mass Concentration of $PM_{2.5}$

c(TSP) .....Atmospheric Mass Concentration of TSP

CAP-LTER ....Central Arizona – Phoenix Long-Term Ecological Research

C_f.....Cunningham Factor

CHY .....Chrysene

CO.....Carbon monoxide

DBA .....Dibenz[*a*,*h*]anthracene

DOC .....Dissolved Organic Carbon

d_p .....Aerodynamic Particle Diameter

DS .....Dust Storm

DU.....Widespread Dust

EPA.....United States Environmental Protection Agency

FG .....Fog

FLT .....Fluoranthene

FLU.....Fluorene

g.....Gravitational Constant

H.....Henry's Law Solubility Constant

h.....Hour

H^*.....Henry's Law Solubility Constant Calculated from K_{OW} and K_{OA}

ha.....Hectare

HZ .....Haze

IND .....Indeno[1,2,3–*c*,*d*]pyrene

$J_{air}(PM_{10})$.....Atmospheric PM_{10} Dry Deposition Flux

J_{air}(TSP) .....Atmospheric TSP Dry Deposition Flux

$k(^{\bullet}NO_3,g)$.....Nitrate Radical Gas Phase Oxidation Rate Constant

$k(^{\bullet}OH,g)$ .....Hydroxyl Radical Gas Phase Oxidation Rate Constant

k(aq) .....Psuedo-First Order Photooxidation Rate in Bulk Water

$k(O(^3P),g)$.....Atomic Oxygen Gas Phase Oxidation Rate Constant

$k(O_3,g)$.....Ozone Gas Phase Oxidation Rate Constant

k(org).....Psuedo First-Order Photooxidation Rate in Liquid Organic Phase

k'(g(.....Pseudo First-Order Gas Phase Oxidation Rate Constants

kg.....Kilogram

km .....Kilometer

K_{OA}.....Octanol – Air Partition Ratio

K_{OW} .....Octanol – Water Partition Ratio

KPHX.....Weather Station at the Phoenix Sky-Harbor International Airport

LWC.....Liquid Water Content

MADIS.....Meteorological Assimilation Data Ingest System

MCAQ.....Maricopa County Air Quality

MCL.....Maximum Contaminant Level

METAR.....Meteorological Terminal Air Report

MFCD .....Maricopa County Flood Control District

NAAQS.....United States National Ambient Air Quality Standards

NO_2 .....Nitrogen dioxide

NOAA.....United States National Oceanic and Atmospheric Administration

NWS.....United States National Weather Service

$O(^3P)$ .....Atomic Oxygen

$O_2(^1\Delta_g)$ .....Singlet Oxygen

O_3 .....Ozone

oAAN.....Aceanthrylene–1,2–dione

oACE.....Acenaphthenequinone

oANT 9,10–anthraquinone

oATR.....9(10*H*)–anthrone

oBAA .....Benz[*a*]anthracene–7,12–dione

oBAP1.....Benzo[*a*]pyrene–1,6–dione

oBAP2.....Benzo[*a*]pyrene–3,6–dione

oBAP3.....Benzo[*a*]pyrene–4,5–dione

oBAP4.....Benzo[*a*]pyrene–6,12–dione

oBAU .....11*H*–benzo[*a*]fluoren–11–one

oBBU .....11*H*–benzo[*b*]fluoren–11–one

oBEP .....Benzo[*e*]pyrene–4,5–dione

oBTR.....7*H*–benzo[*de*]anthracen–7–one

oCOU 2*H*–chromen–2–one

oCRM.....4*H*–chromen–4–one

oCHY Chrysene–1,4–dione

oDBP.....6*H*–benzo[*c*]chromen–6–one

oFLU 9*H*–fluoren–9–one

oNAP.....1,4–naphthoquinone

oPHE1 .....Phenanthrene–1,4–dione

oPHE2 .....Phenanthrene–9,10–dione

oPNE..... 1*H*–phenalen–1–one

oPYR1.....Pyrene–1,6–dione

oPYR2.....Pyrene–1,8–dione

OSHA.....Occupational Safety and Health Administration

oXAN.....9*H*–xanthen–9–one

oxy–PAH.....PAH with One or More Oxygen Atoms in Carboxyl Groups and/or as Heteroatoms in the Ring

PAH.....Polycyclic Aromatic Hydrocarbon

PHE.....Phenanthrene

PM.....Particulate Matter

$PM_{>10}$.....Particulate Matter with Aerodynamic Diameters Greater than 10 Micrometers

PM_{10} .....Particulate Matter with Aerodynamic Diameters of 10 Micrometers or Less

$PM_{2.5}$ .....Particulate Matter with Aerodynamic Diameters of 2.5 Micrometers or Less

p_{PAH} .....Gas Phase PAH Partial Pressure

PYR.....Pyrene

QCLC.....Quality Controlled Local Climatological Data

RA.....Rain

Re.....Reynolds Numbers

RET.....Retene

SO_2.....Sulfur dioxide

SQ.....Squall

SVWTP.....Santan Vista Water Treatment Plant

TOC.....Total Organic Carbon

TS.....Thunderstorm

TSP.....Atmospheric Total Suspended Particulate Matter

TSRA.....Thunderstorm with Rain

TWA.....Time-Weighted Average

VC.....Weather Event in the Vicinity of the Station

VIS.....Visibility

$v_{s,air}$.....Atmospheric Particle Sedimentation Velocity

v_{WG}.....Wind and/or Gust Speed

WBAN.....United States Weather-Bureau-Army-Navy

WOE.....Weight of Evidence

x^{aq}.....Fraction of PAH in the Aqueous Phase

x^{fog}.....The Sum of x^{aq} and x^{org}

x^{g}.....Fraction of PAH in the Gas Phase

x^{org}.....Fraction of PAH in the Liquid Organic Phase

Y_m .....Relative Molar Yield

yr .....Year

η_{air}.....Dynamic Viscosity of Air

θ^{org}.....Liquid Organic Surface Film Coverage

θ^{PAH} .....PAH Surface Film Coverage

ρ_{air}.....Density of Air

ρ_p .....Particle Density

ϕ^{aq}.....Aqueous Phase Volume Fraction

ϕ^{org}.....Liquid Organic Phase Volume Fraction

CHAPTER 1

INTRODUCTION

1.1 PROPERTIES OF ATMOSPHERIC PARTICULATE MATTER

The particulate matter (PM) present in the atmosphere is known to be detrimental to human health. The aerodynamic diameter of PM determines, to some extent, the relative exposure in the lungs (see Figure 1.1). Fine particles are normally defined as PM with aerodynamic diameters less than or equal to 2.5 µm ($PM_{2.5}$) and are small enough to access the alveolar recesses of the lungs. $PM_{2.5}$ can thus deposit and closely interact with lung tissue. Coarse particles refer to PM with aerodynamic diameters between 2.5 and 10 µm. Coarse particles cannot access the alveoli but can access the bronchial tubules. Coarse particles may be exhaled or adhere to mucus and thus interact with lung tissue to a lesser extent than $PM_{2.5}$ (Finlayson-Pitts and Pitts, 1999).

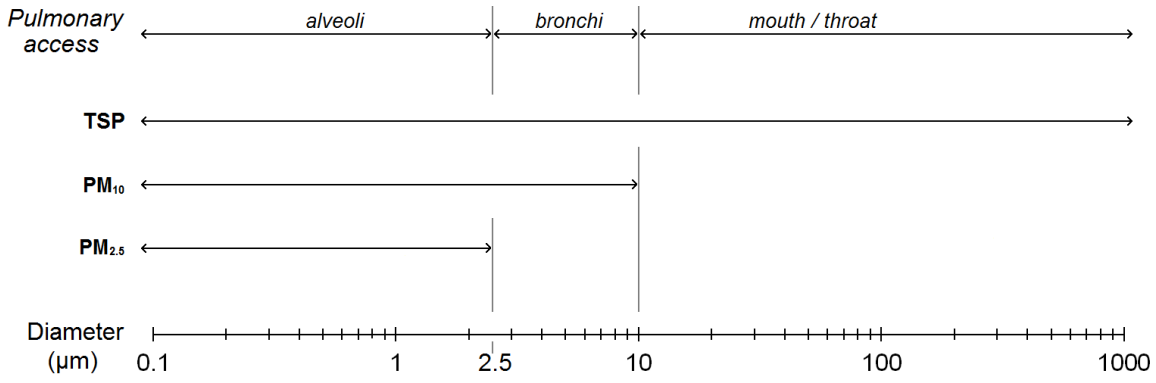

Figure 1.1. Aerodynamic diameters of atmospheric particles and access to respiratory system cavities.

The sum of coarse and fine particles is PM_{10}, or PM with aerodynamic diameters less than or equal to 10 µm. The total suspended particles (TSP) in the atmosphere

includes PM_{10} and PM larger than 10 μm, or $PM_{>10}$. Since the effect of PM exposure varies with diameter, PM is regulated by diameter.

The Clean Air Act of 1963 provided federal funds for research of air pollution control (EPA, 2015). In 1970, modifications to the Clean Air Act required the establishment of regulatory standards for air pollutants and soon thereafter, the U.S. Environmental Protection Agency (EPA) established the National Ambient Air Quality Standards (NAAQS; EPA, 2015). The current NAAQS for PM_{10} and $PM_{2.5}$ are shown in Table 1.1 (EPA, 2013).

Table 1.1

Regulation of Particulate Matter and Polycyclic Aromatic Hydrocarbons

Pollutant	Carcinogenic Classification	Regulatory Scope	Regulatory Concentration	Regulatory Interval	Regulation
$PM_{2.5}$	-	air, ambient	12.0 μg m^{-3} 35 μg m^{-3}	annual[#] 24-hour	EPA, NAAQS[†]
PM_{10}	-	air, ambient	150 μg m^{-3}	24-hour	EPA, NAAQS
PAH	-	air, workplace	200 μg m^{-3}	8-hour[&]	OSHA, PEL[§]
BAA	B2*	water	0.1 μg L^{-1}	-	EPA, MCL[‡]
CHY	B2	water	0.2 μg L^{-1}	-	EPA, MCL
BBF	B2	water	0.2 μg L^{-1}	-	EPA, MCL
BKF	B2	water	0.2 μg L^{-1}	-	EPA, MCL
BAP	B2	water	0.2 μg L^{-1}	-	EPA, MCL
DBA	B2	water	0.3 μg L^{-1}	-	EPA, MCL
IND	B2	water	0.3 μg L^{-1}	-	EPA, MCL

Notes: #, arithmetic mean; †, primary standard (EPA, 2013); &, TWA, time-weighted average; §, Occupational Safety and Health Administration (OSHA, 2016) permissible exposure limit; ‡, MCL, maximum contaminant level; *, EPA WOE (weight of evidence) B2: probable carcinogen with sufficient evidence in animals, for both chronic inhalation and chronic oral (EPA, 2014a); see the text or the Abbreviations Glossary for abbreviations.

1.2 POLYCYCLIC AROMATIC HYDROCARBONS

PAHs (Polycyclic Aromatic Hydrocarbons) are organic molecules with relatively high melting points, low solubilities, and low vapor pressures (Ravindra *et al*., 2008). PAHs are generally considered harmful and seven PAHs are classified as B2 carcinogens ("probable carcinogens, sufficient evidence in animals"; Table 1.1; EPA, 2014a) for both chronic inhalation and chronic oral exposure, namely: benz[*a*]anthracene (BAA), chrysene (CHY), benzo[*b*]fluoranthene (BBF), benzo[*k*]fluoranthene (BKF), benzo[*a*]pyrene (BAP), dibenz[*a,h*]anthracene (DBA), and indeno[1,2,3–*c,d*]pyrene (IND). These seven PAHs are regulated in water (Table 1.1; National Primary Drinking Water Regulations: Maximum Contaminant Levels and Maximum Residual Disinfectant Levels, 2010).

Sixteen PAHs are classified as priority pollutants (EPA, 2014b), namely: the seven aforementioned PAHs, acenaphthylene (ACY), anthracene (ANT), fluorene (FLU), phenanthrene (PHE), fluoranthene (FLT), pyrene (PYR), benzo[*e*]pyrene (BEP), and benzo[*g,h,i*]perylene (BGP).

1.3 SOURCES AND FATE OF PM AND PAHS

The primary sources of PM in the atmosphere include (in order from major to minor) salt condensate from sea spray, dust emissions, vehicular and other anthropogenic emissions, biological debris, and volcanic activity (Rogge *et al*., 1993a; Bond *et al*. 2004; Seinfeld and Pandis, 2006). Secondary PM can arise from atmospheric processing of gases and organic matter (Seinfeld and Pandis, 2006).

PAHs often constitute a small fraction of PM mass (*e.g*., <0.05% of $PM_{2.5}$ in Los Angeles, CA; Rogge *et al*., 1993b) and may be formed concurrently during primary PM

emission. This includes the pyrolysis of organic matter: wildfires, tobacco smoke, automobile exhaust, power plant emissions, and cooking operations (Rogge et al., 1993a; Zhang and Tao, 2004). PAHs are also released to the atmosphere in the gas phase from crude oil and petroleum products; for example, PAHs vaporize from roadway tar sealer and are present in gasoline and diesel vapors (Marr *et al*., 1999; Mahler *et al*., 2012). PAH vapors may adsorb to PM or remain in the gas phase.

The fate of PM is, ultimately, photodegradation and deposition to the Earth's surface. Some of the PM mass can photodegrade over time, such as the organic carbon, which varies by source but is typically less than 30% of the total particulate mass in urban areas (Rogge *et al*., 1993b). The pathway or mechanism of PM reaching the surface of the Earth depends on diameter. PM with aerodynamic diameters less than 1 μm may coagulate into larger particles and / or act as cloud condensation nuclei by up-taking water vapor and growing into droplets (Seinfeld and Pandis, 2006). Such particles can be removed from the atmosphere during precipitation. Larger particles, such as $PM_{>2.5}$, have higher settling velocities than $PM_{2.5}$ and thus may be removed due to gravitational dry deposition (Seinfeld and Pandis, 2006).

Gas phase PAHs may be removed through vapor deposition (adsorption and/or absorption) to the Earth's surface, be scavenged by falling precipitation, or react with atmospheric oxidants such as the hydroxyl radical (Lohmann and Lammel, 2004 Škrdlíková *et al*., 2011; Keyte *et al*., 2013). PAHs bound to PM may share the same atmospheric fate (*i.e*., mechanical deposition) or may be removed by surface reactions (Bidleman, 1988; Ravindra *et al*., 2008; Škrdlíková *et al*., 2011).

The photooxidation kinetics of aqueous phase PAH are faster than liquid-organic phase PAH (Grossman *et al*., 2016) and are of a similar magnitude as PAH oxidation in the gas phase (Chapter 5). Thus, clouds and fog can be an important chemical sink of PAHs.

1.4 RATIONALE AND OBJECTIVES

This work focuses on several aspects of PM and PAH. I investigate haboob and dust storm climatology, PM, and their impact on deposition (Chapters 2 and 3). I also investigate a specific pollutant class (PAH) and its behavior in dust storms (Chapter 4). Finally, I look at how clouds process PAHs in Chapter 5.

There is a need to establish when dust storms occurred in the City of Tempe, especially the haboob dust storms, for which there is no catalog since the 1980's (Nickling and Brazel, 1984). The Nation Weather Service (NWS) records dust events but does not distinguish between types of dust events. In Chapter 2, a clear methodological characterization of haboob events based on meteorological and air pollution observations is established. This is then applied to local datasets from 2005-2015 to gather an objective and systematic climatology of dust storms and haboob events. Then a model is developed and the annual dry deposition is estimated for haboobs and dust storms to evaluate the impact of haboobs on dry deposition fluxes of atmospheric PM. The predicted deposition is compared with literature data.

The impact of dust storms on a local, large body of water, Tempe Town Lake, is investigated in Chapter 3. A recent literature report suggested dust storm induced turbidity in canal water not far from Tempe (Barry *et al*., 2016). Therefore, the coincidence of dust storm deposition and chemistry changes in a long-term dataset of

Tempe Town Lake is investigated. A deposition and dilution model is used to predict dissolved particle masses while a sedimentation model is used to predict particle settling times.

PAHs are ubiquitous in the Earth's atmosphere and are present in the air within and around the City of Tempe, AZ (Cahill, 2013; Clements *et al*., 2016). In Chapter 4, the behavior of this common class of pollutants, PAHs, is investigated in haboobs. It is unknown what affect haboobs have on PAH distribution in Tempe. Haboobs could potentially stir-up, transport, and/or remove PAHs bound to PM. During the summer months of 2013 and 2014, the season when most haboobs occur in Tempe, $PM_{2.5}$ was sampled and analyzed for changes in the relative abundance of PAHs and for changes in PAH isomer ratios. The hypothesis of haboob events altering the PAH concentration and distribution in Tempe, AZ is investigated.

PAHs can travel long distances from their emission sources (Seinfeld and Pandis, 2006). In such cases the PAHs may have aged, for example, after their deposition to soil and prior to resuspension. The PAHs could have undergone atmospheric processing during transport, photochemistry, or even biological modifications. The partitioning and processing of PAH in the vapor and particulate phases is well studied (*e.g*., Lohmann and Lammel, 2004). However, it is unknown to what extent clouds/fog can process PAHs. To determine their impact, the distribution or partitioning of PAHs in a cloud system is modeled in Chapter 5. The PAH (photo)oxidation is calculated. This tests the hypothesis that clouds/fog are an important atmospheric sink for PAHs.

Finally, in Chapter 6, the results and observations are summarized. I conclude by providing suggestions for future research.

CHAPTER 2

THE CHARACTERIZATION OF HABOOBS AND THE DEPOSITION OF DUST IN TEMPE, AZ

2.1 INTRODUCTION

During the North American monsoon season Phoenix, Arizona is reported to experience 2 to 7 dust storms per year (Raman *et al*., 2014). Metropolitan Phoenix is a semiarid urban area with a population of 4.2 million (U.S. Census Bureau, 2013); the region has low annual precipitation ranging from 83 to 240 mm yr^{-1}, and high temperatures with an average of 61 days per year exceeding 40 °C (U.S. NOAA, 2015). The monsoon season is now defined by the National Weather Service (NWS) as June 15 to September 30 (similar to the 'hurricane season'; U.S. NWS, 2016); it is characterized by a change in the general upper atmosphere circulation and an average dew point greater than 12.7 °C. The most intense kind of dust storms Phoenix experiences are fostered by monsoon weather through the interaction of atmospheric water and sunlight. In the vicinity of Phoenix, thunderstorm clouds build during the day as moisture-laden air aloft from the Gulf of Mexico and the Pacific Ocean (Sorooshian *et al*., 2011) is energized by sunlight and rises within the clouds. In the evening, the supply of heated, moist air decreases and there is a net downward movement of moisture as precipitation. Over the semiarid desert, the falling hydrometeors evaporate significantly before reaching the surface which cools surrounding air, causing it to become denser and to displace the dry air below. These powerful downdrafts can produce high winds and turbulent convection over the landscape. These thunderstorm outflows can result in a particular kind of dust storm: an advancing wall of dust hundreds of meters high and tens of kilometers long

known as a haboob, from the Arabic *habūb* ‘blowing furiously / strong wind’ (see Figures 2.1 and 2.2; Sutton, 1925; Idso *et al*., 1972; Idso, 1976).

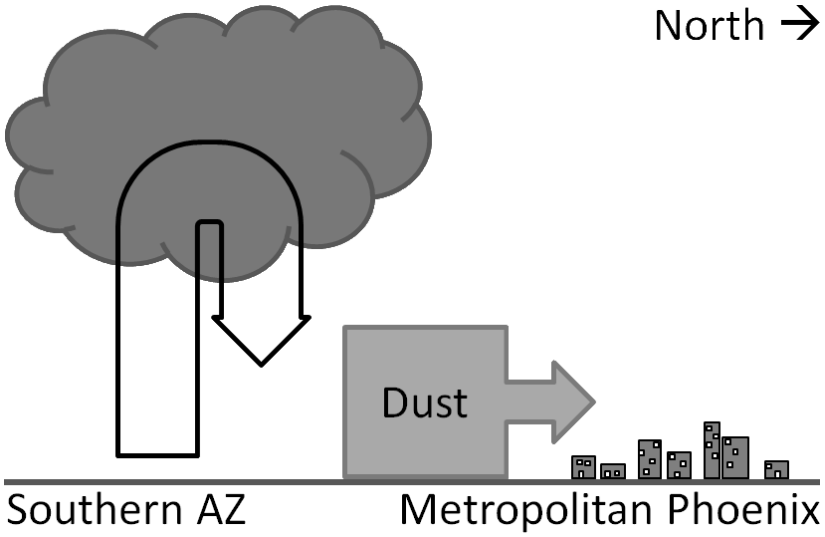

Figure 2.1. Conceptual diagram of haboob initiation in Arizona. Note: not all haboobs originate south of Tempe and the diagram is not to scale.

Haboobs occur in only a few parts of the world, including northern Africa (Sutton, 1925; Roberts and Knippertz, 2012), the Arabian Peninsula (Membery, 1985; Miller *et al*., 2008), and northwest India (there known as *kālī andhī* or *andhī* ‘darkening, blinding storm’; Joseph *et al*., 1980; Joseph, 1982; Goudie and Middleton, 2000). In the US, haboobs have been reported in Arizona and Texas (Warn and Cox, 1951; Idso *et al*., 1972; Brazel and Nickling, 1986; Chen and Fryrear, 2002). In Arizona, haboobs can substantially decrease visibility to less than 1 km (Nickling and Brazel, 1984). Wherever haboobs occur, they are quite intense relative to other types of dust events (Roberts and Knippertz, 2012) and have comparatively short lifetimes of 1 to 4 h in any single location (Sutton, 1925; Brazel and Nickling, 1986).

Figure 2.2. Haboob advancing in Tempe, AZ on August 25, 2015; photo credit: Ariel Anbar

2.1.1 Impact on Air Quality.

Haboobs can have a significant impact on the amount of atmospheric particulate matter (PM) in the metropolitan Phoenix area (Clements *et al*., 2014; Lei and Wang, 2014; Clements *et al*., 2016). Particulate matter is classified by size fractions; PM_{10} and $PM_{2.5}$ are particulate matter with aerodynamic diameters of ≤ 10 μm and ≤ 2.5 μm, respectively. The size of PM determines the extent of penetration into the respiratory tract and therefore the adverse health risk: PM_{10} can penetrate to the bronchi passages while the finer and more hazardous fraction, $PM_{2.5}$, is able to penetrate fully into the alveolar recesses of the lungs (WHO, 2006). Their mass concentrations, $c(PM_{10})$ and $c(PM_{2.5})$ respectively, both increase during haboobs; peak $c(PM_{10})$ can be in the thousands of

μg m^{-3} for several hours and $c(PM_{2.5})$ increases although to a somewhat lesser extent (*e.g.*, tens to hundreds of μg m^{-3}; Clements *et al.*, 2013; Lei and Wang, 2014). The U.S. National Ambient Air Quality Standards (NAAQS) are 12 μg m^{-3} for $c(PM_{2.5})$ and 150 μg m^{-3} for $c(PM_{10})$ over a 24-hour period (U.S. Environmental Protection Agency (EPA), 2013). High haboob-derived PM concentrations which exceed the EPA standards are typically excluded from regulatory decisions regarding NAAQS compliance since they are high-wind, natural-events that are "not reasonably controllable or preventable" and which overwhelm even stringent dust control measures (U.S. EPA, 2006, 2007; ADEQ, 2015).

Besides the impact on air quality, another impact of haboobs is particle deposition. In the early 1970's, rooftop dust deposition in Tempe was reported to be 540 kg $ha^{-1}yr^{-1}$, 12% of which was attributed to 2 haboobs (Péwé *et al.*, 1981). Particle deposition in semiarid regions of southern California and Nevada (which do not experience haboobs) has been reported to be substantially lower, 20 to 200 kg $ha^{-1}yr^{-1}$, over the period 1983 to 2000 (Reheis, 2006). The magnitude of annual haboob deposition and the impact on urban ecosystems is not well known. As the Phoenix population grows, changes in land use could also affect haboobs because the resuspension and transport of dust in and around metropolitan Phoenix will likely co-vary with changes in land cover and in the urban heat island (Li *et al.*, 2016) which in turn affects local precipitation. Identification of haboobs in metropolitan Phoenix from historical data can be challenging since meteorological and radar records often are inadequate in temporal and spatial resolution to capture these short-lived phenomena (Raman *et al.*, 2014). Reliance upon visibility and wind speed data alone can lead to false-positive haboob identifications

since these events can occur with several meteorological phenomena. The METAR (Meteorological Terminal Air Report) weather condition codes provide dust information (*e.g.*, BLDU, blowing dust) but do not distinguish between general dust events and the more intense haboobs.

This work identified and characterized haboobs in Tempe, AZ over the period 2005 to 2014. Air quality impacts were documented and temporal changes in haboob frequency and intensity were investigated. A computational model was used to estimate particle deposition in Tempe. This work is of limited spatial scope since it reports the development of a systematic classification of haboobs. This work exceeds prior location-specific libraries of haboob events in that it employs air quality and meteorological data in haboob classification.

2.2 MATERIALS AND METHODS

2.2.1 Retrieval of meteorological and air quality records.

Metropolitan Phoenix covers a large area (37,700 km^2) and as such, there is heterogeneity in dust deposition throughout the area (Péwé *et al.*, 1981). To maintain consistency a single location near the Arizona State University (ASU) Tempe campus (see Figure 2.3), was selected for dust event identification. The weather station at the Phoenix Sky Harbor International Airport (KPHX) has weather records back to 1930 and was the location used in older dust storm studies (*e.g.*, Brazel and Nickling, 1986). KPHX is also proximal to ASU's Tempe campus as well as to a variety of long-term ecological study sites (*e.g.*, Ball and Guevara, 2015; Bateman *et al.*, 2015; Davis *et al.*, 2015; Giraudeau *et al.*, 2015) for which the deposition predictions of this work could augment the existing research. I retrieved KPHX hourly, quality-controlled local

climatological data from 2005 to 2014 (U.S. NOAA, 2015). Haboob classifications were applied using data from two air quality stations which measure $c(PM_{10})$ were selected in proximity to KPHX, namely, CEPH and TE (see Table 2.1 and Figure 2.3; U.S. EPA, 2015)

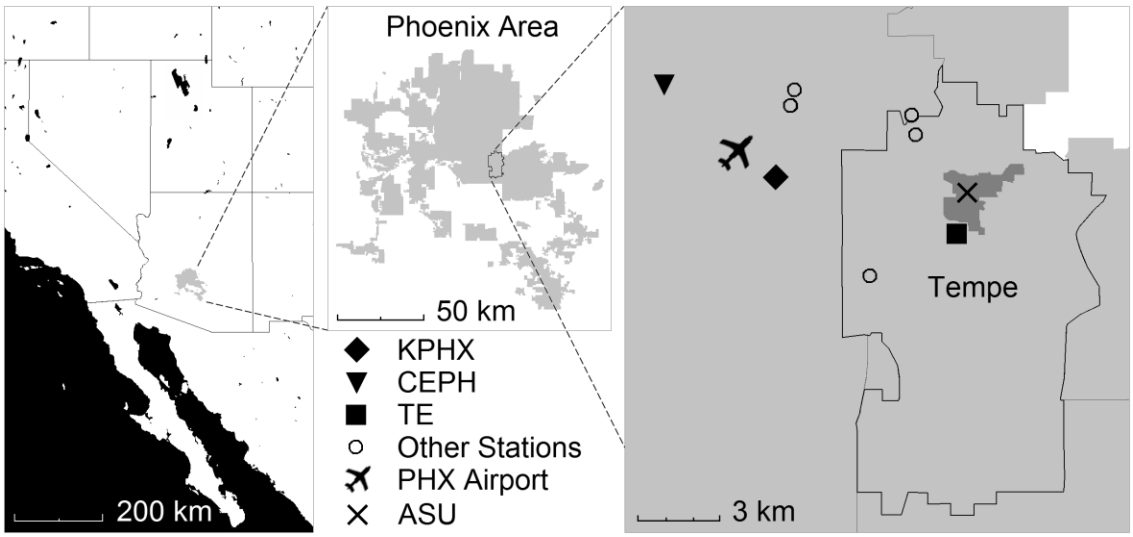

Figure 2.3. Map of the southwest U.S. (left) with gray shading indicating metropolitan Phoenix, an enlargement of metropolitan Phoenix (middle) with the City of Tempe's boundaries as a black line, and the City of Tempe (right) with an × and dark gray shading indicating ASU Tempe campus and nearby meteorological stations and air quality system sites. The filled diamond, triangle and square indicate the station locations of KPHX, CEPH, and TE respectively. Open circles indicate the locations of "Other Stations" which includes MAGC, SA31, SRP01, DIABLO, and VEL. "PHX Airport" is the Sky Harbor International Airport. See Table 2.1 for full station names and station abbreviations in the legend.

Four additional weather stations in Tempe were used to confirm the presence of haboob dust, namely AN014, MAGC, SA31, and SRP01 (MesoWest, 2015). Two additional air quality sites were chosen to better distinguish high smog events from dust events, namely DIABLO and VEL (see Table 2.1 and Figure 2.3; U.S. EPA, 2015).

Table 2.1

Summary of Public Data and Sources

Abbrev-iation	Date Range	Data Type	Station Name	Station ID	Provider
KPHX	2005-Present 1930-Present	QCLCD[†] Meteorological	Phoenix Sky Harbor International Airport	WBAN 23183[‡]	U.S. Weather Bureau[¤]
CEPH	1985-Present 1965-Present	$c(PM_{10})$ [^] Gases	Central Phoenix	AQS*04-013-3002	MCAQ[#,@]
TE	2012-Present 2000-Present	$c(PM_{10})$, $c(PM_{2.5})$ [¢] Gases	Tempe TE	AQS 04-013-4005	MCAQ
DIABLO	2014-Present	$c(PM_{2.5})$, Gases	Diablo	AQS 04-013-4019	MCAQ
VEL	1989-Present 2003-Present	Gases Nephelometry	Vehicle Emissions Lab	AQS 04-013-9998	ADEQ[£,@]
AN014	2010-2014	Meteorological	Tempe	AN014	MCAQ
SA31	2014-2015	Meteorological	Tempe SA31	SA31	MADIS[¶,§]
SRP01	2013-Present	Meteorological	SRP	SRP01	Salt River Project[§]
MAGC	2005-Present	Meteorological	GateWay Community College	MAGC	MFCD[¥,§]

Notes: †, QCLCD, hourly quality controlled local climatological data; ‡, WBAN, Weather-Bureau-Army-Navy; ¤, http://www.ncdc.noaa.gov/qclcd; ^, $c(PM_{10})$, PM_{10} mass concentration; *, AQS, U.S. Environmental Protection Agency Air Quality System; #, MCAQ, Maricopa County Air Quality; @, http://aqs.epa.gov/api; ¢, $c(PM_{2.5})$, $PM_{2.5}$ mass concentration; £ ADEQ, Arizona Department of Environmental Quality; ¶, MADIS, Meteorological Assimilation Data Ingest System; §, http://mesowest.utah.edu; ¥, MFCD, Maricopa County Flood Control District. Stations TE and AN014 are co-located.

2.2.2 Historical haboob identification and categorization.

Hourly weather and air quality data from KPHX for the years 2005 to 2014 were searched for dust event signatures (see flowchart in Figure B1). A dust event was

considered a meteorological condition of reduced visibility (*VIS*), elevated wind and/or gust speed (v_{WG}), and elevated $c(PM_{10})$. To begin, a preliminary list was generated for hours in which any of the following occurred: minimum *VIS* < 16 km (< 10 mi), maximum $v_{WG} > 17$ m s^{-1} (> 40 mi h^{-1}), a 1 h average $c(PM_{10}) \geq 200$ µg m^{-3}, or the occurrence of dust-related METAR weather condition codes (*e.g.*, BLDU, blowing dust; DS, dust storm; DU, widespread dust; HZ, haze; TS, thunderstorm; SQ, squall). The hours identified were then grouped into events. Events were assumed to be separate when the weather and air quality signatures returned or were 'reset to fair weather conditions' for at least 6 hours. There were 422 events which met the preliminary criteria. Some confounding factors which can cause low air visibly were heavy rain, fog, and smog. To avoid false-positives, each event was assessed individually for coincident *VIS* drops, v_{WG} spikes, $c(PM_{10})$ spikes, and appropriate METAR weather condition codes. After removing high smog episodes, fog, heavy rain, and thunderstorms without dust, there were 266 candidate dust events which remained.

There is a characteristic meteorological signature which accompanies thunderstorm outflows and, therefore, haboobs (Idso *et al*., 1972). This signature includes a rapid increase in humidity and air pressure, a rapid decrease in air temperature, and a spike in $c(PM_{10})$, generally ≥ 200 µg m^{-3} for 1 to 3 h (see Figure B2). The individual dust events were inspected for this signature and were categorized as either haboobs or 'other dust'. Non-haboob dust events had longer durations (*i.e.*, 3 to 12 h) of elevated $c(PM_{10})$ without abrupt changes in temperature, humidity, and pressure. Mild haboobs with visibility *VIS* > 11.3 km (> 7 mi) were grouped with the 'other dust' since they were more difficult to positively identify. Following data review, 96 haboob events with *VIS* ≤

11.3 km (≤ 7 mi) were identified for the years 2005 to 2014 (see Table B1 for list). Photographic evidence for haboob events early in this period was often not available. In the latter portion of the 2005-2014 period, social media reports of these events were more common and of the 96 haboob events, 43 were confirmed by photographs of advancing 'walls' of dust obtained from the local press, social media, or web camera records.

2.2.3 Atmospheric Dry deposition model.

Dry deposition in Tempe was estimated using a model similar to that of Sauret *et al*. (2009). The air sedimentation velocities ($v_{s,air}$) for 36 particles sizes (aerodynamic diameters from 0.1 to 320 µm) were calculated with Equation 2.1, where ρ_p is the particle density (1.7×10^6 g m^{-3}), $d_{p,j}$ is the *j*th aerodynamic particle diameter, g is the gravitational constant, $C_{f,j}$ is the diameter-specific particle Cunningham factor (*i.e*., a sliding factor), and η_{air} is the dynamic viscosity of air:

$$v_{s,air,j} = d_{p,j}^2 \, \rho_p \, g \, C_{f,j}/(18 \, \eta_{air}) \quad (2.1).$$

$C_{f,j}$ was calculated as a function of $d_{p,j}$ where $\lambda_{p,air}$ is the particulate mean free path in air (an estimated constant value of 0.066 µm). Calculated $C_{f,j}$ agreed with values given in Seinfeld and Pandis (2006) and Sauret *et al*. (2009):

$$C_{f,j} = 1 + \frac{\lambda_{p,air}}{d_{p,j}}\left(2.514 + 0.8e^{-0.55 \, d_{p,j} \, / \, \lambda_{p,air}}\right) \quad (2.2).$$

Diameter specific Reynolds numbers (Re_j) were calculated as a function of $d_{p,j}$ where ρ_{air} is the density of air:

$$Re_j = \rho_{air} \, v_{s,air,j} \, d_{p,j} \, / \, \eta_{air} \quad (2.3).$$

For particle sizes where the Re_j was > 1, drag was included in the sedimentation velocity calculation and $v_{s,air,j}$ from Equation 2.4 was used in deposition calculations (Seinfeld and Pandis, 2006):

$$v_{\mathrm{s,air},j} = d_{\mathrm{p},j}^{8/7} \left(\frac{4}{55.5} \mathrm{g}\, \rho_{\mathrm{p}}\, C_{\mathrm{f},j}\right)^{5/7} / \left(\rho_{\mathrm{air}}^{2/7}\, \eta_{\mathrm{air}}^{3/7}\right) \quad (2.4).$$

A static value of η_{air} is not adequate for metropolitan Phoenix where diurnal temperatures differ by an average of 12 °C (22 °F) with a range of 2 to 22 °C (4 to 39 °F; U.S. NOAA, 2015).

During thunderstorm outflows, the temperature and pressure both change, causing η_{air} to decrease and therefore $v_{\mathrm{s,air}}$ to increase by as much as 5% in 1 to 2 hours (*e.g.*, 2 August, 2005 in Figure B1). Hourly η_{air} and ρ_{air} were calculated using Mathematica 10 (Mathematica, 2015a, 2015b) as a function of KPHX dry bulb air temperature and air pressure. Values for η_{air} and ρ_{air} varied by time of day and by season, with η_{air} ranging from 0.0171 to 0.0195 g $\mathrm{m^{-1}s^{-1}}$ and ρ_{air} ranging from 1.05 to 1.27 kg $\mathrm{m^{-3}}$ (see Figures B1 and B2).

The dry deposition flux in air (J_{air}) was calculated using Equation 2.5, where $v_{\mathrm{s,air},i,j}$ is the sedimentation velocity of PM with diameter j during a time interval i, x_j is the diameter-specific mass fraction, t_j is the length of a measurement interval (*i.e.*, 1 h), and $c(\mathrm{PM_{10}})_i$ is the $\mathrm{PM_{10}}$ mass concentration during the interval:

$$J_{\mathrm{air}} = \sum_{i=1}^{\mathrm{n}} \left[t_i\, c(\mathrm{PM_{10}})_i \cdot \sum_{j=0.1\mu\mathrm{m}}^{320\mu\mathrm{m}} \left[v_{\mathrm{s,air},i,j}\, x_j \right] \right] \quad (2.5).$$

The PM mass distributions were calculated from distributions reported in the literature (see Figure 2.4). During non-haboob time periods, x_j was the average of 2 distributions (Seinfeld and Pandis, 2006; Sauret *et al*., 2009). Values of x_j were scaled so that the entire $\mathrm{PM_{10}}$ mass fraction was unity:

$$\sum_{j=0.1\mu m}^{10\mu m} x_j = 1 \quad (2.6).$$

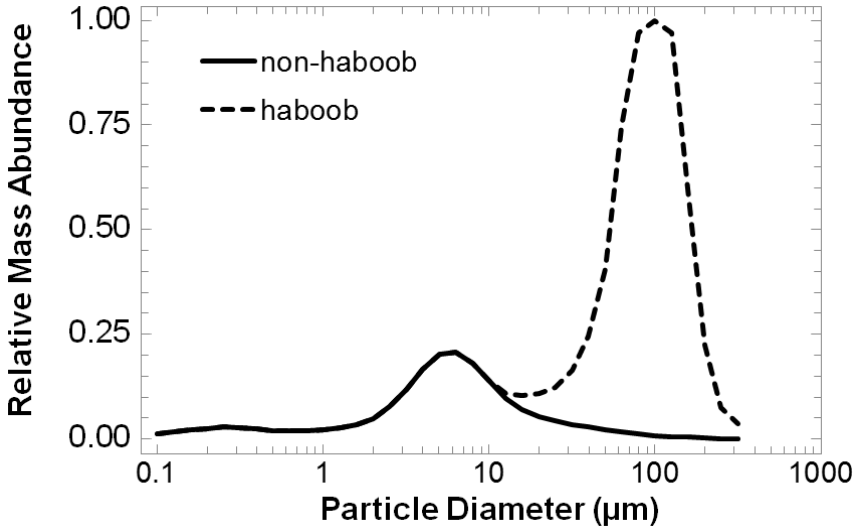

Figure 2.4. Composite PM mass distributions for haboob and non-haboob periods. The haboob distribution had a $\frac{PM_{10}}{TSP}$ mass ratio of 0.20. The non-haboob distribution was the average of literature mass distributions (Sauret *et al*., 2009; Seinfeld and Pandis, 2006). The haboob and the non-haboob distributions differed only for particle aerodynamic diameters > 10 μm. Much of the mass in the haboob distribution was comprised of large particles. See the Figures B3 and B4 for a more detailed explanation.

During haboob time periods, I employed a distinct mass distribution based on dust storm distributions from the literature (Gillette *et al*., 1978; Chen and Fryrear, 2002; O'Hara *et al*., 2006; Box *et al*., 2010). During dust events such as haboobs, much of the particulate mass is comprised of $PM_{>10}$ (PM with d_p > 10 μm). The mass ratio of PM_{10} to the total suspended particulates (TSP), or $\frac{PM_{10}}{TSP}$, has often been reported to be < 0.3 during large dust storms (see Table 2.2) meaning that there was more mass of particles with d_p > 10 μm than the mass with $d_p \leq 10$ μm.

Table 2.2

Dust Storm Mass Distribution Ratios and Deposition

Location	$\frac{PM_{10}}{TSP}$ ¥	J_{air}(TSP)¢ , kg ha^{-1}	Sample Duration	Reference
USA				
Phoenix	n/a	540 yr^{-1}	annual	Péwé *et al*., 1981
Western Texas	0.06*,¤	850 h^{-1}	1 haboob	Chen and Fryrear, 2002
Colorado and Kansas	0.28; 0.30¤	n/a	2 dust storms	Chepil, 1957
Northwest Texas	0.18 – 0.27*	210 – 790 h^{-1}	3 dust storms	Gillette *et al*., 1978
Pennsylvania	n/a	15.3, storm total	1 dust storm†	Miller, 1934
Southern California and Nevada	n/a	20 – 200 yr^{-1}	annual	Reheis, 2006
Europe				
Ukraine	n/a	20 – 6940 mo^{-1}	4 weeks§	Shikula, 1981
Middle East				
Dead Sea, Israel	n/a	255 – 605 yr^{-1}	annual	Singer *et al*., 2003
Negev Desert, Israel	n/a	1100 – 2200 yr^{-1}	annual	Goossens and Offer, 1995
Northern Africa				
Libya	< 0.18 to < 0.77‡	366 – 4210 yr^{-1}	annual	O'Hara *et al*., 2006
Western Chad	n/a	537 yr^{-1} @	annual	Maley, 1980
Northern Nigeria	n/a	991 yr^{-1}	annual	McTainsh, 1980
Northern Nigeria	< 0.67‡	> 850 yr^{-1}	1 dust season	Møberg *et al*., 1991
Southwest Niger	n/a	1640 – 2120 yr^{-1}	annual	Drees *et al*., 1993
Australia and New Zealand				
Sydney, Australia	< 0.85; < 0.87*,^	n/a	2 dust storms	Box *et al*., 2010
South Island, New Zealand	n/a	> 710 to > 6140 yr^{-1}	1 dust season	McGowan *et al*., 1996

Notes: ¥, $\frac{PM_{10}}{TSP}$, mass ratio of PM_{10} to TSP; ¢, J_{air}(TSP), atmospheric TSP dry deposition flux; *, estimated from histograms; ¤, average of 5–20 ft. sampler heights; †, originated in mid-west USA; §, historically, the dust storms during the 4 weeks were unusually severe; ‡, PM_{20} and $PM_{>20}$ were reported; @, calculated with dust density of 0.85 g cm^{-3}; ^, $PM_{>18}$ not reported.

Some $\frac{PM_{10}}{TSP}$ ratios are listed as upper bounds in Table 2.2 as a consequence of: $PM_{>18}$ was not reported (Box *et al*., 2010) or PM_{20} and $PM_{>20}$ were reported but not PM_{10} and $PM_{>10}$ (Møberg *et al*., 1991; O'Hara *et al*., 2006). The composite haboob mass distribution used in this study was identical to the non-haboob distribution for PM_{10}, but for $PM_{>10}$ the haboob x_j values were scaled with the mass ratio $\frac{PM_{10}}{TSP}$ such that Equation 2.7 obtained:

$$\sum_{j>10\mu m}^{320\mu m} x_j = 1 - \frac{PM_{10}}{TSP} \quad (2.7).$$

Thus, the model utilized a particle mass distribution where much of the haboob TSP was $PM_{>10}$ ($\frac{PM_{10}}{TSP}$ = 0.20) while the background (non-haboob) TSP mass was primarily PM_{10} ($\frac{PM_{10}}{TSP}$ = 0.78). A more detailed discussion of the literature and composite distributions is given in Figures B3 and B4. To avoid overestimation of deposition, the non-haboob mass distribution was used for mild haboob events (*i.e*., *VIS* > 11.3 km) and for dust events lacking a clear meteorological signature of a convective thunderstorm outflow.

2.3 RESULTS AND DISCUSSION

2.3.1 Haboob occurrence, characteristics, and frequency.

Most haboobs with *VIS* ≤ 11.3 km (≤ 7 mi) in Tempe over the period 2005 to 2014 occurred in the months of July and August which exhibited median event frequencies of 4 and 2.5 respectively (Figure 2.5). This timeframe coincides with the North American monsoon season and is in agreement with Brazel and Nickling's (1984 and 1986) data for haboobs near Tempe from 1965 to 1980.

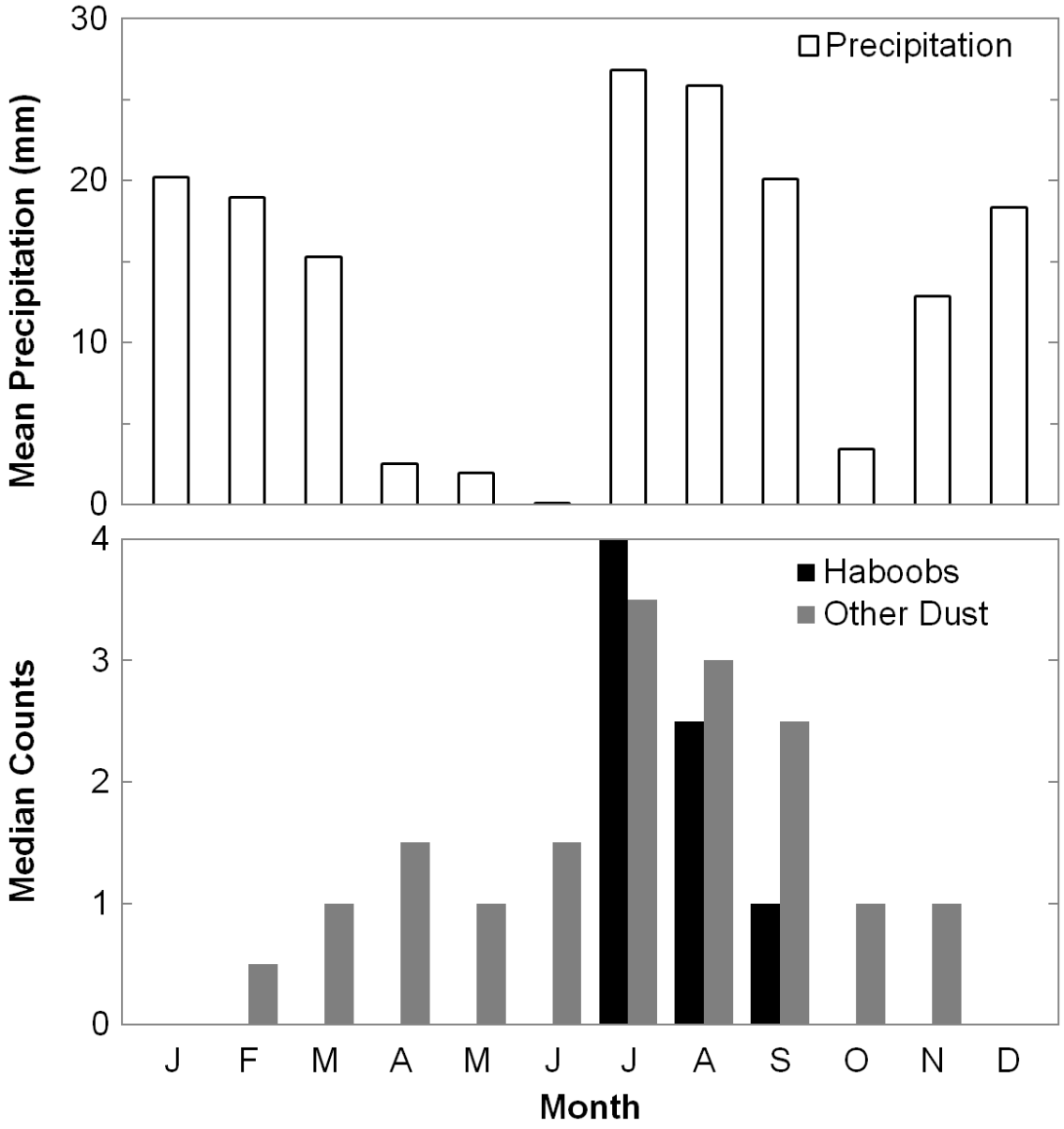

Figure 2.5. Monthly mean precipitation (top) and median dust occurrence (bottom) in Tempe over the period 2005 to 2014. Haboobs were convective outflow events with minimum *VIS* > 11.3 km (7 mi). 'Other dust' comprises events that failed to meet either the visibility or the meteorological criteria for haboobs. Precipitation was bimodal where rains during the North American monsoon season (July to September) coincided with haboobs while winter precipitation coincided with few dust events.

In Figure 2.5, zero median dust event occurrences are indicated as the absence of a bar. In June, the mean annual precipitation was 0.05 mm. The summertime precipitation

pattern and haboob modes are consequences of thunderstorm evolution and convective outflows. Haboobs do not necessarily require precipitation to occur, yet are intrinsically linked to the summer precipitation near metropolitan Phoenix. Thus, the most intense type of dust storm that occurs in Tempe, the haboob, is not only dependent upon relatively hot and dry surface conditions, but also requires significant sources of moisture from outside the region, such as the Gulf of Mexico and Gulf of California (Sorooshian *et al*., 2011). Haboobs do not coincide with the winter rainy periods since winter storms do not have the characteristics necessary to trigger haboob events (*e.g*., convective outflow, surface temperatures, etc.).

The 'other dust' events category included unconfirmed haboobs, mild haboobs (*e.g*., minimum *VIS* > 11.3 km), and dust caused by other meteorological phenomena such as cold fronts. 'Other dust' events occurred in most months of the year with a mode during the monsoon season due to the contribution of mild haboobs. The winter precipitation mode appeared to inhibit dust storms, as indicated by zero median dust event occurrences in December and January (see Figure 2.5). This is in agreement with Nickling and Brazel's 1984 data on dust storms in Tempe for the time period 1965 to 1980.

The number of haboobs and precipitation varied substantially from year to year over the period 2005 to 2014. Haboob occurrences ranged from 3 to 20 yr^{-1} with an annual average of 9.6 yr^{-1} (see Figure 2.6). Annual precipitation ranged from 83 to 240 mm yr^{-1}, with an average of 166 mm yr^{-1}. Such year to year variation was also reported from 1965 to 1980 by Brazel and Nickling when the number of haboobs ranged from 1 to 19 yr^{-1} (1986). In general, fewer haboobs occurred during 2005 to 2014 in years with

greater annual precipitation, in agreement with Brazel (1989) and Holcombe *et al*. (1997). For example, in 2008 and 2010, Tempe received 240 and 230 mm yr^{-1} rain, respectively, and experienced 4 and 3 haboobs, respectively. In drier years, for example 2011 and 2012, Tempe received less rain, 118 and 109 mm yr^{-1}, respectively, and experienced 20 and 19 haboobs, respectively. However, the relationship between precipitation and haboobs in Tempe is complicated by the bimodality of annual precipitation and by many other factors unrelated to precipitation (*e.g*., anthropogenic activity and land use changes; Macpherson *et al*., 2008). During the driest year of this study, 2009, Tempe received 83 mm of precipitation and yet, only experienced 7 haboobs, a below average number. The year 2009 was the only year investigated in this study when annual precipitation was below 100 mm. The simplest explanation of decreased haboob occurrence during 2009 is that it was a manifestation that summer precipitation and haboobs have a mutual source: thunderstorms. However, Goudie (1983) observed that global dust storm occurrence increased as precipitation decreased until reaching a 'hyperaridity' threshold, 100 mm yr^{-1}, below which dust storm occurrence decreased, which was speculated to be due to prior removal of wind-erodible soil, the formation of wind-stable desiccated surfaces, and/or a lack of moisture-associated, dust-storm-initiating weather patterns (*e.g*., thunderstorms, frontal passage). Further investigation would be required to assess whether this hperaridity threshold applies in central AZ. The bimodality of precipitation in Tempe as well as anthropogenic activity and land use change very likely also impact the specific relationship between haboob occurrence and precipitation.

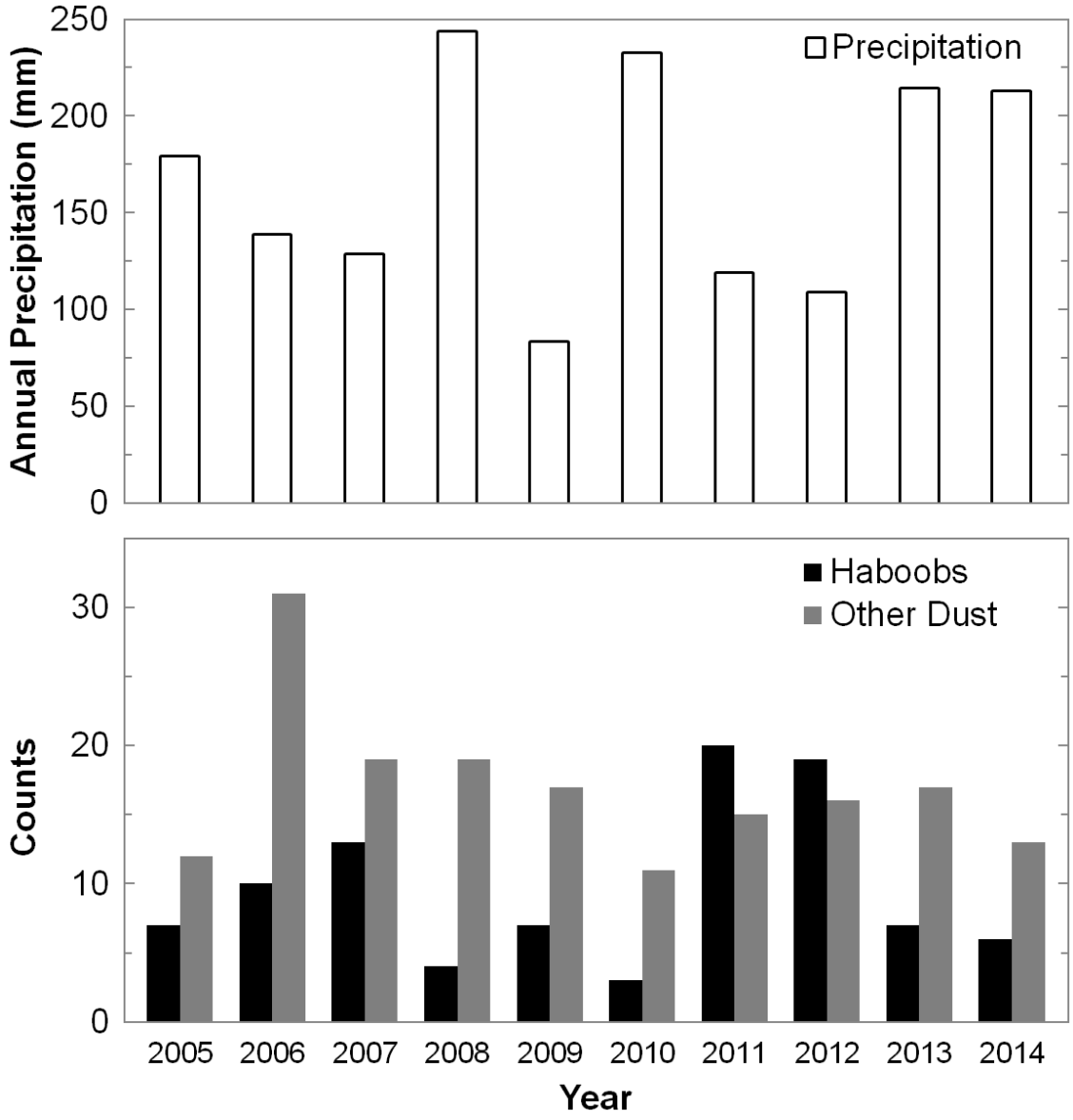

Figure 2.6. The annual precipitation (top) and annual occurrence of dust events (bottom) in Tempe over the period 2005 to 2014. Haboobs were convective outflow events with minimum $VIS \leq 11.3$ km. 'Other dust' events failed to meet haboob visibility or meteorological criteria. There was significant year-to-year variation in precipitation and in haboob occurrence: 83 to 240 mm and 3 to 20 haboobs respectively.

The relationship between precipitation and haboobs in an urban environment is likely to be complex. Land use, land cover, and the disruption of stabilized soil surfaces are affected by a variety of human factors such as economic downturns (*i.e.*, decreased

construction, agricultural, and recreational activities), dust mitigation efforts, and air quality regulations (Hyers and Marcus, 1981; Holcombe *et al*., 1997; Macpherson *et al*., 2008; Clements *et al*., 2014; Upadhyay *et al*., 2015). Precipitation from a thunderstorm may evaporate significantly before reaching the Earth's surface during the initiation of a haboob and may occur far from Tempe; such would not be apparent in the Tempe precipitation records. Metropolitan Phoenix is a highly built–environment and the city has reservoirs that buffer against drought and canals that distribute water year-round. It is, as yet, unclear how much impact diminished precipitation really has on dust production in the area.

The systematic method used in this work provided robust classifications (see Figure 2.7) with significant differences between the mean of haboobs and all other dust events for maximum v_{WG} ($p < 0.001$) as well as maximum $c(PM_{10})$ ($p < 0.001$). The mean v_{WG} of haboobs was larger than 75% of other dust events (see Figure 2.7) and the mean of haboob maximum $c(PM_{10})$, 884 μg m^{-3}, was larger than most (99^{th} percentile) of the other dust events. All of the dust event peak $c(PM_{10})$ were larger than the background mean $c(PM_{10})$ of 33 μg m^{-3}. The differences in the mean minimum *VIS* of haboobs and other dust are a consequence, in part, of the visibility threshold employed in the classification method. Peak $c(PM_{10})$ in the hundreds or thousands of μg m^{-3} is relatively high yet it is sustained for only one or two hours, which may allow one to limit exposure to high PM by seeking shelter from the storm.

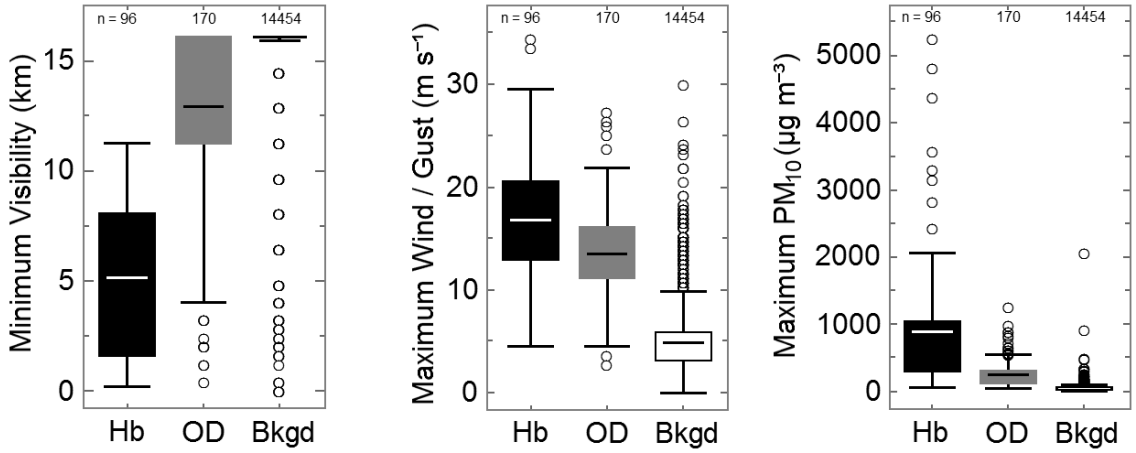

Figure 2.7. Basic characteristics of dust storms in Tempe for the period 2005 to 2014. Minimum visibility (left), maximum wind or gust speed (middle), and maximum PM_{10} concentration (right) are the major factors that distinguish haboobs events (Hb) from other dust events (OD) and background (Bkgd) conditions. In these box plots the horizontal lines are mean values, the box boundaries are the 25th and 75th percentiles, the whiskers are the 10th and 90th percentiles, and the dots are outliers. Haboobs with $VIS \leq$ 11.3 km (7 mi) had much higher PM_{10} concentrations than 'other dust' events. Other dust was events that failed to meet the visibility and meteorological criteria for haboobs. The background data are the 6-hour extremes and include time periods of smog, fog, rain, and fair weather. The small numbers above the columns are the event counts.

2.3.2 Comparison with literature classification methods.

The classification method used in this work bears similarity with classifications previously applied in other U.S. locations. Hagen and Woodruff (1973) and Orgill and Sehmel (1976) identified dust storms from historical records based on 2 criteria: (1) when dust was reported and $VIS < 11.3$ km; or (2) when $11.3 \leq VIS \leq 14.5$ km and $v_{WG} > 5.4$ m s^{-1} (7 mi, 7 to 9 mi and 12 mi h^{-1} respectively). The present work did not employ a wind speed requirement to be considered a dust event. Nevertheless, nearly 97% of all dust events cataloged here had peak $v_{WG} > 5.4$ m s^{-1}. Notably, the past work of Hagen and Woodruff (1973) and Orgill and Sehmel (1976) did not distinguish between types of dust storms or report dust statistics specific to Phoenix.

Lei and Wang (2014) catalogued and characterized dust storms of many kinds (including haboobs) throughout the southwestern U.S. for 10 years. Their methodology did not specify a visibility threshold but was based on dust storms in the literature and in the media that had supporting evidence in meteorological and air quality records. Their method could not be used in Tempe to classify haboobs since there has been a dramatic increase in public awareness and social media attention only in the last few years. Only classifying publicized and reported events in Tempe would have introduced a significant bias.

It is possible to subdivide my haboob category based on intensity using the KPHX visibility data. Brazel and Nickling (1984, 1986) classified dust storms by storm type and by visibility in specific areas of Arizona, including Tempe. They employed visibility thresholds of $VIS \leq 1.6$ km (1 mi) as intense and $1.6 < VIS \leq 11.3$ km (1 to 7 mi) as moderate. Using their classification system, I identified 25 'intense' haboobs and 71 'moderate' haboobs during the time period 2005 to 2014. Another difference between the work of Brazel and Nickling and our current work was that they used 4 meteorological categories for dust while the current work used only 2 categories ('haboob' and 'other dust').

The Australian Meteorological Society visibility threshold for severe dust storms is $VIS \leq 0.2$ km and the threshold for moderate dust storms is <1 km (about 0.12 and 0.63 mi, respectively); higher visibility dust events are not considered storms but blowing dust episodes (O'Loingsigh *et al.*, 2014). Using this classification system, I identified 1 'severe' haboob and 6 'moderate' haboobs in Tempe during the years 2005 to 2014. Indeed the 'severe' haboob (5 July, 2011) was quite exceptional in that it was larger than

any haboob in the preceding 10 years (2001 to 2011, Raman *et al*., 2014); this event caused power outages for ~ 10,000 customers, delayed airline flights, and received much attention even in the national press and social media (*e.g*., Huffington Post, 2011). I included in our catalog haboobs of lesser intensity than a 'dust storm' by international standards because they are noteworthy and disruptive to the large population in metropolitan Phoenix, frequently exceeding the NAAQS 24-hour $c(PM_{10})$ limit (150 μg m^{-3}; U.S. EPA, 2013). Moreover, these smaller haboob events also have high TSP deposition.

Land use in the area directly surrounding KPHX has changed substantially since the systematic categorization of haboobs in Tempe by Brazel and Nickling (1986). Areas that had extensive agricultural fields have been replaced with suburban and industrial development. An approximate boundary between urban and agricultural areas used to be 5 to 10 km south of KPHX but that has expanded to 15 to 20 km south of KPHX (Jenerette *et al*., 2001; Li *et al*., 2014; Maricopa County Assessor's Office, 2016). A direct comparison with the literature to determine whether the number and/or intensity of haboobs in metropolitan Phoenix has changed in since the mid-20th century will require additional locations beyond just the KPHX station and is thus beyond the scope of this paper. Additionally, the nearly one order of magnitude annual variation in haboob occurrences and the relatively short temporal coverage of the present work (10 years) further prevents a more robust temporal comparison.

2.3.3 Uncertainties in the dry deposition model and sensitivity analysis.

The largest uncertainty in the dry deposition in air calculations is the mass distribution employed for haboob events since no measurements are available for the

Phoenix area. It is known that uncertainty in particle mass distributions affects the accuracy of global and local deposition models (Lawrence and Neff, 2009). In the present work, the calculated air deposition was found to increase by 700% between $\frac{\mathrm{PM_{10}}}{\mathrm{TSP}}$ ratios of 0.09 and 0.50 (data not shown). The ratio makes a significant difference since large particles deposit faster than small particles. There are some studies of dust storm particle mass distributions but diameter ranges are sometimes incomplete and the agreement between studies is somewhat limited (Chepil, 1957; Gillette et al., 1978; Møberg *et al*., 1991; Chen and Fryrear, 2002; Singer *et al*., 2003; O'Hara *et al*., 2006; Box *et al*., 2010). I anticipate that dust distributions will differ by location and dust source. Other differences are method related. Many different techniques of determining diameter specific PM mass distributions have been employed in the literature including: multi-stage impactor sampling (Box *et al*., 2010); sedimentation in air (Chen and Fryrear, 2002); sedimentation in aqueous solution (Møberg *et al*., 1991); sedimentation in chlorinated solvent (Chepil, 1957; Chepil and Woodruff, 1957); mechanical sieving (Chen and Fryrear, 2002); measurements with a phase-contrast light microscope (Gillette *et al*., 1978); and laser particle counters (Singer *et al*., 2003; O'Hara *et al*., 2006). Each method of particle size analysis differs in the range of particle sizes reliably quantified and the associated artifacts of analysis.

My model employed $c(\mathrm{PM_{10}})$ to estimate TSP air deposition. $c(\mathrm{PM_{>10}})$ is seldom reported due to the physical constraints of commercially available sampling equipment (*e.g*., standard multistage high-volume samplers). This may be due to the fact that $\mathrm{PM_{>10}}$ is not regulated as an air quality hazard. Since total suspended particle concentration, c(TSP) was not available in Tempe, a synthesized $\frac{\mathrm{PM_{10}}}{\mathrm{TSP}}$ mass ratio of 0.20 was used for

haboobs; this value is within the range of values reported for other locations (see Table 2.2). A few studies in Northern Africa (Møberg *et al*., 1991; O'Hara *et al*., 2006) quantified PM_{20} and $PM_{>20}$ from which a $\frac{PM_{20}}{TSP}$ mass ratio can be determined (Table 2.2). For these, the $\frac{PM_{10}}{TSP}$ mass ratios are estimated as upper bounds since $\frac{PM_{20}}{TSP} > \frac{PM_{10}}{TSP}$. Mass ratios derived from measurements in Australia are similarly given as upper bounds since $PM_{>18}$ was not measured (Box *et al*., 2010) and $\frac{PM_{10}}{PM_{>18}} > \frac{PM_{10}}{TSP}$.

It is likely that the $\frac{PM_{10}}{TSP}$ ratio would be lower for low visibility haboobs than moderate visibility haboobs as the amount of large particles, $c(PM_{>10})$, would be higher. Since detailed and event-specific TSP mass distributions were not available, I employed 0.20 for all haboobs with *VIS* > 11.3 km (> 7 mi). The calculated dry deposition of the 'other dust' events is likely an underestimate since the non-haboob PM mass spectrum was employed, which lacks a large particle ($PM_{>10}$) mode.

The measurement of $c(PM_{10})$ at the CEPH and TE air quality monitoring sites varied both in time and in magnitude. This was to be expected since thunderstorm outflows are directional and may not arrive at different locations throughout metropolitan Phoenix at the same time. In an attempt to minimize these differences, the meteorological and air quality sites used were chosen to be the closest to a reference point: the ASU Tempe campus (Figure 2.3). The dry deposition in other areas of metropolitan Phoenix may differ considerably from the deposition in Tempe.

PM_{10} concentration is sometimes reported as 24 h averages instead of 1 h averages. Using 24 h $c(PM_{10})$ data overestimates haboob dry deposition by 86% (data not shown). The time resolution of a haboob event (1 – 3 h) is too short to be accurately

represented by a 24 h $c(PM_{10})$ value. Employing the haboob particle mass distribution for a full 24 h would erroneously incorporate large particles as a significant fraction of TSP both before and after the haboob events. To avoid such artifacts, I employed 1 h $c(PM_{10})$.

2.3.4 Atmospheric dry deposition.

The dry deposition flux in air, J_{air} for both PM_{10} and TSP was calculated after making simple assumptions about the particle size distributions present in dust storms and employing a $\frac{PM_{10}}{TSP}$ mass ratio of 0.20. The deposition followed trends in haboob occurrence (see Figure 2.8). Most of the haboob deposition occurred during the summer (86%, July to September). Because J_{air}(TSP) is strongly associated with haboob events, there was a distinct maximum in J_{air}(TSP) during the summer monsoon period.

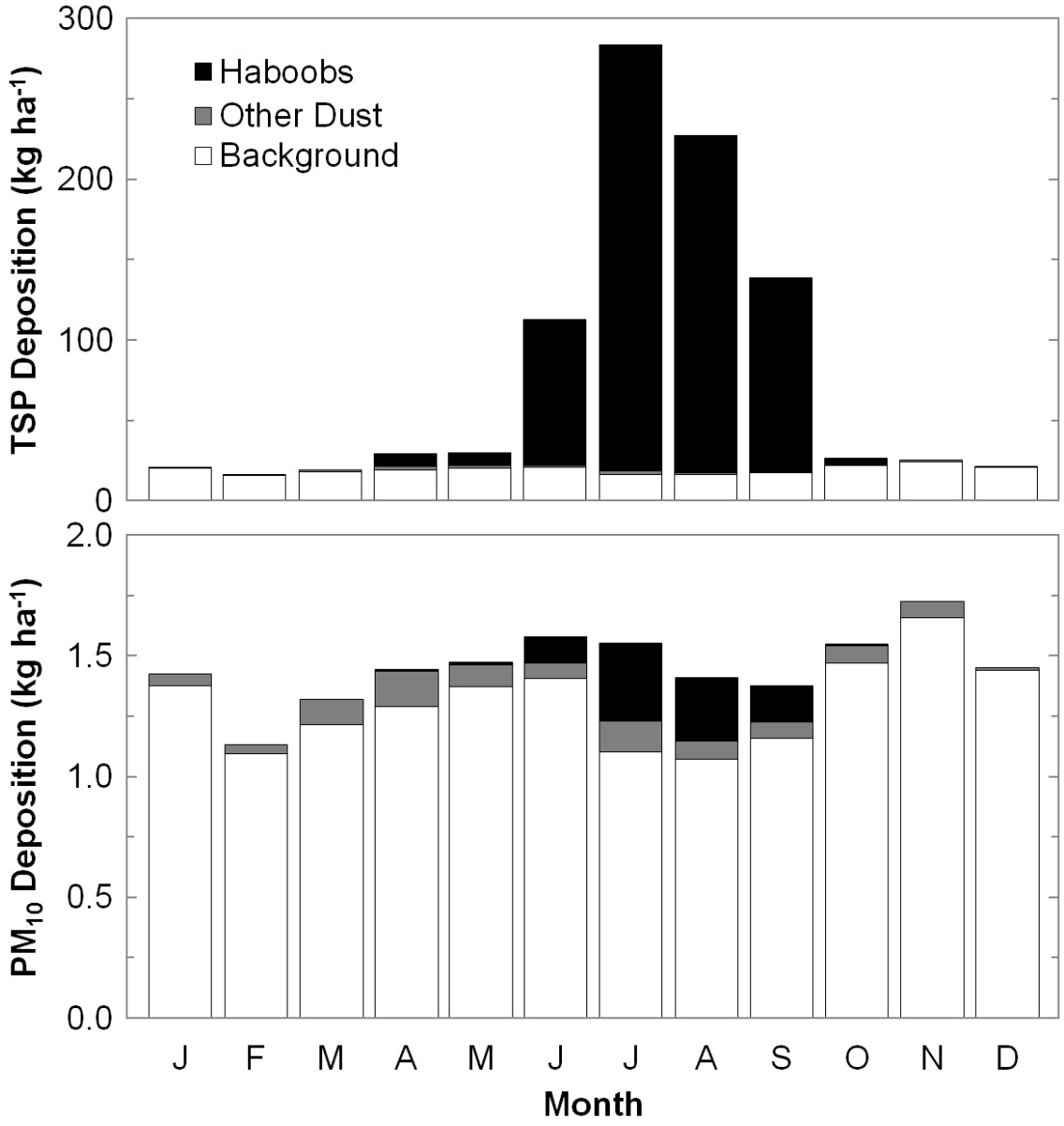

Figure 2.8. Mean monthly TSP (top) and PM_{10} (bottom) dry deposition flux (kg ha^{-1}) in Tempe over the period 2005 to 2014. The haboob contribution to TSP flux is large and occurs only during the summer. PM_{10} flux is a very small fraction of TSP flux and is relatively constant throughout the year. Note the two orders of magnitude difference in the deposition scales.

The PM_{10} dry deposition flux in air, $J_{air}(PM_{10})$, was nearly constant over the course of the year and haboobs contributed very little PM_{10} relative to the background; for example, haboob deposition constituted 21% of overall $J_{air}(PM_{10})$ in July. The

contribution of other dust (events which failed to meet haboob visibility or meteorological criteria) varied somewhat throughout all seasons but was small relative to the calculated background and haboob depositions. Haboob $J_{air}(PM_{10})$ was much smaller than haboob J_{air}(TSP) (0.1% for July). This was expected since deposition velocity of particles varies in approximate proportion with the particle diameter squared (see Equation 2.1).

The year-to-year variation in $J_{air}(PM_{10})$ was small but the year-to-year variation in J_{air}(TSP) was much greater due to the effect of haboobs (Figure 2.9). This was expected since the number and intensity of haboobs varied from year to year. The year 2011 had the highest J_{air}(TSP), 2950 kg ha^{-1}, of which 92% or 2710 kg ha^{-1} occurred during the 20 haboobs which occurred that year. In contrast, the wettest year, 2010, had the lowest J_{air}(TSP), 259 kg ha^{-1}, with 23% or 60 kg ha^{-1} of that being deposited in the 3 haboobs that occurred that year.

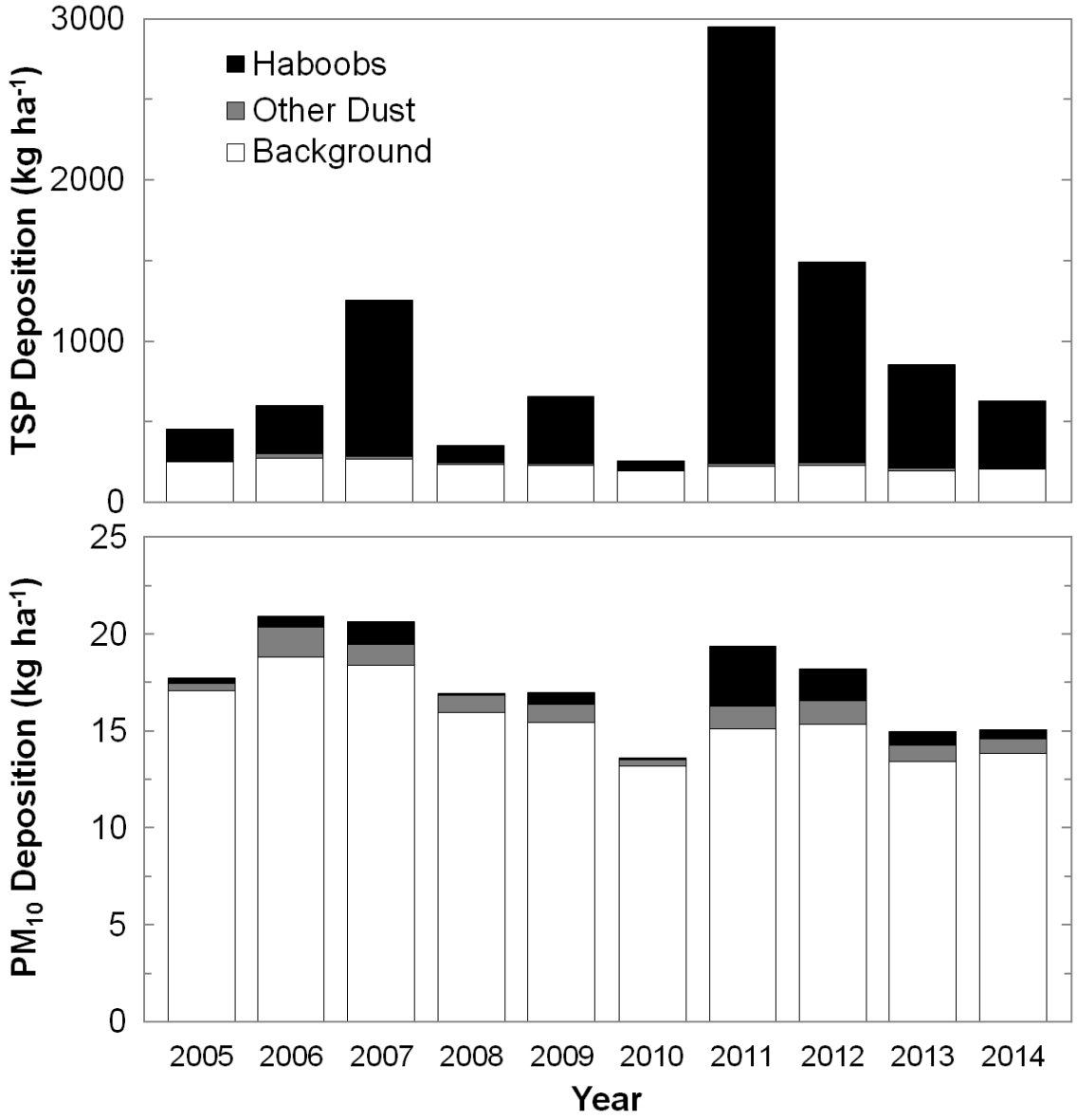

Figure 2.9. Annual TSP (top) and PM_{10} (bottom) dry deposition flux (kg ha^{-1}) in Tempe from 2005 to 2014. The haboob contribution to TSP flux is variable and depends on both on the number and magnitude of events.

On a mass basis, haboob events accounted for 74% of J_{air}(TSP) but only 5% of $J_{air}(PM_{10})$, *e.g.*, Figure 2.10. In contrast, the urban background particle deposition accounted for 90% of the total $J_{air}(PM_{10})$ but only 24% of the total J_{air}(TSP). Most of the deposition mass (98%) was from particles with $d_p > 10$ µm. About 35% of the total

deposition occurred during haboobs with *VIS* ≤ 1.6 km (1 mi) and 39% from haboobs with 1.6 < *VIS* ≤ 11.3 km (1 to 7 mi; see Figure B5). In other words, more than a third (333 kg ha^{-1}) of J_{air}(TSP) was deposited during the most intense quartile of the haboobs (n = 25 out of 96).

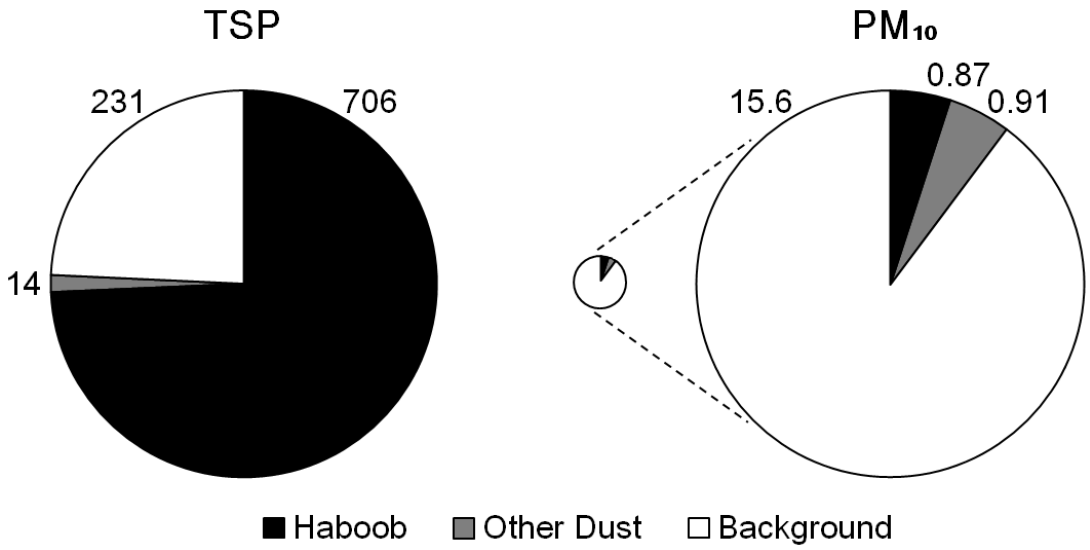

Figure 2.10. Mean annual dry deposition (kg ha^{-1}yr^{-1}) in Tempe for the period 2005 to 2014. The TSP deposition (left) and the PM_{10} deposition (right) for haboobs, other dust and background time periods. The numbers are the deposition quantities in kg ha^{-1}yr^{-1}. The area of the small PM_{10} pie chart is scaled proportionally to the TSP deposition pie chart for comparison.

2.3.5 The comparison of predicted atmospheric deposition with literature.

The J_{air}(TSP) calculated in this work (mean: 950 kg ha^{-1}yr^{-1}) was similar in magnitude to deposition fluxes reported in the literature (see Table 2.2). During a particular rainy year (355 mm precipitation) in metropolitan Phoenix, Péwé *et al*. (1981), reported a rooftop J_{air}(TSP) = 540 kg ha^{-1}yr^{-1}, 12% of which was attributed to 2 haboobs. This compares with the relatively wet year (2010) in this study, with 232 mm rain and J_{air}(TSP) = 259 kg ha^{-1}yr^{-1}, 23% being deposited in 3 haboobs. Excluding haboob

deposition, the J_{air}(TSP) of the sum of background and other blowing dust ranged from 199 to 299 kg $ha^{-1}yr^{-1}$ with a mean of 244 kg $ha^{-1}yr^{-1}$. Smaller J_{air}(TSP) of 20 to 200 kg $ha^{-1}yr^{-1}$ has been reported in Southern California and Nevada, where haboobs did not occur (Reheis, 2006). There was only 1 year where J_{air}(TSP) was calculated to be higher than deposition reported in some locations of northern Africa: 2011 with J_{air}(TSP) = 2950 kg $ha^{-1}yr^{-1}$. In 2011, there were 20 haboobs – the highest in the present work. The estimated 2950 kg $ha^{-1}yr^{-1}$ was less than the deposition of 6940 kg ha^{-1} reported in a series of dust storms over a period of 4 weeks in the Ukraine (Shikula, 1981), less than the 6140 kg $ha^{-1}yr^{-1}$ reported in New Zealand (McGowan *et al*., 1996), and less than the deposition of 4210 kg $ha^{-1}yr^{-1}$ reported in Waddan, Libya (O'Hara *et al*., 2006). A single haboob in western Texas (Chen and Fryrear, 2002) was reported to deposit 850 kg $ha^{-1}h^{-1}$ which was higher than any single haboob identified in the present study, the highest being 362 kg $ha^{-1}h^{-1}$ during the 30 June, 2013 haboob (maximum $c(PM_{10})$ = 5250 μg m^{-3}; minimum *VIS* = 1.2 km (0.75 mi); maximum v_{WG} = 21 m s^{-1} (47 mi h^{-1})). The deposition values calculated within this study were consistent with literature data in arid environments.

2.4 CONCLUSIONS

I cataloged the occurrence of haboobs over the time period 2005 to 2014 using a method based on meteorological and air quality measurements. The major factors that distinguish haboobs events from other dust events and background conditions were event minimum visibility, maximum wind or gust speed, and maximum PM_{10} concentration. There were between 3 and 20 haboob events yr^{-1} with a somewhat lower number of haboob events occurring in years with higher annual precipitation. The relationship

between precipitation and haboob occurrence is complex due to the bimodality of seasonal precipitation as well as the mutual source of haboobs and monsoon precipitation. There was a strong seasonal pattern in haboob occurrence with the vast majority of haboobs occurring during the North American monsoon season (*i.e.*, June to September) and no events occurring in the winter.

The calculated PM dry deposition in Tempe compares well with literature deposition reported for other arid environments when haboob deposition is included in the model. Annual J_{air}(TSP) ranged from a low of 259 kg ha^{-1} in 2010 to a high of 2950 kg ha^{-1} in 2011. The contribution of large particles ($PM_{>10}$) is greater than the contribution of PM_{10} to deposition: the average annual J_{air}(TSP) was 950 kg ha^{-1}yr^{-1} while J_{air}(PM_{10}) was 17 kg ha^{-1}yr^{-1}. My haboob mass distribution was compiled from literature studies, many of which provided only partial information across the range of particle sizes in the deposition model. Thus, there is a need to measure the TSP mass distribution in metropolitan Phoenix.

This study characterized haboobs at a single location in metropolitan Phoenix in an effort to minimize the spatial-temporal heterogeneity of haboobs. There is a need to investigate the spatial differences in haboobs throughout metropolitan Phoenix and in surrounding areas. There may also be a need to investigate meteorological and air quality characteristics in the desert to the south where measurements are currently limited.

CHAPTER 3

THE EFFECT OF HABOOB DEPOSITION ON TEMPE TOWN LAKE CHEMISTRY

3.1 INTRODUCTION

The Central Arizona – Phoenix (CAP) area experiences intense dust events, known as haboobs (Idso *et al*., 1972; Nickling and Brazel, 1984; Chapter 2). The summer monsoon season fosters thunderstorm development which sometimes produces haboob events (Brazel and Nickling, 1986; Chapter 2). These dust storms dramatically reduce visibility due to high levels of particulate matter (PM) suspended in the air (Figure 3.1; Lei and Wang, 2014). CAP also experiences blowing-dust episodes that are generally less intense than haboobs; in most cases, these are caused by high winds associated with cold-front passage (Brazel and Nickling, 1986). Every year, haboobs and blowing-dust episodes have been estimated to deposit 706 and 14 kg ha^{-1} of particles, respectively (or 74% and 1.4% of the total annual deposition) near Tempe Town Lake (Chapter 2).

Figure 3.1. Haboob approaching Tempe Town Lake and ASU (Arizona State University) from the south in Tempe, AZ on August 25, 2015; photo credit: Ariel Anbar. The haboob shown here is over 1100 m tall and tens of km wide.

3.1.1 Tempe Town Lake.

Tempe Town Lake is a man-made lake in downtown Tempe, AZ (Figures 3.1 and 3.2). Construction of the lake started in 1997 and was completed in 1999 (City of Tempe, 2016). It has an average depth of 3.8 m (range 2.1 to 5.8 m) and a water capacity of about 3.7×10^6 m^3 (City of Tempe, 2016). The lake is situated in the dry bed of the Salt River and the river banks are contained by concrete levees. During the period of this study, the water was contained between two inflatable dams that could be lowered as needed during high river flows (> 10 000 cfs ≈ 283 m^3 s^{-1}; City of Tempe, 2015). In spring 2016, the

downstream dam was replaced with a steel gate dam. In 1999, Tempe Town Lake was filled with Colorado River water from the Central Arizona Project. Since that time, the dams have been opened/lowered and the lake emptied/refilled at various times to accommodate high river flows from the Verde and Salt rivers and to accommodate dam release events. The lake can also receive storm water from Indian Bend Wash (Figure 3.2) and from urban storm drains.

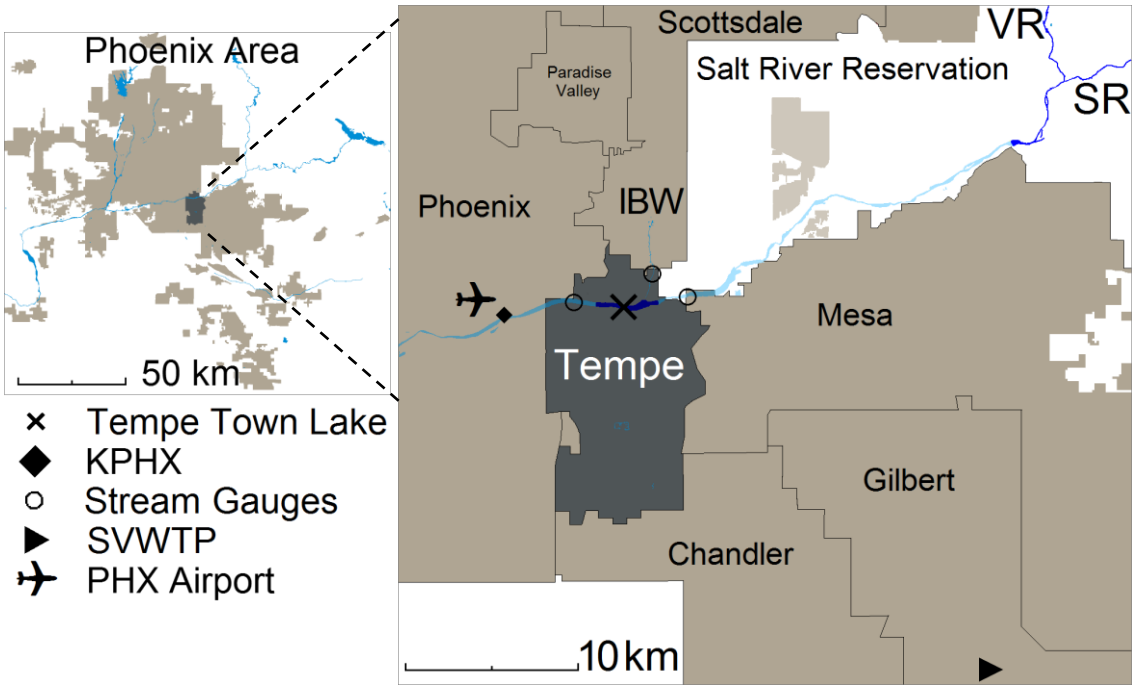

Figure 3.2. Map of Tempe Town Lake in the City of Tempe, AZ. Notes: ×, Tempe Town Lake in dark blue; VR, Verde River; SR, Salt River; IBW, Indian Bend Wash; river beds that are normally dry are in faded blue; the triangle shape, SVWTP is the Santan Vista Water Treatment Plant; open circles indicate stream flow gauges; ♦ KPHX, the weather station at the (PHX) Phoenix Sky Harbor International Airport.

Tempe Town Lake is generally somewhat alkaline with pH ranging from 7.5 to 9.5 (McLean, 2007; City of Tempe, 2015; Hartnett, unpublished). High pH values are due to a combination of CO_2 drawdown by algae and the fact that the underlying rock is predominantly granite (*i.e.*, silicate) which has inherently low carbonate buffering

capacity. Changes in dissolved ions have been correlated with hydrological inputs from upstream, including those that occur during rain events (McLean, 2007; Hartnett *et al*., in prep.) but currently, it is unclear if or how dust storms impact the chemistry of Tempe Town Lake.

The influence of dust storms on surface water turbidity has been recently demonstrated in canal water collected ~30 km to the south-east of Tempe Town Lake (Barry *et al*., 2016). These authors found the turbidity of water entering the Santan Vista Water Treatment Plant (SVWTP) was elevated from Feb to Apr 2011 and from Feb to Apr 2012, a time when haboobs do not generally occur but general blowing dust events do occur (Chapter 2). During the same time frame, PM_{10} (air-borne particles with aerodynamic diameters less than 10 μm) in the vicinity of the water treatment plant increased several times. This observation of increased PM_{10} is consistent with wintertime cold-front blowing-dust episodes that also occur near Tempe Town Lake (see Chapter 2). However, the turbidity of CAP canal water did not appear to increase during monsoon season dust storms (haboobs; *e.g*., Barry *et al*., 2016).

Tempe Town Lake occasionally receives input from the Verde and Salt Rivers, which are the source of the canal water feeding the Santan Vista Water Treatment Plant. While the water sources for these two systems are sometimes related, they are functionally distinct and spatially separated. The canals and the urban lake have significant differences in residence time, water flow, biological activity, and human impacts. Therefore, a separate analysis must be done to see what impact, if any, dust storms have on the surface water chemistry of Tempe Town Lake.

This chapter investigates temporal correlations between dust deposition event occurrence and water quality in a long-term biogeochemical dataset for Tempe Town Lake. Two models are used to estimate particle dissolution, dilution, and settling in Tempe Town Lake.

3.2 METHODS

The deposition of atmospheric particles in Tempe Town Lake is modeled under two end-member scenarios: (1) the complete, instantaneous dissolution of particles and (2) no dissolution of particles. This dual approach is employed since the timescales of dissolution and the extent to which particles can dissolve in the lake are unknown.

3.2.1 Deposition and dissolution in Tempe Town Lake.

The mass of a dissolved chemical species, $m(t)$ [mg] in Tempe Town Lake introduced via atmospheric deposition, dissolving immediately, and its subsequent dilution as water flows through the lake – that is, ignoring biogeochemical reactions, arrival of new solute from source waters (*i.e.*, $r_{in} = 0$), and solute precipitation – may be described via Equation 3.1 where r_{dep} and r_{out} are the rates at which the mass of the chemical species enter the lake by dry deposition of air-borne particles and leave by discharge, respectively:

$$\frac{dm(t)}{dt} = r_{dep} - r_{out} \quad (3.1).$$

r_{out} is a function of $m(t)$, the rate of flow leaving Q_{out} [L h^{-1}], and the lake volume V [L]. Thus, the rate of a dissolved species being discharged from Tempe Town Lake is:

$$r_{out} = Q_{out} \frac{m(t)}{V} \quad (3.2).$$

r_{dep} is a product of lake surface area (A = 89 ha) and the dry deposition flux in air J_{air} [kg ha^{-1} h^{-1}]:

$$r_{dep} = J_{\text{air}} \cdot A \cdot 10^6 \text{mg kg}^{-1} \quad (3.3).$$

Therefore, the concentration in the lake during hour *i* of a dissolved chemical species arising from dry deposition is:

$$c(t_i) = \frac{r_{dep,i}}{Q_{out,i}} + \left(c(t_{i-1}) - \frac{r_{dep,i}}{Q_{out,i}}\right) e^{(-t\, Q_{out,i}\, /\, V)} \quad \text{for } Q_{out} > 0 \quad (3.4),$$

$$c(t_i) = \frac{r_{dep,i}}{V} t + c(t_{i-1}) \quad \text{for } Q_{out} = 0.$$

The lake residence time t_R [h] was calculated with Equation 3.5:

$$t_R = \frac{V}{Q_{out}} \quad (3.5).$$

3.2.2. Particle settling in Tempe Town Lake.

In contrast to the scenario of complete particle dissolution (Equations 3.1 – 3.4), a scenario of purely settling particles in Tempe Town Lake (*i.e.*, no dissolution and Q_{out} = 0) was calculated using Equation 3.6 (adapted from Seinfeld and Pandis, 2006). In this equation, $v_{\text{s,water},j}$ is the water settling velocity of the j^{th} particle diameter ($d_{\text{p},j}$), g is the gravitational acceleration at Tempe Town Lake [9.79 m s^{-2}] (Mathematica, 2015c), ρ_{p} is the particle density [1.7×10^3 kg m^{-3}] (Sauret *et al.*, 2009), ρ_{water} is the lake water density at 30 °C [995.6 kg m^{-3}] (Mathematica, 2015d), and η_{water} is the dynamic viscosity of lake water at 30 °C [0.000797 kg m^{-1} s^{-1}] (Mathematica, 2015e):

$$v_{\text{s,water},j} = d_{\text{p},j}^2 \, \text{g} \left(\rho_{\text{p}} - \rho_{\text{water}}\right) / (18\, \eta_{\text{water}}) \quad (3.6).$$

Water temperatures of 30 °C are typical during the summertime in Tempe Town Lake (City of Tempe, 2015). As a comparison, the particle settling velocity was also calculated at 10 °C, representative of wintertime water temperatures (see Appendix C).

The mean-free path $\lambda_{p,water,j}$ of a particle in the lake due to Brownian movement was derived from the diffusion coefficient and mean thermal speed resulting in Equation 3.7 (adapted from Seinfeld and Pandis, 2006) where k_B is the Boltzmann constant [1.38× 10^{-23} kg m^2 s^{-2} K^{-1}] and T [K] is the absolute lake temperature:

$$\lambda_{\mathrm{p,water},j} = \frac{1}{6\,\eta_{\mathrm{water}}}\sqrt{\rho_{\mathrm{p}}\,k_{\mathrm{B}}\,T\,d_{\mathrm{p},j}\,/\,3} \quad (3.7).$$

The diameter-specific depth $h_{p,j}$ of a particle in the lake was calculated as:

$$h_{\mathrm{p},j} = v_{\mathrm{s,water},j}\,t \pm \lambda_{\mathrm{p,water},j} \quad (3.8).$$

3.2.3 Retrieval of public data.

Long-term biogeochemical measurements have been made in Tempe Town Lake (Hartnett, unpublished; McClean, 2007; City of Tempe, 2015), the Verde River, and the Salt River. To test my hypothesis, I employ the dates and times of haboob and blowing dust events determined in my prior work (see Chapter 2) as well as several CAP-LTER (Central Arizona – Phoenix Long-Term Ecological Research) long-term data sets (Marusenko *et al*., 2011), some of which has been published and tested for other hypotheses (Hartnett *et al*., in prep.; Hartnett, unpublished; McClean, 2007).

Weekly measurements of pH, temperature, water clarity, and dissolved oxygen were retrieved from the City of Tempe (2015). Dissolved organic carbon (DOC), trace metals, and conductivity measurements reported in Hartnett *et al*. (in prep.) were also compared with modeled deposition. Stream flow measurements (15-minute resolution) were obtained from the U.S. National Water Information System (2016) for gauges 09512162 (Indian Bend Wash at Curry Rd.) and 09512165 (Salt River at Priest Dr.) as well as from the Flood Control District of Maricopa County (2016) for gauges 4573

(Price Drain at Loop 202), 4548 (Salt River at Val Vista Dr.), 4583 (Salt River below Granite Reef), and 4603 (Indian Bend Wash near McKellips Rd). Hourly precipitation records for KPHX (the Phoenix Sky-Harbor International Airport weather station) were retrieved from the quality-controlled local climatological database provided by the U.S. National Centers for Environmental Information (2016).

3.3 RESULTS AND DISCUSSION

There were 96 haboobs and 170 blowing dust events near Tempe Town Lake from 2005 to 2014 (Chapter 2). These events were compared with the long-term CAP-LTER biogeochemical data (City of Tempe, 2015; Hartnett *et al*., in prep.; Hartnett, unpublished). I hypothesized that dust deposition was altering Tempe Town Lake chemistry. To test the hypothesis, I employed the two endmember models.

3.3.1 Atmospheric dry deposition into Tempe Town Lake.

The impact of particulate flux into Tempe Town Lake in the first endmember model (particles fully dissolving in the lake and their dilution by flow through the lake) was investigated. Between 0.01 and 50 mg L^{-1} dissolved PM arising solely from atmospheric dry deposition is predicted to be present in the lake (Figure 3.3). The large range in dissolved particulate mass is a result of extreme dust events when deposition is high as well as solute dilution during heavy precipitation events.

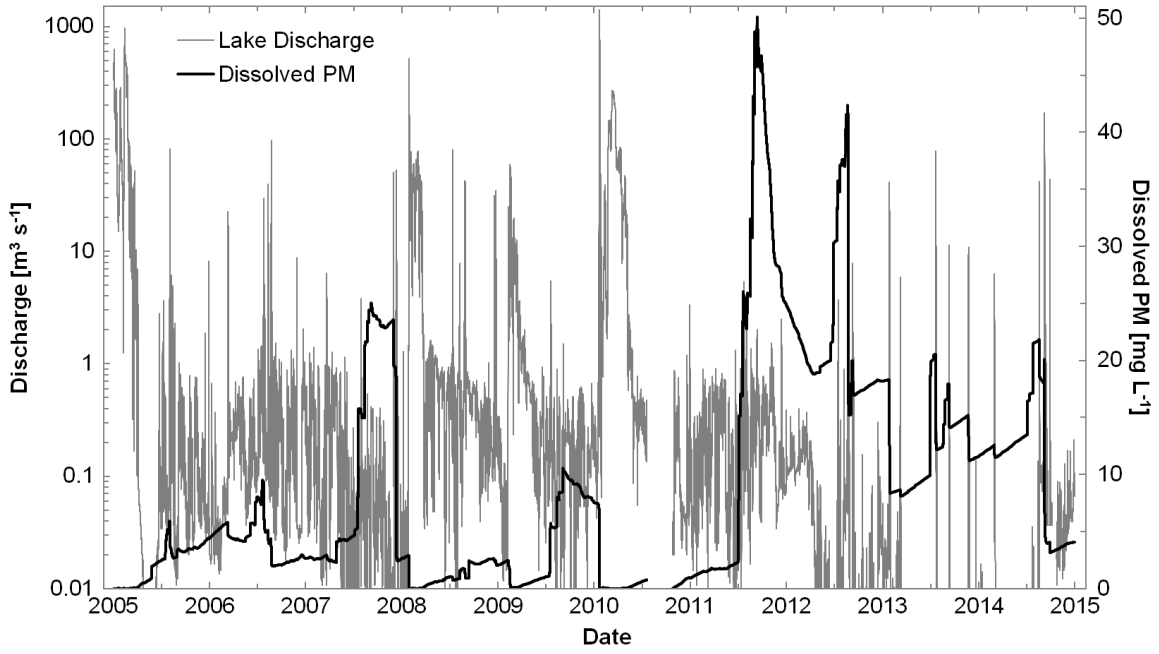

Figure 3.3. Time series plot of lake discharge flow (grey line) and the predicted dissolved particle mass concentration (black line) in Tempe Town Lake. During large flow events, the dissolved PM concentration decreases due to dilution. During large deposition events, such as haboobs, the dissolved PM concentration increases.

Tempe Town Lake receives a large amount of runoff (*e.g.*, > 3 $m^3 s^{-1}$) only infrequently: the immediate area receives ≥ 10 mm rain on fewer than six days per year (U.S. National Centers for Environmental Information, 2016). The lake is designed to function as a river channel when receiving flood waters and has reached release rates of up to 1161 $m^3 s^{-1}$ (Feb 12, 2005; U.S. National Water Information System, 2016) which equates to a flow velocity of about 1.7 m s^{-1} and a lake residence time of about 44 minutes. However, the discharge flow is generally < 1 $m^3 s^{-1}$ and sometimes zero (67% and 21% of the hourly discharge rates respectively; Figure 3.3) resulting > 42 day to indefinite instantaneous residence times.

3.3.2 Particle settling in Tempe Town Lake.

In the second end-member scenario where particles settle within the lake according to Stoke's Law without dissolving, much of the particle mass settles relatively quickly during haboobs. The predicted summertime settling times of particles at 30 °C is shown in Figure 3.4. Much of the particles deposited during haboob events are larger than 10 µm in aerodynamic diameter (Chapter 2) and consequently 69% of particles settle to the bottom of the lake in 1 hour or less (Figure 3.4).

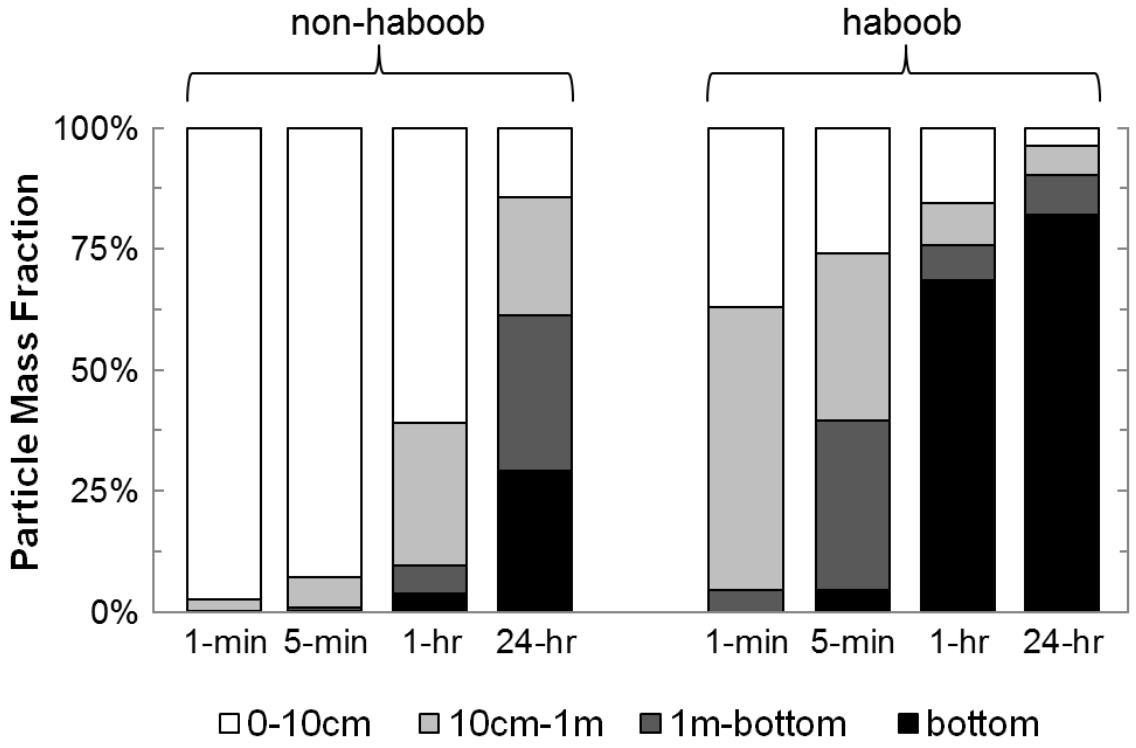

Figure 3.4. The predicted settling of a non-haboob distribution (left) and a haboob distribution (right) of particles within Tempe Town Lake in a non-dissolution, no-flow scenario, at 30 °C. The shaded bars indicate the percent of overall particle mass contained in three depth layers or on the lake bottom. In less than 24 hours, 60% of the mass in a non-haboob particle distribution will settle below 1 m depth. In 1 minute, 63% of the mass in a haboob particle distribution settles 10 cm or more and during 1 hour, 69% reaches the lake bottom.

The comparative calculation at wintertime lake water temperatures (10 °C) yielded similar results (Figure C1). Even if the lake is polymictic with daily mixing timescales, the Stokes sedimentation would occur faster for most particles, that is particles with $d_p > 2.5$ µm. Nevertheless, the water-borne particles with $d_p < 2.5$ µm can remain in the upper 10 cm of the lake for 12 hours or more if settling alone is considered. The mean free path of particles ($d_p = 0.1$ to 320 µm) due to Brownian motion is on the order of tens of nanometers at the temperature range of the lake (8.4 to 33 °C). Thus, particle movement in the lake is likely dominated by gravitational sedimentation, barring high-flow resuspension.

3.3.3 Large deposition events which coincide with lake chemistry changes.

During the ten year time period investigated (2005 to 2014), there were some deposition events which coincided with changes in Tempe Town Lake chemistry (Table 3.1). Specifically, water clarity, DOC, and conductivity exhibited changes that might have been associated with haboobs (Figures 3.5 – 3.7; Hartnett *et al*., in prep.). One of the changes was after a moderate haboob on June 26, 2012. The DOC measurement taken approximately 9 h after the haboob event was 7.3 mgC L^{-1} (53%) larger than the previous measurement (Table 3.1; Figure 3.5, blue rectangle). As a comparison, the lake had a relatively consistent DOC concentration of 5.8±1.0 mgC L^{-1} (n=16) during the prior two months.

Table 3.1

Haboob Events Which Coincide with Changes in Tempe Town Lake Chemistry

Date	Dissolved PM Δ [mg L^{-1}]	Parameter	Absolute Δ	Relative Δ [%]
7/11/2011	9.2 ±0.1	Clarity	-9.4 †	28%
7/25/2011	6.9 ±0.2	Clarity	-9.8	38%
8/29/2011	11.4 ±0.1	Clarity	-13	54%
6/27/2012	1.6 ±0.1	DOC	7.3 ±0.2 ‡	53%
7/22/2012	1.5 ±0.1	DOC	1.1 ±0.2	15%
9/4/2012	2.7 ±0.1	DOC	0.75 ±0.23	11%
8/23/2013	1.8 ±0.7	Conductivity	9*	1%
9/6/2013	1.4 ±0.9	Conductivity	10	1%
9/6/2013	1.4 ±0.9	DOC	0.63 ±0.36	12%
7/8/2014	3.1 ±0.8	DOC	0.13 ±0.03	3%
7/28/2014	3.8±0.7	Clarity	-3.1	8%

Notes: negative absolute changes are decreases in measurements; †, inches of clarity; ‡, DOC (dissolved organic carbon) in mgC L^{-1}; *, units are µS cm^{-1}; the dissolved PM changes are predictions while the absolute changes in clarity, DOC, and conductivity are observations.

On the week of June 22 – 30, 2012, no water was discharged from the lake (Q_{out} = 0) and there was no water flowing immediately upstream (Salt River, Indian Bend Wash). Similarly, Price Drain at Loop 202 had minimal flow during the week (≤ 0.25 m^3 s^{-1}) and no flow the evening of the haboob. The data for canal flow into the lake was not publically available but was insufficient to cause an outflow. This precludes the dilution of deposited particles by lake flow. Furthermore, there was no precipitation reported locally during June 22 – 30, 2012 (at KPHX).

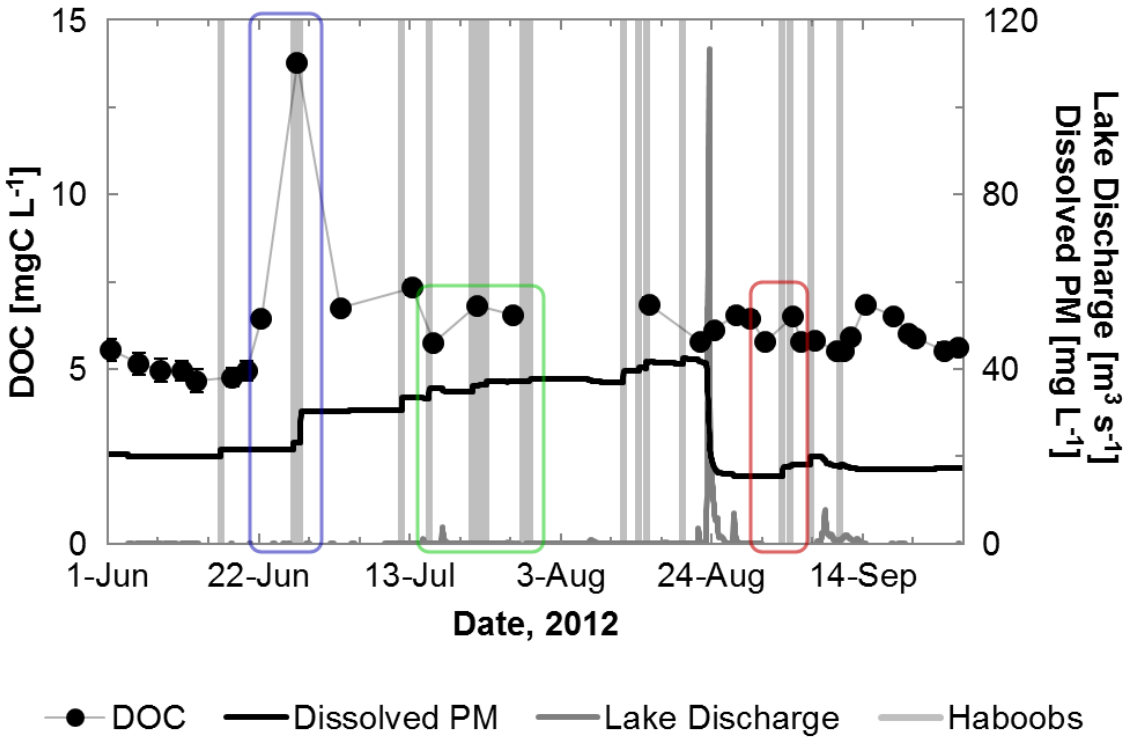

Figure 3.5. Dissolved organic carbon (black circle symbols), predicted particle dissolution (black line), and lake discharge (grey line) in Tempe Town Lake for summer 2012. Haboob events are indicated by vertical lines. The blue, green, and red shapes highlight a discussion in the main text.

The organic carbon content of haboob dust (specifically, air-borne total suspended particulate matter or TSP) is unknown for the Tempe area. The sources of the particles carried by haboobs into Tempe have not been recently characterized but likely include a combination of desert particles, agricultural soils, and urban particles. Péwé *et al*. (1981) collected Tempe haboob dust in the 1970's and performed mineralogical characterization. Their samples were primarily comprised of minerals: 55-60% SiO_2, 11-14% Al_2O_3, and 4-5% iron oxides with 8-12% mass loss upon ignition – which is related to organic matter and carbonate content. Recently studies reported the organic carbon content of soils throughout the Phoenix area as 0.07–3.7% (mean 1.2%; McCrackin *et al*., 2008) of which an average of 31% was black carbon (which is generally insoluble in water; Hamilton and

Hartnett, 2013). Higher organic carbon contents have been reported in road-side soils throughout the Phoenix area: approximately 0.4 to 5% (median 1.4%; calculated as organic matter 50% carbon by mass; Marusenko *et al*., 2011). A study of the PM generated in the resuspension of soil samples from the Phoenix-area reported 1.3% organic carbon in PM_{10} from desert samples and 2% organic carbon in PM_{10} from agricultural samples (Upadhyay *et al*., 2015).

Fine particles in the lake, for example $d_p < 2.5$ µm arising from atmospheric $PM_{2.5}$ may be richer in organic carbon content as the fine particles are often anthropogenic in origin (Chapter 1). Nevertheless, the mass arising from $d_p < 2.5$ µm particles during a haboob is estimated as 5% of the TSP (Chapter 2). For the purposes of this Chapter, I employed a soluble organic carbon content of 1% in PM depositing in Tempe Town Lake.

The haboob on June 26, 2012 deposited a peak of about 42 kg ha^{-1} h^{-1} and a 3-hour cumulative deposition of 62 kg ha^{-1}. Using Equation 3.4 and assuming complete mixing, this equates to 1.6 mg L^{-1} new mass and 0.016mgC L^{-1} new soluble organic carbon added to Tempe Town Lake (Figure 3.5 and Table 3.1). This is substantially less than the observed increase in DOC of 7.3 mgC L^{-1}. If complete mixing is not assumed, *e.g*., if particles completely dissolve in the top 10 cm of the lake but do not diffuse below 10 cm, the haboob deposition on June 26, 2012 could have temporarily increased surface DOC concentrations by 0.65 mgC L^{-1} (top 10 cm), which is nonetheless an order of magnitude smaller than the observed increase. Thus, haboob dust deposition on June 26, 2012 was likely insufficient to wholly cause the 7.3 mgC L^{-1} increase in Tempe Town

Lake DOC observed 9 hours later. The increase may have been caused by biological or other processes in the lake.

Haboob deposition coincided with two more DOC increases in the summer of 2012 (Table 3.1). The endmember dissolution model predicts 1.5 mg L^{-1} new PM mass on July 22 and 2.7 mg L^{-1} on August 4, 2012 (see green and red highlights in Figure 3.5). This would equate to 0.015 and 0.027 mgC L^{-1} new dissolved organic carbon which is less than the observed 1.1 and 0.75 mgC L^{-1} DOC increases. If lake heterogeneity is assumed (*i.e.*, mixing is confined to the upper 10 cm of the lake), then haboob deposition could have caused 0.61 and 1.1 mgC L^{-1} increases in DOC on the two respective days, which is of the same order of magnitude as the observed DOC increases (Table 3.1).

In the summer of 2013, two haboob events (highlighted in magenta and yellow in Figure 3.6) on August 20 and September 5 coincided with 9 and 10 µS cm^{-1} increases in conductivity on August 23 and September 6 (1% increases each; Table 3.1). The corresponding endmember model masses added to the lake are 1.8 and 1.4 mg L^{-1} (Figure 3.6). The dissolution of ionic compounds originating from deposited PM would contribute to increasing water conductivity and may be responsible for these small (1%) increases. However, larger deposition events with predicted PM added masses > 10 mg L^{-1} did not coincide with increases in lake conductivity.

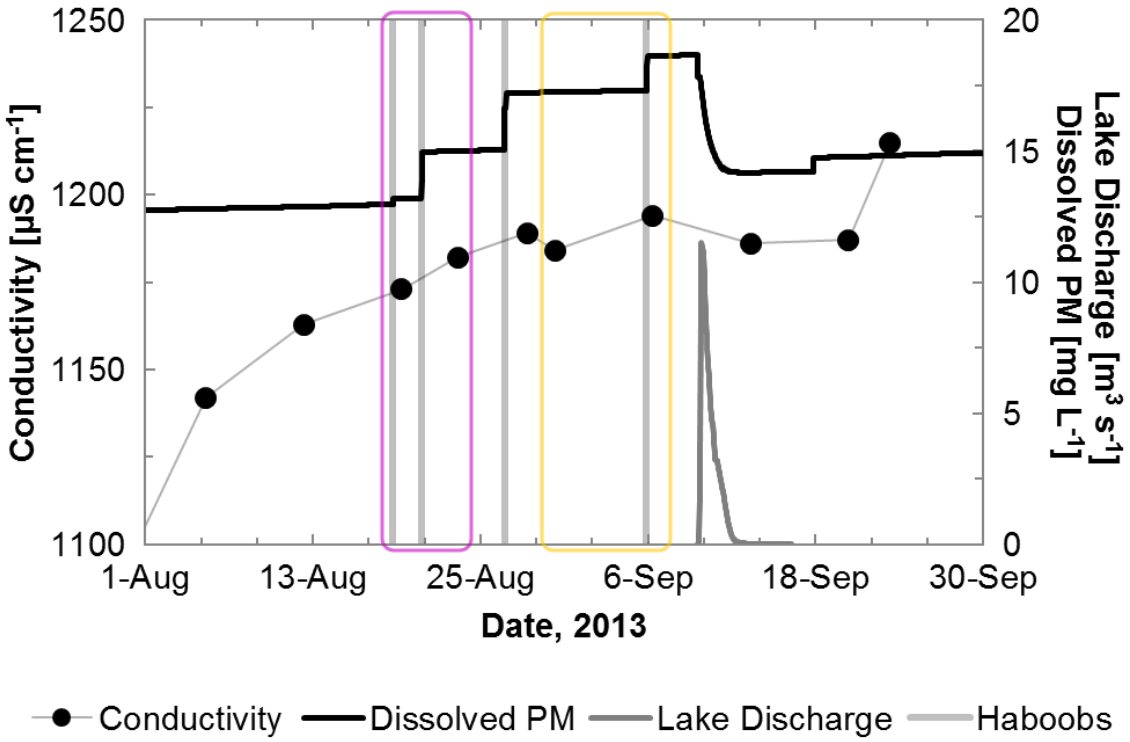

Figure 3.6. Conductivity (black circle symbols), predicted particle dry deposition (black line), and lake discharge (grey line) in Tempe Town Lake for summer 2013. Haboob events are indicated by vertical lines. The magenta and yellow shapes highlight a discussion in the main text.

Several large deposition events occurred in the summer of 2011 and added a predicted 9.2, 6.9, and 11.4 mg L^{-1} dissolved PM mass to the lake (Table 3.1). These coincided with 28 to 54% decreases in Tempe Town Lake clarity on July 11, July 25, and August 29, as highlighted in Figure 3.7 in cyan, purple and orange, respectively. However, not every deposition event was accompanied by a decrease in water clarity, for example August 8, 2011 in Figure 3.7.

Many factors can contribute to changes in water clarity in surface water, such as high-flow resuspension of settled particles. The decreased clarity on July 5, 2011 may have been affected by the modest lake release (attributed to flow through the lake) of 5.3

$m^3 s^{-1}$ which occurred on the same day and which totaled 7% of the lake volume during a 24-hour period (see purple highlight in Figure 3.7). The associated lake residence time at peak outflow was calculated to be 8 days.

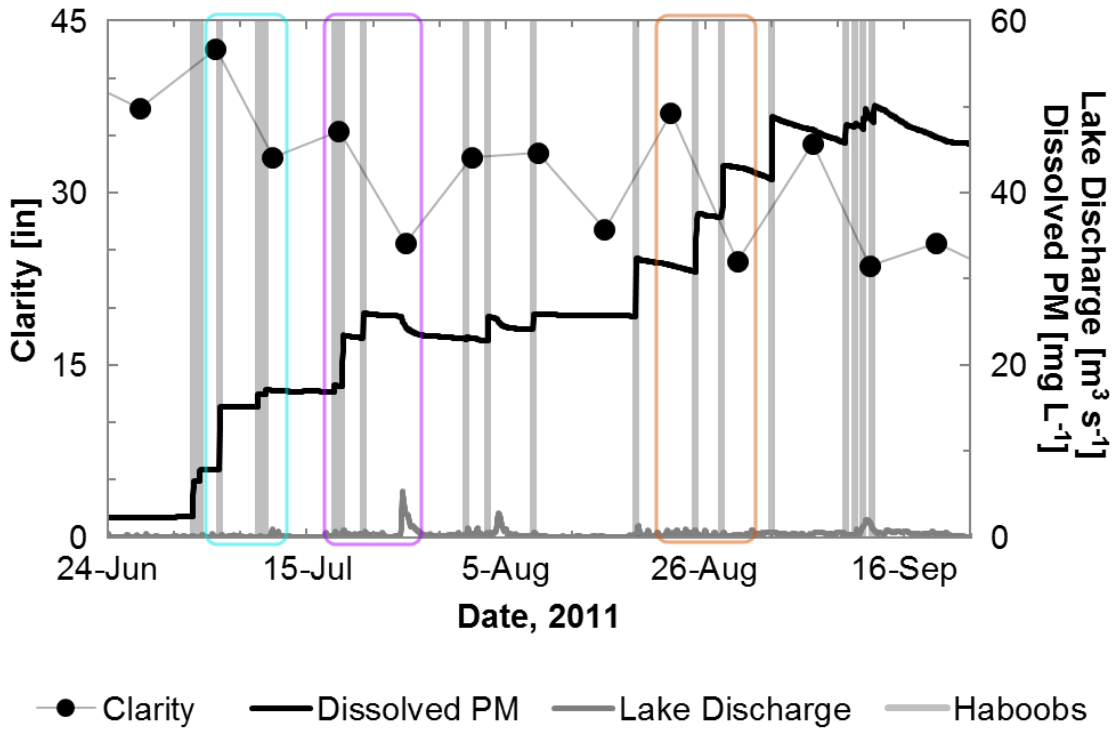

Figure 3.7. Water clarity (black circle symbols), predicted particle dry deposition (black line), and lake discharge (grey line) in Tempe Town Lake for summer 2011. Haboob events are indicated by vertical lines. The cyan, purple and orange shapes highlight a discussion in the main text.

Despite the findings of Barry *et al*. (2016) that wintertime dust events sometimes affected canal water turbidity, the present work reports inconclusive findings of dust-storm alteration of Tempe Town Lake clarity during all seasons of the year. A few large-deposition haboob events, such as during the summer of 2011, may have affected water clarity in the lake. However, consistent effects were not apparent during the 96 haboobs and 170 blowing dust events over the ten years I investigated.

The application of the two endmember models of either complete dissolution or non-dissolution provides a preliminary view of dust deposition impacts on the lake. Dissolution would need to occur on timescales of tens of seconds to avoid substantial particle sedimentation to the lake bottom. If dissolution were indeed rapid enough, haboobs could be responsible for some of the changes in biogeochemical measurements. A much more complex model would be required to more precisely predict the dissolved mass originating from atmospheric dry deposition in the lake. The timescale of dissolution is unknown and will depend on the particle sizes, particle surface morphology, and particle composition.

3.4 SUMMARY

The deposition of haboobs was compared in time with changes in Tempe Town Lake chemistry. An endmember model was developed for particle dissolution and dilution in the lake and a second endmember model was developed for predicting particle settling times. During the time frame investigated, 2005 to 2014, there was no clear evidence of haboob deposition events producing a discernable signal in Tempe Town Lake chemistry. The dissolution endmember model predicts lower increases in DOC than observed meaning that dust deposition does not fully account for the DOC increases that coincide with some haboobs. A few deposition events did coincide with changes in lake conductivity and water clarity. Dust storms may have well impacted the lake but not in a consistently discernable manner.

The particle settling endmember model predicted sedimentation times of non-dissolving particles on the order of minutes and hours. During a haboob, 69% of the particle mass is predicted to settle to the bottom of the lake in 1 hour or less. Since

particle dissolution timeframes were not known, an endmember dissolution approach was employed. A more complex model of dissolution would be required to predict real dissolution timescales in Tempe Town Lake. Future research is warranted to identify haboob redistribution and haboob biochemical impact on other systems, such as soil, in the CAP urban ecosystem.

CHAPTER 4

PAH IN HABOOB PARTICULATE MATTER

4.1 INTRODUCTION

Polycyclic aromatic hydrocarbons (PAHs) are ubiquitous in the atmosphere from pristine to urban environments (Xie *et al*., 2007; Nizetto *et al*., 2008; Mancilla *et al*., 2016). PAH are considered semivolatile species, with most occurring both in the gas and in the particle phase. The partitioning between the phases is dependent on temperature, vapor pressure of the PAH under consideration, and the particulate matter population present (Fernandez *et al*., 2002; Eiguren-Fernandez *et al*., 2004; Delgado-Saborit *et al*., 2013). Typically smaller PAH, like naphthalene (NAP), are predominately in the gas phase while higher molecular weight PAH such as benzo[*a*]pyrene (BAP) are predominately associated with the particle phase.

PAHs have been extensively studied in air pollution studies because of health concerns despite overall low concentrations in the pg m^{-3} range in urban areas and accounting for only a small fraction of total organic carbon (< 0.2%, Rogge *et al*., 1993b). Several PAH are known or suspected to cause cancer (ATSDR, 1995; Ravindra *et al*., 2008). A subset of 16 PAHs is categorized as priority pollutants by the Environmental Protection Agency (EPA, 2014b).

PAH have various sources, which are usually grouped as either petrogenic (from petroleum) or pyrogenic (products of incomplete combustion). PAH are present in crude oil and thus are released in oil spills, vaporize from roadway tar sealer and are present in gasoline and diesel vapors (Marr *et al*., 1999; Mahler *et al*., 2012). PAH are also formed during pyrolysis of organic matter: wildfires, tobacco smoke, automobile exhaust, power

plant emissions, and cooking operations (Rogge et al., 1993a; Zhang and Tao, 2004). Many sources have distinct relative abundances of specific PAH isomers (Figure 4.1) which lead to the use of ratios as diagnostic tools to characterize the sources of PAH. For example, following a review of 38 source studies, Yunker *et al*. (2002) employed an IND (indeno[1,2,3–*cd*]pyrene) and BGP (benzo[*g*,*h*,*i*]perylene) isomer ratio, $\frac{\text{IND}}{\text{IND} + \text{BGP}}$, of 0.0 to 0.2 for petroleum sources, 0.2 to 0.5 for petroleum combustion, and 0.5 to 1.0 for grass, wood, and coal combustion.

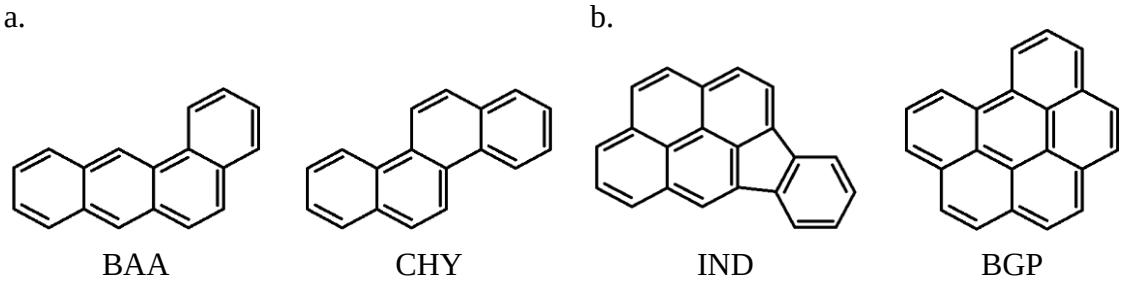

Figure 4.1. A few examples of PAH isomers employed in tracer ratios. Panel a. shows $C_{18}H_{12}$ isomers BAA (benz[*a*]anthracene) and CHY (chrysene); panel b. shows $C_{22}H_{12}$ isomers IND (indeno[1,2,3–*cd*]pyrene) and BGP (benzo[*g*,*h*,*i*]perylene).

In the Phoenix area, PAHs have been reported in particulate matter (PM) at concentrations *c*(PAH) of 20 to 1460 pg m^{-3} (Cahill, 2013), the majority of which was in $PM_{2.5}$ or PM with aerodynamic diameters of less than 2.5 μm. It has also been reported that PAHs in soils in the Phoenix area are related to automobile emissions (Marusenko *et al*., 2011).

A haboob is a type of severe dust storm which occurs in the Phoenix area during the summer monsoon seasons (Nickling and Brazel, 1984; Brazel and Nickling, 1986; Chapter 2). When thunderstorms mature in the early afternoon, falling hydrometeors cool the air which produces a dense air mass that descends rapidly to the surface of the earth.

The displacement of air causes an outflow: a turbulent, directional movement of air and dust (Sutton, 1925; Idso *et al*., 1972; Idso, 1976). Visibility is reduced due to increases in $PM_{>2.5}$ (PM larger than an aerodynamic diameter of 2.5 μm) and, to a lesser extent, increases in $PM_{2.5}$ (Lei and Wang, 2014). In these haboob events the total particle mass concentrations increase for one to three hours in both the $PM_{2.5}$ and PM_{10} fractions: for example, on July 3, 2014, the $PM_{2.5}$ increased by 37 μg m^{-3} (a factor of 4.2×) and PM_{10} increased by 2006 μg m^{-3} (a factor of 61×; Figure A2). While most of the haboob PM is likely soil derived, it might also contain urban particles which generally have higher amounts of atmospheric pollutants (such as metals or organic pollutants) than rural PM. To the best of my knowledge, no detailed chemical characterization of haboob PM has ever been reported. Hence, it is unknown how anthropogenic pollutant concentrations change in haboob storms, especially whether or not their concentrations increase. It is further unknown if any changes are persistent after a haboob event or merely transient, like the sharp increases in particulate mass (Lei and Wang, 2014).

In this chapter, the impact of haboobs on atmospheric concentrations of a specific class of pollutants, PAH, is investigated. Concentrations of PAH have been monitored before, during, and after haboob dust storms. Their variability is discussed relative to total particle mass concentrations. Diagnostic ratios are applied to investigate if the sources of haboobs change in dust storms and how atmospheric PAH relate to soil PAH in the Phoenix region.

4.2 METHODOLOGY

The concentrations of PAH were determined in $PM_{2.5}$ for nine days during June 30 to July 9, 2014. There was one haboob and one ‘other dust’ event that occurred during

this time (Chapter 2). A national holiday (July 4th) was on a Friday, creating for many residents what is sometimes called a three-day weekend. Barbeque and firework use were abundant.

Ambient aerosols were collected on the roof of the Life Sciences building on the Arizona State University Tempe Campus *via* high volume (HiVol) samplers (Tisch Environmental, Village of Cleves, OH) equipped with a TE 231 impactor stage (Tisch Environmental, Village of Cleves, OH), allowing the for collection of $PM_{2.5}$. OM samples were collected onto pre-fired (600 °C, baked overnight) quartz fiber filters (QM-A, Whatman, Pittsburgh, PA). Filters were handled at all times with solvent-washed metal tweezers. Samples were collected for 24-hours, unless a dust storm occurred, for which 3- to 6-hour samples were collected. The filters were stored at –20 °C until the time of extraction. Field blanks were collected by loading filters onto the HiVol stages.

Extractions were performed with triply cleaned glassware and metalware. The cleaning procedure included: first washing with soap and tap water, then with deionized water, and finally with ultrapure deionized water (18.2 MΩ cm; Milli-Q, Millipore, Billerica, MA). After air drying, all were rinsed with 2–propanol (Optima grade, Fisher Scientific, Rochester, NY), air dried again, then wrapped in new aluminum foil. Glass beakers and glass bottles were pre-fired at 450 °C for 12-hours as a last cleaning step.

A deuterated internal PAH standard consisted of 250 µg mL^{-1} of the following in dichloromethane (Optima grade, Fisher Scientific, Rochester, NY): benzene–d_6, naphthalene–d_8, acenaphthene–d_{10}, phenanthrene–d_{10}, pyrene–d_{10}, chrysene–d_{12}, perylene–d_{12}, benzo[*e*]pyrene–d_{12}, dibenz[*a*,*h*]anthracene–d_{14}, and coronene–d_{12} (SPEX

CertiPrep). Authentic PAH standards were prepared from a commercial mixture (76-Big-Mix, SPEX CertiPrep).

The $PM_{2.5}$ samples and field blanks were divided into pieces with a metal razor blade (cleaned as above) and placed into glass jars with lids (cleaned as above), spiked with 20 µL deuterated internal standard mixture, and ultrasonically extracted with three sequential 25 mL aliquots of dichloromethane. The three 25 mL extraction aliquots were combined and reduced to 2 mL volume under a gentle stream of nitrogen gas (ultra-high purity; Praxair, Phoenix, AZ), dried with anhydrous sodium sulfate (Sigma Aldrich), filtered through 25 mm diameter pre-fired quartz fiber filters (QM-A, Whatman, Pittsburgh, PA), reduced to 100 µL volume under the aforementioned nitrogen gas, and transferred *via* gas tight syringe to 2 mL capped amber vials (PTFE/silicon septa; Restek, Bellefonte, PA) with a glass insert (Restek, Bellefonte, PA). Following extraction, samples were stored at –20 °C until the time of analysis.

Samples, standards, and blanks were analyzed by GC/MS (Agilent 6890/5973 inert, Agilent Technologies, Santa Clara, CA), operating in splitless mode at 300 °C and 2 µL injections. Separation was achieved with an Agilent HP-5MS column (0.25 mm × 30 m × 0.25 µm) and the following temperature program: holding 65 °C for 10 minutes, then ramping 10 °C per minute to 300 °C and finally holding 300 °C for 20 minutes. The MS source was operated at 230 °C and 70 eV EI with a 5 minute solvent delay. Ions 50 to 550 m/z (mass [Da] / charge ratio) were monitored in scan mode.

As a means of comparison with the samples collected on ASU Tempe Campus, $PM_{2.5}$ air concentration data for the closest monitoring site: 04-013-4005 (TE) were retrieved from the EPA Air Quality System (AQS; EPA, 2015). The ASU sampling site is

about 850 m north of AQS TE. Quality controlled meteorological data in the vicinity of ASU was retrieved from NOAA (2015) for the Phoenix Sky-Harbor Airport (KPHX). PAH soil concentrations at 60 sites throughout the region surrounding ASU were retrieved from CAP-LTER (Central Arizona – Phoenix Long-Term Ecological Research) data catalog (Hall and Marusenko, 2009).

4.3 RESUTLTS AND DISCUSSION

4.3.1 PAH concentrations.

PAH concentrations in Tempe (AZ) $PM_{2.5}$ ranged from 1 – 1140 pg m^{-3} (Table 4.1). For Tempe, the concentrations were separated into background and haboob time periods. The background time periods were samples when there was no dust storm. The summertime typical Tempe background $PM_{2.5}$ PAH concentrations *c*(PAH) were on the same order of magnitude as those reported in urban areas in southern California throughout all seasons of the year (Eiguren-Fernandez *et al*., 2004; Table 4.1) but less than those reported during the winter at a roadside in Birmingham, United Kingdom (Delgado-Saborit *et al*., 2013). The $PM_{2.5}$ *c*(PAH) in urban locations throughout the greater Houston area, Texas during all seasons of the year ranged from the same order of magnitude to an order of magnitude higher than Tempe (Fraser *et al*., 2002). The higher *c*(PAH) in $PM_{2.5}$ in some areas of Houston and in Birmingham is likely due to seasonal effects where *c*(PAH) is higher during the wintertime. Cahill (2013) measured up to a factor of 84× higher *c*(PAH) in PM during the wintertime relative to the summertime, which is attributed to wintertime low wind speeds and boundary layer temperature inversions (Sorooshian *et al*., 2011). In the case of Birmingham, the sampling location was roadside, which further increased *c*(PAH) relative to Tempe (not roadside).

Table 4.1

A Comparison of PAH $PM_{2.5}$ Concentrations during a Haboob, Non-Dust, and Background Time Periods in Tempe with Literature Measurements

PAH*	2014-07-03 haboob[#]	2014-07-08 dust event	Background mean (range)[§]	Houston, Texas[†]	Southern California[‡]	Birmingham, United Kingdom[♦]
PHE	339	92	69 (8 – 103)	60 – 370	1 – 37	840
ANT	133	22	22 (5 – 55)	20 – 380	0.2 – 3	250
FTH	265	134	75 (9 – 118)	40 – 550	5 – 48	1400
ACP	497	11	23 (5 – 35)			
PYR	1139	141	127 (38 – 188)	60 – 670	6 – 70	1350
BAA	394	26	34 (21 – 79)	10 – 1290	6 – 41	440
CHY + TRI	53	48	22 (6 – 61)	20 – 1340[◊]	8 – 57[◊]	850[◊]
BKF	148	76	57 (9 – 163)	<10 – 870	6 – 53	560
BJF	25	6	7 (1 – 14)			
BEP	147	40	23 (3 – 48)			260
BAP	953	102	76 (31 – 144)	<20 – 870	9 – 100	180
PYL	35	7	8 (1 – 14)			
IND	81	21	22 (7 – 44)	<40 – 960	12 – 100	430
BGP	124	47	23 (6 – 44)	<10 – 1260	23 – 193	440
DBA	235	47	28 (7 – 58)	<10 – 900	2 – 12	240
COR	200	55	56 (29 – 132)			350

Notes: *, concentrations are in pg m^{-3}; #, two sequential samples were taken during the haboob; §, background was the non-dust time periods from June 30 – July 9, 2014; †, Fraser *et al*., 2002; ‡, Eiguren-Fernandez *et al*., 2004; ♦, Delgado-Saborit *et al*., 2013; ◊, only chrysene was reported; PHE, phenanthrene; ANT, anthracene; FTH, fluoranthene; ACP, acephenanthrylene; PYR, pyrene; BAA, benzo[*a*]anthracene; CHY, chrysene; TRI, triphenylene; BKF, benzo[*k*]fluoranthene; BJF, benzo[*j*]fluoranthene; BEP, benzo[*e*]pyrene; BAP, benzo[*a*]pyrene; PYL, perylene; IND, indeno[1,2,3-*cd*]pyrene; BGP, benzo[*g,h,i*]perylene; DBA, dibenz[*a,h*]anthracene; COR, coronene.

4.3.2 Haboob-related $PM_{2.5}$ and PAH changes.

Examination of $PM_{2.5}$ during the 2012 to 2014 monsoon seasons revealed that $PM_{2.5}$ increased briefly during haboobs (n = 31) by a factor of 0.2× to 23.5× (mean = 5.1×) of that of the background $PM_{2.5}$ during the previous 24 hours (Table 4.2).

Table 4.2

A Comparison of the July 3, 2014 Haboob and the July 8, 2014 Dust Event with the Haboob Mean Characteristics for 2012 to 2014

Date	2014-07-03	2014-07-08	Haboob Mean
Classification*	haboob	other dust	(haboob)
Maximum $PM_{2.5}$ [µg m^{-3}] #	46.0	43.3	46.8
Relative $PM_{2.5}$ increase [×]	4.2	5.2	5.1
Minimum Visibility [km]&	1.6	14.5	5.1
Maximum Gust [m s^{-1}]&	25	14	16.9
Maximum PM_{10} [µg m^{-3}]#	1059	424	789
Wind Direction [degrees]&	160 – 170	100 – 110	Not determined

Notes: *, classification in Chapter 2; #, at site AQS TE (04-013-4005); &, at KPHX.

There was also an increase in 16 PAHs' *c*(PAH) in $PM_{2.5}$ during the haboob on July 3, 2014 (Figure 4.2, Table 4.1). The increases varied by PAH and ranged from a factor of 0.6× for CHY to 23.6× for ACP (mean = 6.5×) greater than the background *c*(PAH) during the previous 72 hours (Figure 4.2). All the PAHs were influenced by a haboob more than by background holiday activities (July 4th through 6th; Figure 4.2).

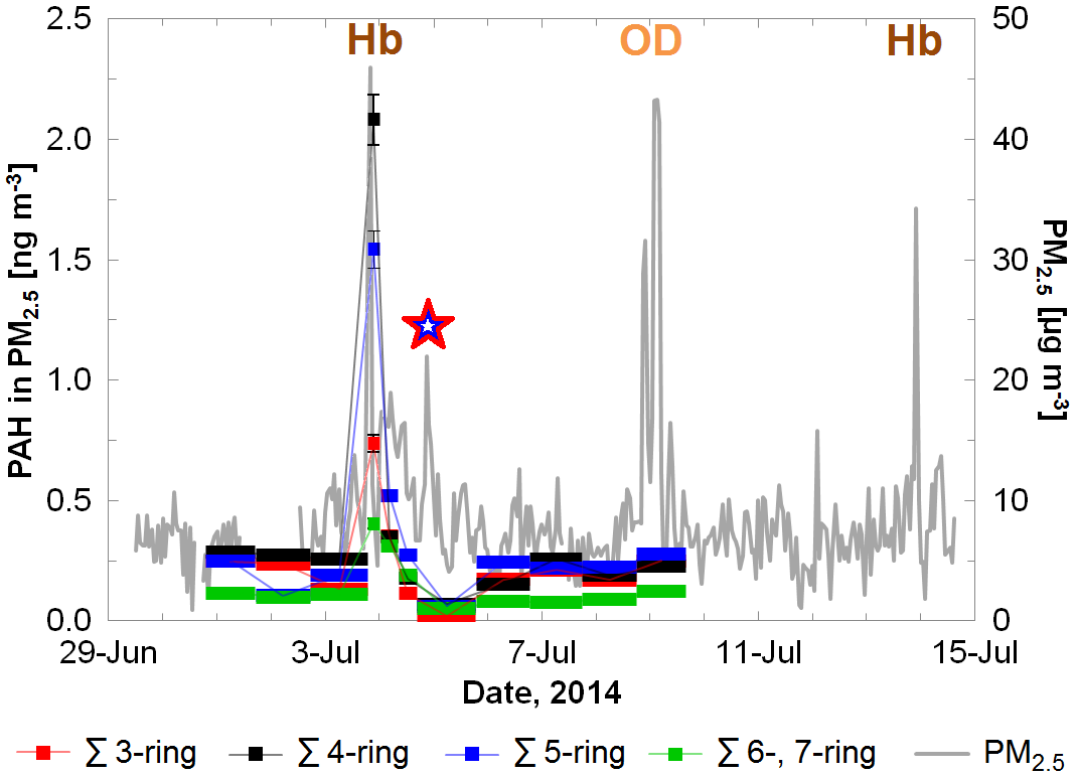

Figure 4.2. The increase of PAH concentrations in $PM_{2.5}$ during a haboob (Hb) but not during an 'other dust' (OD) event. The sums of 3-, 4-, 5-, and 6-,7-ring PAHs are in red, black, blue, and green rectangles respectively. The duration of the sampling can be seen in the horizontal width of the PAH markers. AQS TE (04-013-4005) $PM_{2.5}$ is in gray. The red and blue star denotes the increase in $PM_{2.5}$ due to holiday fireworks. Note the difference in scales of PAHs and $PM_{2.5}$.

The relative increase in $PM_{2.5}$ during the July 3, 2014 haboob was a factor of 4.2× which is below the average, 5.1× but above the median, 3.4× for 2012 to 2014 monsoon season $PM_{2.5}$ data. The maximum $PM_{2.5}$ of 46 µg m^{-3} on July 3, 2014 is typical for the three monsoon seasons where the mean of the maxima is $PM_{2.5}$ 46.8 µg m^{-3}. Thus, this particular haboob may be representative of typical haboobs in terms of $PM_{2.5}$ increases. However, the visibility of 1.6 km (1 mi) was lower, the peak gust speed of 25 m s^{-1} (56 mph) was higher, and the peak PM_{10} of 1059 µg m^{-3} (PM with aerodynamic diameters < 10 µm; station AQS TE) was higher than the average for haboob extrema (5.1 km, 16.9

m s^{-1}, and 789 µg m^{-3} respectively; Chapter 2) meaning that it was a relatively 'stronger' haboob than average.

The *c*(PAH) did not appear to increase during a dust event that occurred on July 8, 2014 despite the increase in $PM_{2.5}$ by a factor of 5.2 (Figure 4.2, Table 4.1). There were a few differences between the events. The July 3rd haboob had gust speeds up to 25 m s^{-1} while the dust event on July 8th had lower gust speeds: maximum of 14 m s^{-1} (Table 4.2). The dust event on the 8th may have been a weak haboob when it reached ASU: there was a weak thunderstorm outflow weather signature. However, due to the uncertainties associated with the classification of weak haboobs, it was categorized as "other dust" in Chapter 2.

Thunderstorm outflows are known to be heterogeneous throughout the area (Péwé *et al.*, 1981) and do not all originate from the same direction. Indeed, the wind direction reported nearby ASU (KPHX) was about 165 compass degrees (originating from the SSE) during the July 3rd haboob and was about 100 degrees (nearly east) on the 8th (U.S. National Oceanic and Atmospheric Administration, 2015). To the SSE of ASU is an urban region extending 16 km or more whereas to the ENE (*i.e.*, a bit north of 100 degrees), there are agricultural fields and open desert 5 to 10 km away. PAH emission is often the result of anthropogenic activities and *c*(PAH) are generally higher in urban areas than rural areas. The difference between the dust storms was further investigated through the use of diagnostic ratios to see if the relative differences in *c*(PAH) might be reflected in the observation of different PAH profiles.

4.3.3 PAH diagnostic ratios in $PM_{2.5}$ and soils.

Several PAH isomer ratios were calculated (Table 4.3) for the haboob, the other dust event, and the background samples. These were compared to the soil PAH diagnostic ratios reported in Marusenko *et al*. (2011). The PAHs in $PM_{2.5}$ during the haboob and during background time periods had generally higher ratios of $\frac{\text{BAA}}{\text{BAA + CHY}}$ than soils throughout the Phoenix area while the other dust event had a signature similar to the soils (Figure 4.3). The background PAHs at ASU are probably largely anthropogenic in origin, to which the haboob PAH isomer ratios bore similarity. This agrees with the wind direction data suggesting an influx of anthropogenic PAHs from SSE of ASU rather than resuspension of soil PAHs while the July 8th other dust event was an influx resuspended soil $PM_{2.5}$ originating from the east or ENE of ASU.

The $\frac{\text{IND}}{\text{IND + BGP}}$ ratio during most of the background time periods in Tempe was between 0.2 and 0.5 (Figure 4.3), which is indicative of automobile emissions (Yunker *et al*., 2002); the exceptions were three sampling periods when the $\frac{\text{IND}}{\text{IND + BGP}}$ ratio was > 0.5, suggesting PAH originating from combustion of other fuels (*i.e*., not gasoline or diesel fuels) such as barbeques. One of the three sampling periods with a $\frac{\text{IND}}{\text{IND + BGP}}$ ratio > 0.5 was during the daytime hours of the July 4th holiday, when barbeque use is higher. The other two exceptions occurred on the Tuesday after the holiday weekend and on the Monday prior to the holiday weekend and bear no apparent significance.

The literature $\frac{\text{IND}}{\text{IND + BGP}}$ ratios at urban locations where vehicular emissions may be a dominant source of PAH in $PM_{2.5}$ (Table 4.3) were of similar magnitude to most of the background time periods in Tempe.

Table 4.3

A Comparison of PAH $PM_{2.5}$ ratios during a Haboob, Non-Dust, and Background Time Periods in Tempe with Literature Measurements

Parameter	2014-07-03 haboob	2014-07-08 dust event	Background mean (range)[§]	Houston, Texas[†]	Southern California[‡]	Birmingham, United Kingdom[♦]
Relative increase factor	0.6 – 23.6	-0.6[&] – 2.4	n/a*	n/a	n/a	n/a
BAA / (BAA + CHY)	0.70	0.35	0.63 (0.34 – 0.80)	0.22 – 0.49	0.38 – 0.53	0.34
IND / (IND + BGP)	0.38	0.31	0.49 (0.28 – 0.76)	0.29 – 0.55	0.31 – 0.45	0.49
ANT / (ANT + PHE)	0.28	0.20	0.26 (0.08 – 0.43)	0.18 – 0.51	0.03 – 0.58	0.23
FTH / (FTH + PYR)	0.19	0.49	0.36 (0.20 – 0.51)	0.40 – 0.53	0.26 – 0.45	0.51

Notes: §, background was the non-dust time periods from June 30 – July 9, 2014; †, Fraser *et al*., 2002; ‡, Eiguren-Fernandez *et al*., 2004; ♦, Delgado-Saborit *et al*., 2013; &, the negative number is a relative decrease; *, n/a is not applicable; PHE, phenanthrene; ANT, anthracene; FTH, fluoranthene; PYR, pyrene; BAA, benzo[*a*]anthracene; CHY, chrysene; IND, indeno[1,2,3-*cd*]pyrene; BGP, benzo[*g,h,i*]perylene.

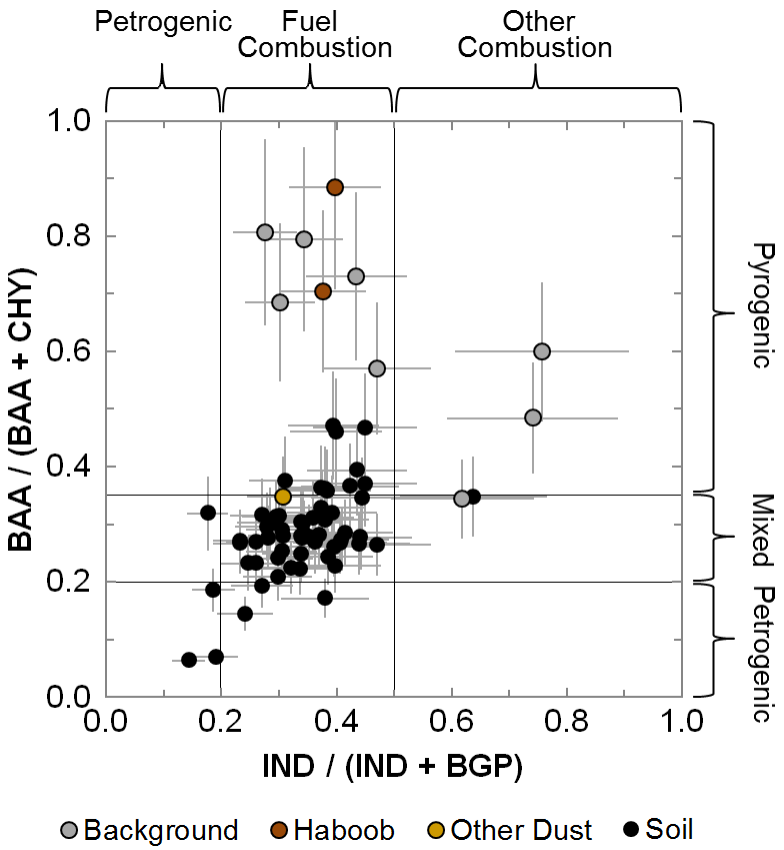

Figure 4.3. PAH diagnostic ratios of haboob, background, other dust data (brown, grey, and tan circles respectively) during the time period of June 30 to July 9, 2014. Soil data (black circles) is as reported in Marusenko *et al*. (2011) and Hall and Marusenko (2009). See text for abbreviations.

The magnitude of the background and haboob $\frac{\text{BAA}}{\text{BAA + CHY}}$ ratios further would suggest a pyrogenic PAH origin, which is consistent with an anthropogenic PAH influx. The PAH isomer ratios of somewhat more volatile PAHs, $\frac{\text{ANT}}{\text{ANT + PHE}}$ and $\frac{\text{FTH}}{\text{FTH + PYR}}$, are likely less applicable to $PM_{2.5}$ in the Phoenix area during the summer when temperatures exceed 40 °C for approximately 61 days per year (NOAA, 2015). Nevertheless, the $\frac{\text{FTH}}{\text{FTH + PYR}}$ ratio differentiates most of the urban background $PM_{2.5}$ samples from the soil samples (Figure 4.4). One of the two haboob samples bears similarity with soil $\frac{\text{FTH}}{\text{FTH + PYR}}$

ratios while the other does not. It is possible that the source of the haboob dust was not constant throughout the period of the haboob, which could be manifested in a PAH isomer ratio difference. The $\frac{\text{ANT}}{\text{ANT + PHE}}$ isomer ratio does not appear to differentiate $PM_{2.5}$ from soils and would suggest a pyrogenic origin for nearly all the $PM_{2.5}$ and soil samples (Figure 4.4).

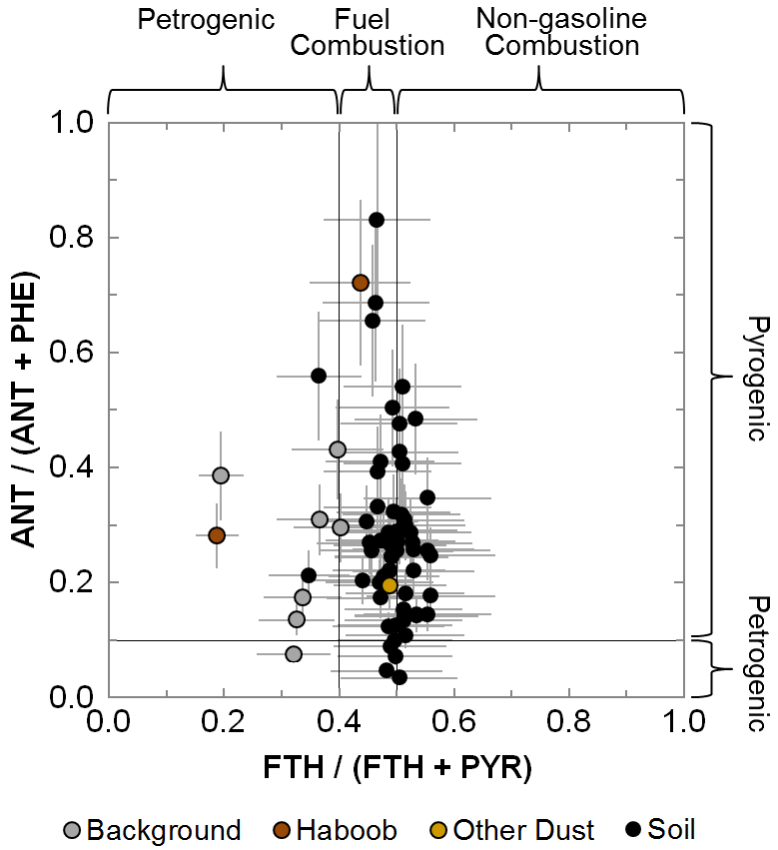

Figure 4.4. PAH isomer ratios of haboob, background, other dust data (brown, grey, and tan circles respectively) from June 30 to July 9, 2014. Soil data (black circles) is as reported in Marusenko *et al*. (2011) and Hall and Marusenko (2009). See text for PAH abbreviations.

The diagnostic ratios of the summertime background samples in Tempe (Table 4.3) compared well with urban literature ratios in southern California (year-round; Eiguren-Fernandez *et al*., 2004), the Houston area (year-round; Fraser *et al*., 2002), and

Birmingham (wintertime; Delgado-Saborit *et al*., 2013). The background diagnostic ratios were generally indicative of the combustion of petroleum fuels (gasoline and diesel) while fewer samples were indicative of other fuels or mixed fuel pyrolysis.

4.4 SUMMARY

The concentrations of PAHs have been determined in $PM_{2.5}$ samples in Tempe (AZ) during the summer of 2014. The background (*i.e*., non-dust storm) PAH concentrations and diagnostic ratios observed in Tempe are consistent with summertime literature observations of similar urban/suburban environments.

The $PM_{2.5}$ concentrations and PAH in $PM_{2.5}$ concentrations during a haboob storm were found to be higher than antecedent background concentrations by a factor of 4.2× and 6.5× respectively. However, PAH concentrations did not increase during an 'other dust' event a few days later when $PM_{2.5}$ concentrations increased by a factor of 5.2×. The haboob $PM_{2.5}$ PAH diagnostic ratios were compared to those in and were found to be different than those in soils of the Phoenix area yet similar to urban background $PM_{2.5}$ while the other dust event was similar to soil diagnostic ratios. An inspection of wind direction and PAH isomer ratios in $PM_{2.5}$ relative to soil suggests an urban / anthropogenic PAH source to the SSE of ASU during the July 3, 2014 haboob while the July 8, 2014 other dust event may have originated from rural/agricultural areas to the ENE of ASU. The data suggests that the quantity of PAH in $PM_{2.5}$ during haboobs and other dust events depends on the direction of the storm path and therefore the PM source.

CHAPTER 5

THE IMPACT OF PARTITIONING AND OXIDATIVE PROCESSING OF PAH IN FOGS AND CLOUDS ON ATMOSPHERIC LIFETIMES OF PAH

5.1 INTRODUCTION

Polycyclic aromatic hydrocarbons (PAHs) are ubiquitous in the atmosphere. They are formed during the incomplete pyrolysis of organic matter and emitted by vehicles, cigarette smoke, wildfires, fireplaces, smoked foods, and coal power plants (Rogge *et al*., 1993a; Zhang and Tao, 2009). Many PAHs are classified as suspected human carcinogens and one (benzo[*a*]pyrene) is a known human carcinogen (U.S. EPA, 2014a). The most often studied and most abundant PAHs are fluorene (FLU), acenaphthylene (ACY), anthracene (ANT), fluoranthene (FLT), pyrene (PYR), benzo[*a*]anthracene (BAA), benzo[*e*]pyrene (BEP), benzo[*a*]pyrene (BAP), perylene (PRL), dibenz[*a,h*]anthracene (DBA), and benzo[*g,h,i*]perylene (BGP) with typical atmospheric concentrations of 0.002 to 25 ng m^{-3} while the smallest PAH, naphthalene (NAP), has typical atmospheric concentrations of 20 to 500 ng m^{-3} (total of gas and particle phases; Fraser *et al*., 2002; Eiguren-Fernandez *et al*., 2004; Delgado-Saborit *et al*., 2013).

PAHs have relatively high boiling points (218 to 525 °C or higher) but nevertheless demonstrate semi-volatile behavior with nanograms per meter cubed quantities of gas phase PAHs in the atmosphere (*e.g*., phenanthrene, PHE 0.15 ng m^{-3}; Delgado-Saborit *et al*., 2013). Observational studies have shown the partitioning of PAHs in the absence of fogs and clouds (*i.e*., distribution between the gas and particulate phases) to be dependent upon temperature and the molecular weight of the PAH (Fernandez *et al*., 2002; Eiguren-Fernandez *et al*., 2004; Delgado-Saborit *et al*., 2013).

For example, Delgado-Saborit *et al*. (2013) reported PAHs with molecular weights of < 202 Da to be > 80% in the gas phase while PAHs > 250 Da were 30% or less in the gas phase. When fogs and clouds are present, PAHs are found in the aqueous phase (*e.g*., BAP 2×10^{-7} g L^{-1}; Herckes *et al*., 2002) despite the very low water solubilities of PAHs (1.4×10^{-7} to 3.2×10^{-2} g L^{-1}; Pearlman *et al*., 1984). Capel *et al*. (1991) proposed three mechanisms to account for PAH presence in fog water: dissolved organic compounds that act as co-solvents for PAHs, organic compounds acting as surfactants at the droplet surface or in colloids, and PAHs bound to scavenged particles. They found that filtering fog water isolated most PAHs (Leuenberger *et al*., 1988; Capel *et al*., 1991) which lead Capel *et al*. (1991) to conclude that scavenged particles were the largest reservoir of PAHs in fog. Nonetheless, Capel *et al*. (1990) found that the surface tension in fog water is lower than in pure water, which is a manifestation of surfactant (surface film) and/or co-solvent behavior. Valsaraj demonstrated PAH adsorption to water surfaces (Valsaraj, 2004; Valsaraj, 2009) and to surfactant-like organic matter on water surfaces (Donaldson and Valsaraj, 2010; Chen *et al*., 2011).

There have been few atmospheric PAH multiphase (*i.e*., > two phases) studies. Lei and Wania (2004) employed partition ratios to predict PAH distribution in clouds. Ehrenhauser *et al*. (2012) compared the observed PAH distribution in fog with simple predictions using partition ratios. While the phase distribution and reactions within a three-phase system are not well known for PAHs, partition ratios have been measured and estimated for octanol-water systems (Wang *et al*., 1986; Hansch *et al*., 1995; de Maagd *et al*., 1998), octanol-air systems (Alaee *et al*., 1996; Harner and Bidleman, 1998a; Bamford *et al*., 1999; Odabasi *et al*., 2006; Ma *et al*., 2010), and water-air

systems, *i.e*., Henry's law constants (ten Hulscher *et al*., 1992; Reza and Trejo, 2004; Sander 2015). (Photo)chemical degradation rate constants of many PAHs in the various phases have been measured or calculated (Calvert *et al*., 2002) and the products of PAH oxidation reactions have been reported in the gas (Helmig *et al*., 1992; Helmig and Harger, 1994; Lane *et al*., 1996; Mihele *et al*., 2002; Wang *et al*., 2007; Lee and Lane, 2010), aqueous (Sigman *et al*., 1996; Mallakin *et al*., 2000; Kong and Ferry, 2003; Woo *et al*., 2009; Sanches *et al*., 2011) and organic phases (Jang and McDow, 1997; Fioressi and Arce, 2005). To the best of the authors' knowledge, only one study has published PAH photochemical degradation rate constants in organic / aqueous liquid mixtures (Grossman *et al*., 2016) and this was limited to ANT and PYR. The conclusion of their study was that ANT and PYR processing in the aqueous phase is faster than in a liquid organic phase and thus chemical reactions in the aqueous phase should be considered in identifying chemical sinks of PAHs, in addition to deposition processes. Previously, PAH processing in the atmospheric aqueous phase was considered to be negligible (Lohmann and Lammel, 2004) due to the very low solubility of PAHs. Gas phase PAH reactions and heterogeneous reactions on particulate matter surfaces are considered the main sink of PAHs where atmospheric lifetimes range from 1 to 300 hr (Keyte *et al*., 2013). It has been suggested that dry deposition is the main physical (*i.e*., non-chemical) loss process of PAHs and therefore their atmospheric lifetime is constrained by the particle lifetime (Bidleman, 1988; Škrdlíková *et al*., 2011). Removal by wet deposition (rain) is considered to be at least ten times less efficient than dry deposition (Škrdlíková *et al*., 2011).

During droplet nucleation and scavenging processes, it is unknown what fraction of PAHs bound to PM (particulate matter) will dissolve into the atmospheric aqueous phase. Open questions remain as to the role of surface films on PAH uptake by fog and cloud droplets and whether PAHs incorporate into or onto atmospherically representative droplets. This is in part due to analytical constraints of sample size and PAH detection limits. Many studies of PAH uptake from the gas phase by surface films on water have employed planar or cylindrical surfaces which do not have the same surface area to volume ratios as cloud droplets (Moza *et al*., 1999; Chen *et al*., 2006; Chen *et al*., 2011). A few studies of PAH uptake from the gas phase have employed 92 μm droplets (Raja and Valsaraj, 2006) or modeled 1000 μm droplets (Ma *et al*., 2013) which were greater than the 5 to 20 μm droplets found in fogs and clouds (Zak, 1994). Other studies have employed concentrations of PAHs far exceeding those found in typical fogs and clouds (Kahan and Donaldson, 2007; Chen *et al*., 2011; Styler *et al*., 2011). Measurements on relatively planar surfaces or on surfaces with very high PAH loading may overestimate the coverage of drops by surface films.

The atmospheric oxidation of PAHs to oxy–PAHs (PAHs with one or more oxygen atoms in carboxyl groups and/or as heteroatoms in the ring) increases their solubility (Delgado-Saborit *et al*., 2013). This conversion affects the phase distribution of PAHs and therefore their atmospheric lifetimes. In addition, it has been shown that oxidation may increase PAH toxicity (Straub *et al*., 1977; McConkey *et al*., 1997). Oxy–PAHs are further oxidized to smaller products. PAH removal must be considered not only in terms of phase distribution in multiple atmospheric phases but also in terms of PAH reactivity and the physical distribution of first- and higher-generation products.

Predicting PAH lifetimes and fate in the atmosphere without considering all aspects of their distribution and reaction in fogs and clouds might substantially overestimate their lifetime.

5.2 DATA REVIEW

5.2.1 Partition ratios to describe the distribution between gas, aqueous and organic phases.

Three constants describe the equilibrium partitioning between the gas, organic and aqueous phases, respectively. The dimensionless 1–octanol water partition ratio, K_{OW} (Equation 5.1), describes the equilibrium distribution of PAH concentrations between water and octanol ($[PAH]_{aq}$ and $[PAH]_{org}$, respectively). 1-octanol is assumed in the present study as a proxy of a liquid organic (org) phase in atmospheric particulate matter; K_{OW} and can be considered a measure of hydrophobicity.

$$K_{OW} = \frac{[PAH]_{org}}{[PAH]_{aq}} \quad (5.1).$$

The dimensionless octanol-air partition ratio K_{OA} describes the partitioning between the PAH concentrations in 1–octanol and air $[PAH]_g$:

$$K_{OA} = \frac{[PAH]_{org}}{[PAH]_g} \quad (5.2).$$

The Henry's law constant H [mol L^{-1} atm^{-1}] describes gas-aqueous partitioning as a function of p_{PAH} [atm], the partial pressure of PAHs in the gas phase:

$$H = \frac{[PAH]_{aq}}{p_{PAH}} \quad (5.3).$$

Literature values for PAH K_{OW} and K_{OA} are summarized in Table D1.

Values for H were calculated with the law for ideal gases, K_{OW}, and K_{OA} where R is the universal gas constant [0.08206 L atm mol^{-1} K^{-1}], and T is the absolute temperature [K]:

$$H^* = \frac{K_{OA}}{K_{OW} RT} \quad (5.4).$$

The asterisk superscript is included in Equation 5.4 to distinguish *H* measured in or estimated to represent a pure-water / gas system from a system from *H** calculated from K_{OW} and K_{OA}. The *H** together with available literature *H* are summarized in Table D1.

When literature partition ratios were unavailable they were estimated with U.S. EPA's EPISuite, which is a collection of software for the prediction of chemical release potential in the environment. The EPISuite K_{OW} estimation methodology is based on dividing a molecule into fragments followed the summation of fragment coefficients with correction factors for intramolecular effects. EPISuite estimates K_{OA} through a rearrangement of Equation 5.4 using K_{OW} and literature *H*. When unavailable, EPISuite estimates *H* from the sums of bond contributions and correction factors.

There is an internal inconsistency between the three partitioning ratios *H*, K_{OW}, and K_{OA} which has been attributed to octanol and water being mutually partially soluble (Ma *et al*., 2010). K_{OW} is measured in octanol that is 'wet' or saturated with water and in water that is saturated with octanol. *H* is measured in an ideal aqueous solution and K_{OA} is measured in 'dry' or anhydrous octanol. The exceptions to this internal inconsistency are the EPISuite estimated K_{OA} values since EPISuite employs Equation 5.5, a rearrangement of Equation 5.4, to determine them:

$$K_{OA} = K_{OW}\, R\, T\, H \quad (5.5).$$

Since the aim of the current work is to predict the distribution of PAHs when all three phases are present, it was desirable to employ constants that were measured in octanol-saturated water and water-saturated octanol. K_{OW} met this requirement and was selected as an independent parameter in Equation 5.4. Of the remaining two partition

ratios, neither was consistent with K_{OW}. Nevertheless, K_{OA} was selected as an independent variable since it was assumed that H was more uncertain due to the low water solubilities of PAHs. Therefore, the dependent variable was H^*. The H^* likely have a bias which systematically produces high values relative to H due to the 'wet octanol' and 'dry octanol' mismatch between K_{OW} and K_{OA} respectively. However, this 'bias' would actually not be a bias in the gas/aq ratio for atmospheric systems since there all three phases are present and therefore the organic phase is not dry and the aqueous phase is not organic-compound-free. The magnitude of the 'bias' has been quantified in terms of K_{OW} (calculated based on H and K_{OA}) and is reported to be negligible for NAP (two-rings) but for IND (six-rings), K_{OW} is an order of magnitude lower than a theoretical partition ratio based on immiscible octanol and water (Ma *et al*., 2010). Indeed, the H^*calculated with Equation 5.4 were approximately within an order of magnitude of literature and EPISuite values (Table D1 and Figure D1).

As expected, PAH H^* were generally greater than PAH literature H (Figure D1) since the water phase in K_{OW} is octanol-saturated, which increases PAH solubility, decreases K_{OW} and increases H^*. For example, at 25 °C the calculated H^* of PHE was 52±29 M atm^{-1}which was about a factor of two higher than a literature value for H, 21±4 M atm^{-1} (Alaee *et al*., 1996). Here, the uncertainty in the H^* of PHE was estimated as the propagation of K_{OW} and K_{OA} uncertainties: $\log_{10}^{-1}(4.57 \pm 0.08)$ (de Maagd *et al*., 1998) and $\log_{10}^{-1}(7.68 \pm 0.33)$ (Odabasi *et al*., 2006) respectively and the uncertainty in H was estimated as the standard error of prediction from the data given in Alaee *et al*. (1996).

The agreement between H^* and H of within an order of magnitude was considered adequate for PAHs since there are notable (half an order of magnitude)

uncertainties in H, K_{OW} and K_{OA} as well as the previously mentioned bias due to the 'wet octanol' and 'dry octanol' mismatch. Many EPISuite H values fell on the 1:1 line with H^* (Figure D1) since EPISuite uses Equation 5.5 to estimate K_{OA} where no literature value exists.

5.2.2 Chemical loss processes of PAHs: kinetic constants.

Literature rate constants k were are listed for oxidation reaction of gas-phase PAHs (Table D2) with various oxidants, which included the hydroxyl radical $k(^{\bullet}\mathrm{OH},\ \mathrm{g})$, ozone $k(\mathrm{O_3},\ \mathrm{g})$, atomic oxygen $k(\mathrm{O}(^3\mathrm{P}),\ \mathrm{g})$, and nitrate radical $k(^{\bullet}\mathrm{NO_3},\ \mathrm{g})$. Measurements of the gas-phase oxidation kinetics for PAHs with four or more rings (BAA, CHY, BAP *etc*.) and most oxy–PAHs were largely absent from the literature due to their lower volatility (Calvert *et al*., 2002). Some of the missing gas-phase rate constants were estimated with EPISuite.

Two pseudo first-order photooxidation rate constants were used for the condensed phase: the photooxidation rate in bulk water k(aq) and in liquid organic phase k(org). Aqueous phase oxidizing agents are known to include singlet oxygen ($O_2(^1\Delta_g)$) and $^{\bullet}$OH, both of which can be formed from the reaction of ground-state dissolved oxygen O_2(aq) with photo-excited PAHs; thus aqueous PAHs photodegrade in a self-catalyzing process when O_2(aq) is present (Pierlot and Aubry, 1997; Miller and Olejnik, 2001; Kong and Ferry, 2003; Clark *et al*., 2007). When liquid organic phases are in contact with water, $O_2(^1\Delta_g)$ is an important PAH oxidant; however, in anhydrous liquid organic phases, PAH removal is slower and/or occurs by a different reaction pathway (Plata *et al*., 2008).

There are few literature PAH k(org) measured in a liquid organic phase (Table D2): ANT and PYR in 1–octanol (Grossman *et al*., 2016), ANT and PYR in methanol

(Grossman *et al*., 2016), and BAA, CHY, BAP, and BEP in toluene (Plata *et al*., 2008). Analogous photooxidation rates of PAHs have been reported on the waxy epidermidis of spruce needles (Niu *et al*., 2003). The *k*(org) in 1–octanol, methanol, and toluene were within an order of magnitude of *k*(needle epidermidis) for ANT, PYR, BAA, CHY, BAP and BEP (Figure D2). Grossman *et al*. (2016) reported a systematic decrease in *k*(org) for decreasing solvent polarity, which is seen in Figure D2 where *k*(1–octanol) is five to seven times smaller than *k*(methanol). Irradiation intensity also affects *k*(org) as evidenced in Figure D2 where *k*(1–octanol) is about five to seven times smaller than *k*(toluene) notwithstanding toluene being less polar than 1–octanol. The intensity employed by Plata *et al*. (2008) was close to 888 W m^{-2} while Grossman *et al*. (2016) employed about 17 W m^{-2} and Niu *et al*. (2003) reported a mean irradiation intensity of 620±50 W m^{-2}. Ten PAH *k*(org) were calculated as a function of the linear regression of *k*(toluene) vs. *k*(needle epidermidis) (see 1 / 7.2 line in Figure D2). For NAP, ACP, BAU, BBU, and RET neither a literature rate constant nor an estimated rate constant was available. Therefore, the photooxidation in the liquid organic phase for those five PAHs was not included in the model.

The product identities and the product yields of the oxidation of PAHs were derived from experimental studies in the literature. The major products of PAH (photo)oxidation are monocyclic aromatics and non-aromatic organic compounds (Moza *et al*., 1999; Mallakin *et al*., 2000; Kong and Ferry, 2003; Woo *et al*., 2009). The scope of the current work is limited to polycyclic aromatic products, *i.e*., oxy–PAHs, which are minor products of PAH photo(oxidation) and which have relative molar yields (Y_m) of a few percent or less. Literature Y_m were consistently < 3% for reactions with three of the

gas-phase oxidants and the condensed phases: $Y_{\mathrm{m}}(^{\bullet}\mathrm{OH},\ \mathrm{g})$; $Y_{\mathrm{m}}(\mathrm{O}_3,\ \mathrm{g})$; $Y_{\mathrm{m}}(\mathrm{O}(^3\mathrm{P}),\ \mathrm{g})$; $Y_{\mathrm{m}}(\mathrm{aq})$; and $Y_{\mathrm{m}}(\mathrm{org})$ (Table D3). With the exception of $Y_{\mathrm{m}}(^{\bullet}\mathrm{NO}_3,\ \mathrm{g})$, an estimate of 1% was used for products with the native-ring backbone intact while 0.1% was used for ring-rearranged / ring-opened products for reactions without literature Y_{m}. Literature $Y_{\mathrm{m}}(^{\bullet}\mathrm{NO}_3$, g) of PAH oxidation to oxy–PAH products was only available for PHE → oPHE2 (33 ± 9%) and was more than an order of magnitude higher than other Y_{m}. It is probable that $^{\bullet}\mathrm{NO}_3$ reacts with PAHs in a way that suppresses somewhat the fragmentation of PAHs into monocyclic and acyclic compounds thus increasing the production of oxy–PAHs. Since it was unclear whether all $Y_{\mathrm{m}}(^{\bullet}\mathrm{NO}_3,\ \mathrm{g})$ would be close to 33%, the missing $Y_{\mathrm{m}}(^{\bullet}\mathrm{NO}_3,\ \mathrm{g})$ values were not estimated.

Some literature Y_{m} were based on irradiation spectra that were not atmospherically representative, that is, the setup did not include filters to correct the UV irradiation intensity spectrum to be representative of sunlight at the surface of the Earth (*e.g.*, UV lamps without air mass filters; Woo *et al*., 2009; Sanches *et al*., 2011). In those instances, the same products were assumed while the yield was not. Probable products and estimated conversion quantities are indicated by parentheses in Table D3. Molecular structures of PAHs and their oxidation products (oxy–PAHs) are given in Figure D3.

5.3 MODEL DESCRIPTION

A box model was applied to calculate PAH equilibrium partitioning and processing in three phases: gas, aqueous, and liquid organic (Figure 5.1). The model was initialized with gas phase concentrations of oxidants (Table 5.1); these concentrations were held constant throughout the simulations and reflect typical oxidant levels for remote daytime conditions ($^{\bullet}\mathrm{OH}$, $\mathrm{O}^3\mathrm{P}$, O_3) and nighttime ($^{\bullet}\mathrm{NO}_3$). For simplicity, both

$^{\bullet}NO_3$ and $^{\bullet}OH$ chemistry were simulated simultaneously; they do not affect each other in the model. The model was initialized with 21 PAHs at environmentally relevant concentrations (Table 5.1).

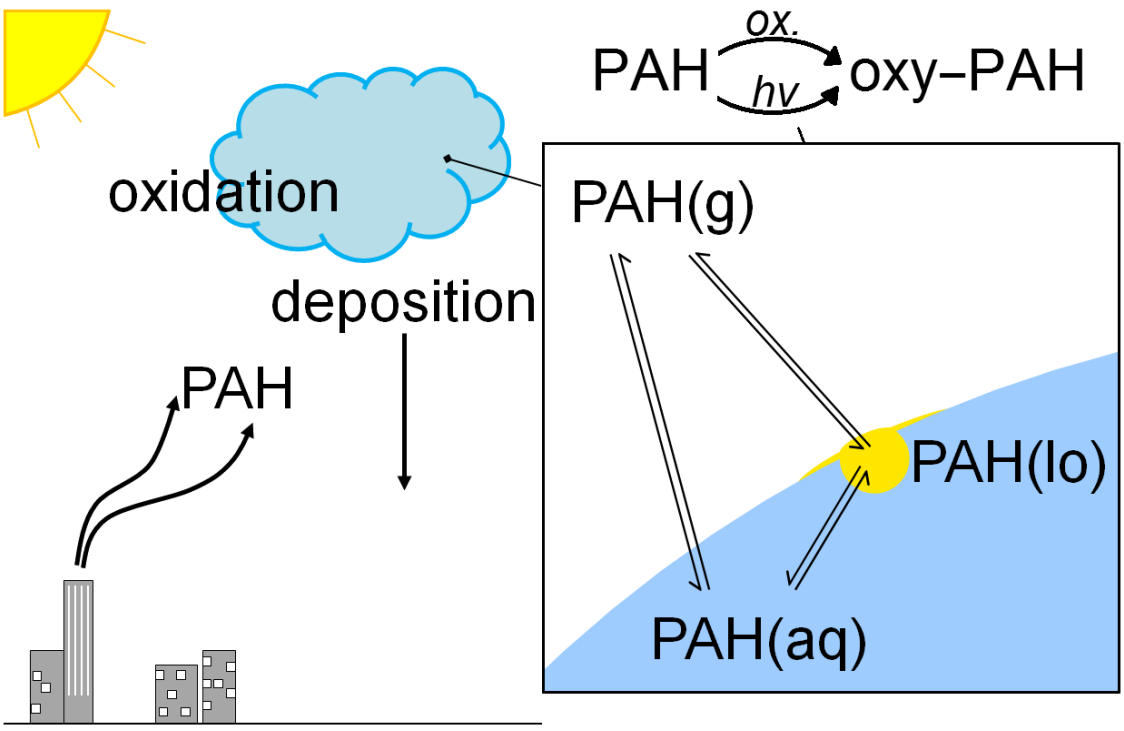

Figure 5.1. Schematic of the PAH multiphase (gas, aqueous, liquid organic) (photo)oxidation model.

PAH concentrations decreased over the course of the simulations due to oxidative loss. Of the 21 PAHs, 15 are known to form oxy–PAH products commonly reported in fog, cloud, gas or aerosol samples. Initial concentrations of oxy–PAHs were zero and increased as a function of loss of the 15 PAHs. The model did not include PAH loss by dry or wet deposition.

Table 5.1

Initialization of the Box Model

Parameter	Abbreviation / Symbol	Initial Values
aqueous phase volume fraction	ϕ^{aq}	3×10^{-7} vol/vol
liquid organic phase volume fraction	ϕ^{org}	3×10^{-12} vol/vol
hydroxyl radical	$^{\bullet}OH$	3×10^{6} molecules cm^{-3}
ozone	O_3	30 ppb
atomic oxygen	$O(^3P)$	200 molecules cm^{-3}
nitrate radical	$^{\bullet}NO_3$	1×10^{9} molecules cm^{-3}
nitrogen dioxide	NO_2	8×10^{13} molecules cm^{-3}
naphthalene	NAP	100 (20 – 500) ng m^{-3}
acenaphthylene	ACY	4.1 (1 – 17) ng m^{-3}
acenaphthene	ACE	4.1 (1 – 17) ng m^{-3}
9*H*–fluorene	FLU	8.7 (3 – 25) ng m^{-3}
phenanthrene	PHE	13 (7 – 23) ng m^{-3}
anthracene	ANT	0.5 (0.1 – 2.5) ng m^{-3}
fluoranthene	FLT	0.4 (0.09 – 2) ng m^{-3}
pyrene	PYR	2.3 (0.4 – 13) ng m^{-3}
acephenanthrylene	ACP	0.4 (0.09 – 2) ng m^{-3}
11*H*–benzo[*a*]fluorene	BAU	0.06 (0.01 – 0.4) ng m^{-3}
11*H*–benzo[*b*]fluorene	BBU	0.06 (0.01 – 0.4) ng m^{-3}
benzo[*a*]anthracene	BAA	0.12 (0.04 – 0.35) ng m^{-3}
chrysene	CHY	0.23 (0.13 – 0.42) ng m^{-3}
retene	RET	0.08 (0.02 – 0.35) ng m^{-3}
benzo[*b*]fluoranthene	BBF	0.04 (0.012 – 0.16) ng m^{-3}
benzo[*k*]fluoranthene	BKF	0.03 (0.006 – 0.1) ng m^{-3}
benzo[*a*]pyrene	BAP	0.04 (0.01 – 0.2) ng m^{-3}
benzo[*e*]pyrene	BEP	0.03 (0.003 – 0.26) ng m^{-3}
indeno[1,2,3–*cd*]pyrene	IND	0.05 (0.013 – 0.2) ng m^{-3}
dibenz[*a,h*]anthracene	DBA	0.01 (0.002 – 0.1) ng m^{-3}
benzo[*g,h,i*]perylene	BGP	0.08 (0.02 – 0.32) ng m^{-3}

Notes: PAH concentrations are an overview from the literature of the totals of all three phases and are representative of total PAH levels (gas + particulate) in urban areas; ranges are in parenthesis (Eiguren-Fernandez *et al*., 2004; Albinet *et al*., 2007; Delgado-Saborit *et al*., 2013). The concentrations of all oxidants were held constant.

An aqueous phase volume fraction (ϕ^{aq}) of 3×10^{-7} was used and is equivalent to a liquid water content (LWC) of 0.3 g m^{-3}, consistent with observations of dense fogs and

clouds (Raja *et al*., 2008; Ervens *et al*., 2013). A liquid organic phase volume fraction (ϕ^{org}) of 3×10^{-12} was calculated with Equation D1 and corresponds to 5 mgC L^{-1} water-insoluble organic carbon (OC; assuming a liquid organic phase of 70% C by mass and a density of 0.7 g cm^{-3}, *i.e*., a ratio of organic matter to organic carbon (OM/OC) of 1.4). These volume fractions were comparable to the liquid water and particle volume fractions employed by Lei and Wania (2004) ($\phi^{\mathrm{aq}} = 3\times10^{-7}$ and $\phi^{\mathrm{PM}} = 1\times10^{-12}$ respectively) in a cloud PAH model. The incorporation of ϕ^{aq} and ϕ^{org} into Equations 5.1, 5.2 and 5.4 permitted the derivation of Equations D2 – D10, where PAH concentrations are in terms of total air volume.

The model included monodispersed 10 µm diameter water droplets with constant ϕ^{aq} and ϕ^{org}. pH and temperature were held constant with pH = 6 and T = 25 °C, respectively. During each time step (1 s), the PAHs and oxy–PAHs concentrations changed due to chemical reactions. Following that, the new equilibrium concentrations of PAHs and oxy–PAHs between all three phases were calculated using Equations D4 – D7 before the next time step. Simulations were performed over three hours. The assumption of equilibrium has been used in many models (Lei and Wania, 2004 and references therein; Lohmann and Lammel, 2004; Lammel *et al*., 2009) even though equilibrium may not always exist.

5.4 MODEL RESULTS AND DISCUSSION

5.4.1 Predicted phase partitioning.

PAHs with two to four rings such as NAP and CHY were predicted to be primarily in the gas phase ($x^{\mathrm{g}} > 93\%$) at 25 °C while DBA (five rings), IND (six rings), and BGP (six rings) were predicted to have a significant fraction in droplets ($x^{\mathrm{g}} < 11\%$)

with aqueous phase fractions x^{aq} of 2 to 5% and liquid organic phase fractions x^{org} of and 85 to 91% (Figure 5.2).

All of the monocarbonyl oxy–PAHs were predicted to be predominantly gas phase (x^{g} > 82%) while the dicarbonyl oxy–PAHs were principally in droplets (x^{g} < 32%; x^{aq} 32 to 97%; x^{org} < 0.1 to x^{org} = 68%) with the exception of oANT (x^{g} = 76%). The oxy–PAHs with the greatest x^{aq} was the dicarbonyl oPHE2 with x^{aq} = 97%. The PAHs were predicted to be mostly absent from the aqueous phase, where the five-ring PAH BBF had the greatest x^{aq} = 6%.

In log-log space, the phase 'boundaries' seen in the K_{OW} - K_{OA} parameter space corresponded to $\log_{10} K_{OA}$ = 11.52, $\log_{10} K_{OA} = \log_{10} K_{OW}$ + 6.52, and $\log_{10} K_{OW}$ = 5. Their magnitudes are a consequence of the ratio of the aqueous and liquid organic phase volumes in Equations D2 and D3. The five- and higher-ring PAHs and the four- and higher-ring oxy–PAHs approached or passed the liquid organic phase 'boundary' with x^{org} > 9%, DBA having the highest x^{org} = 91%.

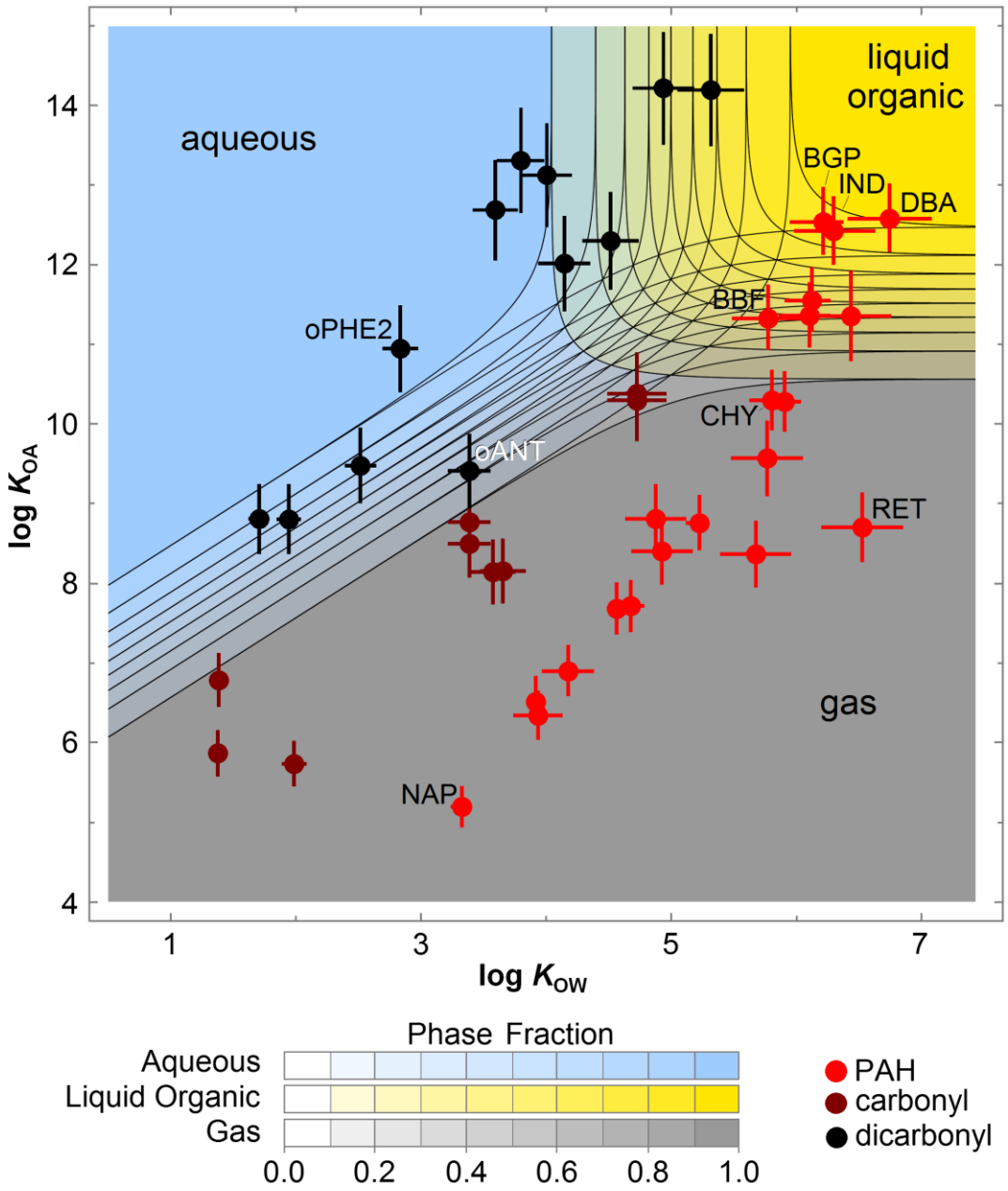

Figure 5.2. Predicted PAH and oxy–PAH phase fractions at 25 °C. The calculated fractions in the aqueous, liquid organic, and gas phases are in blue, yellow, and greyscale respectively. PAH literature and EPISuite K_{OW} and K_{OA} values are indicated as red circle symbols, monocarbonyl oxy–PAHs as dark-red, and dicarbonyl oxy–PAHs as black circle symbols. Error bars show literature reported error (95% CI, Odabasi *et al*., 2006) or 5% if an error was not reported.

The oxy–PAHs are less hydrophobic than PAHs and indeed many of the oxy–PAHs were predicted to partition into the aqueous phase more than their PAH counterparts. This difference was expected since the presence of oxygen atoms in oxy–PAHs increases intermolecular attractions and water solubility, as evidenced by their smaller K_{OW} (Table D1). The dicarbonyl oxy–PAHs were predicted to have a greater aqueous phase fraction than monocarbonyl oxy–PAHs (Figure 5.2) with x^{aq} ranging from 24 to 97% and 0.2 to 11% respectively. The number of rings in PAHs and oxy–PAHs had less of an effect on x^{g} and x^{aq} than the number of carbonyl groups.

The species which were predicted to be primarily gas phase (*i.e.*, $x^{g} > 0.5$) were the two-, three-, and four-ring PAHs (e.g., NAP and CHY) and the monocarbonyl oxy–PAHs (dark-red circle symbols in Figure 5.2).

To the best of the authors' knowledge, the only reported study of PAH and/or oxy–PAH fractionation between the gas and fog droplet phases is Ehrenhauser *et al*. (2012). They demonstrated the deviation of observed aqueous/gas partitioning (analogous to *H**) from literature *H* for PHE, ANT, PYR, ACE, FLU, and BAP. These PAHs have greater x^{fog} (the sum of x^{aq} and x^{org}) at 2 to 7 °C than theoretical x^{aq} in a pure water / gas system at 25 °C. While temperature undoubtedly influenced x^{fog}, the role of organic compounds in droplets also influenced x^{fog} and is considered in greater detail later in the discussion.

Ehrenhauser *et al*. (2012) did not tabulate observed x^{fog} and therefore a direct comparison with the predicted x^{fog} of the present work cannot be made at this time. However, an indirect approach can be employed to compare this work with literature observations. In the absence of fogs and clouds, PAHs and oxy–PAHs are known to

fractionate between the gas and condensed phases (Eiguren-Fernandez *et al.*, 2004; Alam *et al*., 2013). The predicted partitioning of PAHs and oxy–PAHs where the aqueous volume is 15% as large as the liquid organic volume (*i.e.*, $\phi^{aq} = 4.5\times10^{-13}$) shown in Figure D4 is representative of hygroscopic particles at ambient relative humidity (Lohmann and Lammel, 2004). Under those conditions the partitioning of PAHs in the gas and liquid organic phases is predicted to be nearly the same in Figures 5.2 and D4. Thus notwithstanding the differences in the gas / particulate system as compared to the gas – droplet system, some similarities are seen in Table 5.2 for PAHs x^{g}: as the PAH molar mass and K_{OA} increase, x^{fog} increases.

The difference between Figures 5.2 and D4 demonstrates a lesser fraction of some oxy–PAHs (especially the two- and three-ring dicarbonyls) that would be gas phase when fogs or clouds are present relative to when fogs or clouds are absent. Hence, there is a water-enhanced decrease in the gas phase fraction of some oxy–PAHs. An enhanced uptake from the gas phase of various hydrocarbons with oxygen groups at air / water surfaces was reported by Goss (1994). They demonstrated that the enhanced uptake of compounds capable of strong intermolecular attractions with water (*i.e.*, hydrogen bonding) was not well described by K_{OW} values alone but was well described by vapor pressure that has been corrected for hydrogen binding in the solvent. In the current model, the use of both K_{OA} and K_{OW} indirectly provides information on both vapor pressure and aqueous-intermolecular attractions (including hydrogen bonding). The vapor pressure of oxy–PAHs is inversely proportional with H in Equation 5.3 and therefore is inversely proportional to $K_{OA}/(K_{OW}RT)$ by Equation 5.4. K_{OW} is a description of the

difference in strength of octanol-solute and water-solute intermolecular attractions and repulsions, which includes hydrogen-bonding differences.

5.4.2 Chemical removal of PAHs and formation of oxy–PAHs.

In order to compare chemical loss rates in each phase, the gas phase rate constants $k(\mathrm{g})$ were multiplied by the oxidant concentrations to obtain pseudo first order rate constants, *i.e.*, loss rates $k'(\mathrm{g})$ [s^{-1}]. Many rate constants were missing which confounded a direct comparison of all kinetic processes. For example, $k'(O_3,\ \mathrm{g})$ were only available for five PAHs. Of the processes for which rate constants were available, $k'(^{\bullet}NO_3,\ \mathrm{g})$ and $k'(O(^3P),\ \mathrm{g})$ were three to five orders of magnitude smaller than $k'(^{\bullet}OH,\ \mathrm{g})$ and $k'(O_3,\ \mathrm{g})$ as seen in Figure 5.3a. The $k'(O_3,\ \mathrm{g})$ were smaller by three orders of magnitude than $k'(^{\bullet}OH,\ \mathrm{g})$ except for ACY, which is likely due to the ease of O_3 reacting with the double bond in the five-membered ring of ACY (Calvert *et al*., 2002).

To determine the importance of the different reactions for each PAH, the loss rates were weighted by their fractions in each phase (x^{g}, x^{org}, x^{aq}) and compared in Figure 5.3b. In general, $x^{\mathrm{g}}k'(^{\bullet}OH,\ \mathrm{g})$ was largest of the volume-weighted rates of all phases for two-, three-, and four-ring PAHs since they are primarily gas phase ($x^{\mathrm{g}} > 0.92$) at 25 °C. The $x^{\mathrm{g}}k'(^{\bullet}OH,\ \mathrm{g})$ of BBF, BBK, BAP, and BEP were the same order of magnitude as $x^{\mathrm{org}}k(\mathrm{org})$ since $x^{\mathrm{g}} < 0.6$ at 25 °C. For IND, DBA, and BGP, $x^{\mathrm{org}}k(\mathrm{org})$ in the liquid organic phase kinetics exceeded $x^{\mathrm{g}}k'(\mathrm{g})$ due to their very low gas phase fractions (x^{g} 0.08 to 0.10; Table 5.2 and Figure 5.3b). For ANT, PYR, BAA, and BAP the $k(\mathrm{aq}) > k'(^{\bullet}OH,\ \mathrm{g})$ while the volume-weighted rates $x^{\mathrm{aq}}k(\mathrm{aq}) < x^{\mathrm{g}}k'(^{\bullet}OH,\ \mathrm{g})$.

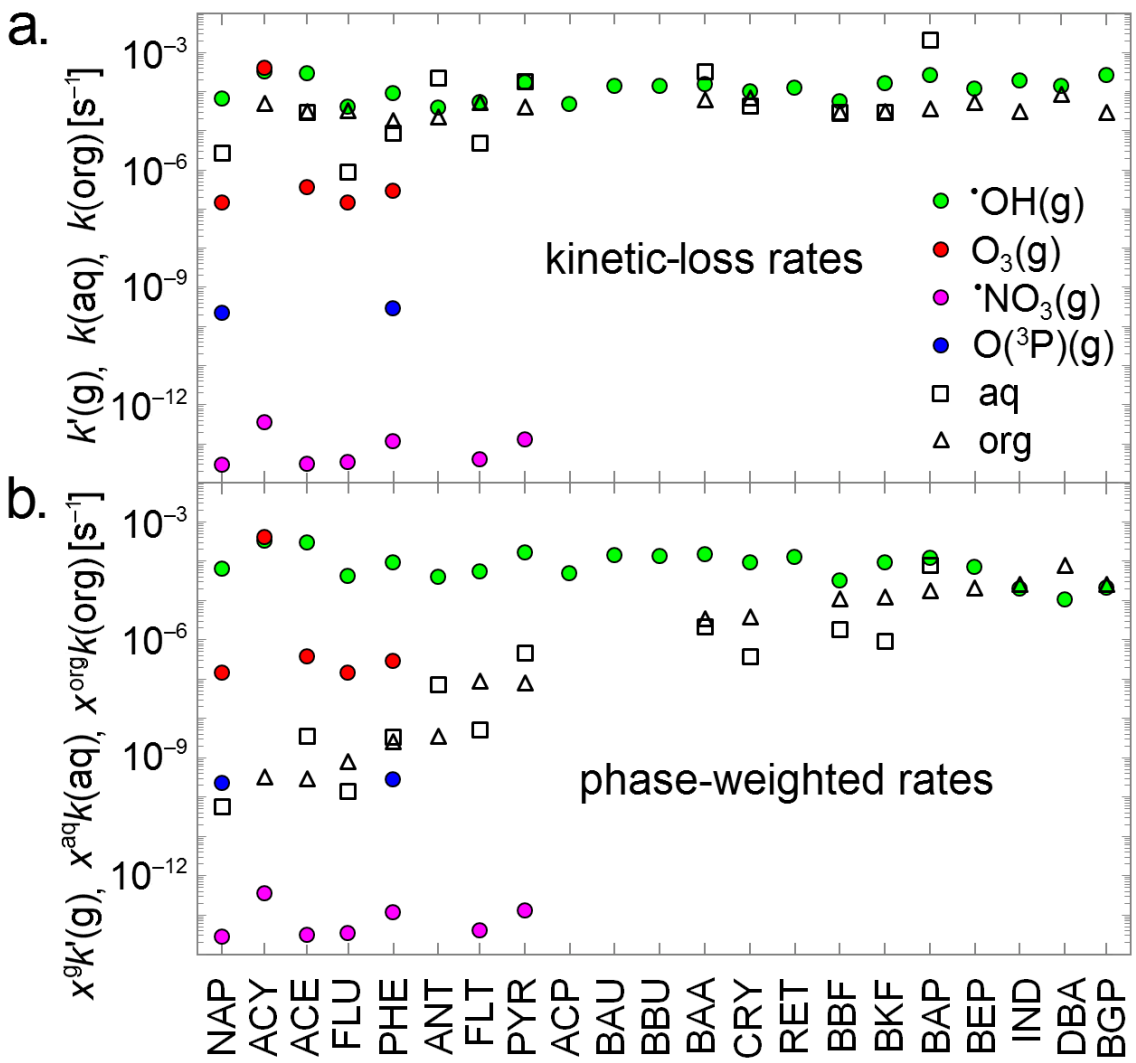

Figure 5.3. A comparison of pseudo-first order rate constants (a) and a comparison of pseudo-first order rate constants weighted by phase fractions x^{phase} (b). Gas phase rate constants included oxidation by hydroxyl radical ($^{\bullet}OH$), ozone (O_3), nitrate radical ($^{\bullet}NO_3$), and excited oxygen ($O(^3P)$). Pseudo-first order photooxidation rates are given for the aqueous (aq) and liquid organic (org) phases. The temperature is 25 °C for all rate constants. See Glossary of Abbreviations and Terms for PAH abbreviations.

PAH lifetimes were calculated using

$$\tau[\mathrm{s}] = \frac{1}{\sum(k')} \qquad (5.6).$$

At 25 °C, chemical lifetimes in fogs and clouds τ_{rxn}^{fog} were 0.3 to 4.7 hours (Table 5.2). This is shorter than or comparable to lifetimes due to chemical loss in the

absence of an aqueous phase. The chemical lifetime in the gas and particulate phases $\tau_{rxn}^{\mathrm{g,PM}}$ is estimated to range from 1 to 300 hours (Table 5.2; Keyte *et al*., 2013). $\tau_{rxn}^{\mathrm{fog}}$ is also shorter than physical loss processes: The lifetime of PAHs due to dry deposition τ_{drydep} is estimated to be 1 to 14 days and wet deposition τ_{wetdep} is 5 to 15 months (Bidleman, 1988; Škrdlíková *et al*., 2011). These lifetimes exceed the typical lifetime of aerosol particles in the atmosphere, τ_{dep}^{PM}, which are generally estimated as about one week.

Table 5.2

PAHs and oxy–PAHs Chemical Lifetimes τ and Fractions in the Gas Phase

PAH	τ (hours; fog model; 25 °C) [a]	τ (hours; no fog) [b]	x^g (fog model; 25 °C) [c]	x^g (no fog; –0.5 to 4 °C) [d]	x^g (no fog; 13 to 20 °C) [e]	x^g (no fog; 7 to 26 °C) [f]
NAP	2.5	13	> 0.99		0.98	> 0.99
ACY	0.29	1	> 0.99	0.97	> 0.99	
ACE	0.56	5	> 0.99	0.96	0.99	> 0.99
FLU	4.0	21	> 0.99	0.92	> 0.99	> 0.99
PHE	1.8	9	> 0.99	0.95	0.97	> 0.99
ANT	4.3	2	> 0.99	0.93	0.98	0.98 to > 0.99
FLT	3.1	14 to 25	> 0.99	0.87	0.76	< 0.01 to 0.99
PYR	1.1	5 to 6	> 0.99	0.91	0.72	< 0.01 to 0.99
ACP	3.5		> 0.99			
BAU	1.2		> 0.99			
BBU	1.2		0.99			
BAA	1.1	3 to 11	0.94	0.87	0.13	< 0.01 to 0.91
CHY	1.7	9 to 27	0.93	0.77	0.15	< 0.01 to 0.95
RET	1.3		> 0.99			
BBF	4.3	34 to > 330	0.57	0.30	0.03	< 0.01
BKF	1.7	8 to 21	0.57	0.11	0.04	< 0.01
BAP	0.92	2 to 5	0.46	0.16	0.10	< 0.01
BEP	2.0	10 to 15	0.59	0.11		
IND	4.7	6 to 9	0.10	0.08	0.03	< 0.01
DBA	2.9	34 to > 330	0.08	0.14	0.25	< 0.01
BGP	4.6	5	0.08	0.06	0.08	< 0.01

Notes: a, chemical lifetimes predicted in this study; b, gas / particle chemical lifetimes predicted by Keyte *et al*. (no fog present; 2013); c, fraction in the gas phase when a fog or cloud is present, predicted in this study; d, Alam *et al*., 2013; e, Liu *et al*., 2010; f, the range between six sites' annual averages (Eiguren-Fernandez *et al.*, 2004).

The final amounts of oxy–PAH products were influenced by a variety of factors, including PAH Y_m and chemical loss processes of oxy–PAHs. After three hours, 28% of the original carbon mass in PAHs was predicted to remain as carbon in PAHs and 0.93% as carbon in oxy–PAHs. The other 71% of the original carbon mass was not speciated in this work but would include monocyclic aromatics and non-aromatic organic compounds (Moza *et al*., 1999; Mallakin *et al*., 2000; Kong and Ferry, 2003; Woo *et al*., 2009).

5.4.3 Uncertainty in partitioning in the model predictions and variability in real fogs and clouds.

The main uncertainties in predicting PAH and oxy–PAH phase partitioning were the uncertainties in partition ratios. The lack of experimental K_{OW} for sixteen of the twenty five oxy–PAHs and experimental K_{OA} and H for all of the oxy–PAHs required estimates to be used. These uncertainties may well be on the same order of magnitude as variabilities in field measurements.

5.4.4 The influence of salts and co-solvents.

It is known that small-molecule (*e.g*., methanol, ethanol, and propanol) co-solvents can enhance PAH solubility (Fan and Jafvert, 1997; Yap *et al*., 2012). In fog in very polluted regions or in deliquesced aerosol water (*i.e*., low LWC), high concentrations of dissolved salts and organics can cause deviations from Henry's law. The salt effects on solubility are generally smaller than temperature effects over atmospherically relevant ranges. For example, Whitehouse (1984) reported 1 to 15% salting out PHE, ANT, and BAP for a salinity increase from 0 to 4‰ and a 24% salting-in effect for BAA over the same salinities; however, there was a 50 to 70% decrease in solubility when temperature decreased from 25 to 8 °C. Typically, fog water salinity is

about two orders of magnitude lower (0.07‰; Collett *et al*., 2008) than applied in the previous study. Shahpoury *et al*. (2015) found that ionic compounds had little impact on the scavenging of PAHs by rain when the salinity in rain increased from approximately 0.002 to 0.03‰. Therefore, under the fairly dilute conditions simulated in this work, it can be expected that ionic 'salting in' or 'salting out' effects are minor.

5.4.5 Influence of temperature on partitioning.

The temperature of this model was 25 °C, while typical fog and cloud observations in recent literature range from 0 to 19 °C (Capel *et al*., 1990; Erel *et al*., 1993; Herckes *et al*., 2002; Reyes-Rodríguez, *et al*., 2009; Ervens *et al*., 2013). The use of 25 °C was constrained by the availability of partition ratios and rate constants. Very few temperature-dependent partition ratios and rate constants have been published for PAHs and oxy–PAHs (Harner and Bidleman, 1998a; Frerichs *et al*., 1990; Lei *et al*., 2000; Odabasi *et al*., 2006).

Generally, the vapor pressure increase is greater than the solubility increase which results in lower $H^*$and K_{OA} at lower temperatures. The increase in water solubility is greater than the solubility increase in 1–octanol which results in lower K_{OW} as temperature increases. Therefore, K_{OA}, K_{OW}, and H^* increase with temperature. $H^*$is most affected by changes in temperature followed by K_{OA} and then K_{OW}. The change in K_{OA} and K_{OW} is seen in Figure D5a resulting in higher x^g at 25 °C than at 1 °C (x^g = 0.94 and $x^g \sim 0.4$ respectively). BAA was the only PAH of this study with temperature-dependent K_{OA} and K_{OW} partition ratios available (Lei *et al*., 2000; Odabasi *et al*., 2006). Assuming other PAHs have similar temperature dependencies, the x^g at 25 °C are 0.2 to 0.6 greater than x^g at 1 °C (Figure D5b) for PAHs whose K_{OA} are near the gas phase

boundary at 25 °C (*i.e.*, log K_{OA} ~ 10 to 12), including BAA, CHY, BBF, BKF, BAP, and BEP. Extrapolation of the oxy–PAH K_{OA}, K_{OW}, and x^g changes as a function of temperature were not attempted in Figure D5b since oxy–PAHs have additional (and stronger) intermolecular interactions that PAHs do not have, such as hydrogen bonding and dipole – dipole interactions.

My model calculations likely overestimated x^g for some PAHs in the presence of fogs and clouds as temperatures are typically lower than 25 °C and therefore under typical cloud/fog conditions the condensed phase may represent an even larger sink for PAHs as demonstrated by my analysis.

5.4.6 Heterogeneous surface reactions.

Heterogeneous reactions of PAHs adsorbed at the air / water interface have been reported for several PAHs (Valsaraj, 2004; Chen *et al*., 2006; Raja and Valsaraj, 2006; Kahan and Donaldson, 2007; Donaldson and Valsaraj, 2010; Styler *et al*., 2011). However, this work did not include heterogeneous PAH reactions at the air / water interface since it was assumed that the dissolution of PAHs in a liquid organic phase was lower in energy than the deposition of PAHs onto a water surface. A consideration of organic surface films on droplets is given later in the discussion. This work further did not include heterogeneous reactions of PAHs adsorbed at a water / solid interface, such as what might occur at the surface of a hygroscopic sub-micrometer particle entrained in the interior of a droplet. A comparison of CHY kinetic rate constants measured in water with those measured in a solution of smectite clay in water revealed little difference: Kong and Ferry (2003) reported $k(\text{smectite, aq}) = 4.3 \times 10^{-5}$ s^{-1} while Zepp and Schlotzhauer (1979) reported $k(\text{aq}) = 4.4 \times 10^{-5}$ s^{-1} and Fasnacht and Blough (2002) reported $k(\text{aq}) =$

9×10^{-5} s^{-1}. These are of similar magnitude as $k(\text{org}) = 6.8 \times 10^{-5}$ s^{-1} (Plata *et al*., 2008), $k(\text{aq, 10\% methanol}) = 1.4\times 10^{-5}$ s^{-1} (Kong and Ferry, 2003), and less than an order of magnitude smaller than CHY $k'(^{\bullet}\text{OH, g}) = 1.0 \times 10^{-4}$ s^{-1} (Calvert *et al*., 2002 with $[^{\bullet}\text{OH}] = 3 \times 10^{6}$ molecules cm^{-3}).

5.4.7 Coverage of the droplet surface by an organic film.

The geometry of the organic phase was not specified in this model other than each phase was in contact with the other two, *i.e*., no complete organic film on the drop surface (Figure 5.1). Many researchers have concluded that PAHs adsorb to water surfaces as hydrophobic surface layers (Moza *et al*., 1999; Valsaraj, 2004; Chen *et al*., 2006; Raja and Valsaraj, 2006; Kahan and Donaldson, 2007; Chen *et al*., 2011; Styler *et al*., 2011). Gill *et al*. (1983) estimated it would require 300 mg L^{-1} organic matter for the entire surface of fog drops with diameters 1 to 10 µm to be coated with an organic monolayer film. Depending on the compound, this equates to 180 to 250 mgC L^{-1} which is greater than the TOC reported in typical fog and clouds (0.1 to 40 mgC L^{-1}; Erel *et al*., 1993; Herckes *et al*., 2002; Raja *et al*., 2008; Reyes-Rodríguez, *et al*., 2009; Ehrenhauser *et al*., 2012; Ervens *et al*., 2013; Herckes *et al*., 2013; Herckes *et al*., 2015).

To more precisely estimate surface coverage, the dimensionless PAH surface film coverage θ^{PAH} was calculated in this work (Equation 5.7) from the total PAH surface area, $A^{\text{PAH}}\left[\text{m}^2\ \text{m}_{\text{air}}^{-3}\right]$, of the carbon backbone plane (*i.e*., the PAHs lying flat on the water surface; Chen *et al*., 2011) and the total fog droplet surface area, $A^{\text{fog}}\left[\text{m}^2\ \text{m}_{\text{air}}^{-3}\right]$. Equations D11 – D14 were used to find A^{PAH} and A^{fog}. Similarly, the liquid organic surface film coverage θ^{org} (Equation 5.8) was calculated from the cross-sectional area of an alkyl chain following Equation D15:

$$\theta^{\mathrm{PAH}} = A^{\mathrm{PAH}}/A^{\mathrm{fog}} \quad (5.7).$$

$$\theta^{\mathrm{org}} = A^{\mathrm{org}}/A^{\mathrm{fog}} \quad (5.8).$$

This work predicted (Equation 5.7) very small θ^{PAH}; for example, $\theta^{\mathrm{NAP}} = 1 \times 10^{-3}$, $\theta^{\mathrm{PYR}} = 3 \times 10^{-5}$, $\theta^{\mathrm{BAP}} = 5 \times 10^{-7}$, and $\theta^{\mathrm{DBA}} = 1 \times 10^{-7}$. Even if all TOC (5 mgC L^{-1}) was completely water immiscible and had the molecular dimensions of 1–octanol, the coverage of the droplet would be $\theta^{\mathrm{org}} < 1.3\%$ for 10 μm droplets (Equation 5.8). Thus, under all circumstances, the surface of a typical fog or cloud droplet would be too large to be wholly covered with an organic monolayer.

5.5 SUMMARY

The phase distribution of PAHs and oxy–PAHs was predicted using a multiphase box model that includes gas, aqueous and organic phases. At 25 °C, PAHs with two, three and four rings were predicted to be primarily in the gas phase ($x^{\mathrm{g}} > 92\%$) while five- and six-ring PAHs partitioned significantly into droplets ($x^{\mathrm{fog}} > 40\%$). At lower temperatures, such as those typical of fogs and clouds, the fraction of PAHs in the aqueous phase is expected to be even higher.

The oxidation of PAHs in the multiphase system was predicted to result in significantly shorter lifetimes (< 5 hours) than dry and wet deposition processes (1 – 14 days, 5 – 15 months, respectively) and shorter or comparable lifetimes of PAHs relative to oxidation in the gas / particulate system (1 to 300 hours). At 25 °C, gas-phase $^{\bullet}$OH was the predicted to be an important but not always dominant process of removal of PAHs; the k(aq) of ANT, RYR, BAA, and BAP were > $k'(^{\bullet}\mathrm{OH,\ g})$. Even though PAHs are not very soluble, the aqueous phase cannot be neglected as their sink due to the large aqueous volume (*vs*. organic volume) and the relatively fast aqueous reactions. The fraction

weighted loss rates $x^{\mathrm{g}}k'(^{\bullet}\mathrm{OH},\ \mathrm{g})$ for BBF, BKF, BAP, BEP were the same order of magnitude as $x^{\mathrm{org}}k(\mathrm{org})$ but for IND, DBA, BGP, $x^{\mathrm{org}}k(\mathrm{org}) > x^{\mathrm{g}}k'(^{\bullet}\mathrm{OH},\ \mathrm{g})$.

The surface of typical fog and cloud droplets (d = 10 μm, TOC < 50 mgC L^{-1}) was predicted to be too large to be completely covered by a liquid organic surface film. Consequently, a multiphase geometry where each phase is in contact with the others was employed.

The most sensitive parameters that may require more studies include temperature dependent K_{OW} and K_{OA} values; many in this model were estimates from the EPISuite and/or reported only at 25 °C. As an example, BAA is expected have x^{g} = 0.94 at 25 °C and x^{g} ~ 0.4 at 1 °C. Additionally, liquid-organic and aqueous-phase photooxidation rate constants were unavailable for many of the PAHs and most of the oxy–PAHs. Despite their low water solubilities, PAHs process faster when clouds and fog are present than in cloudless conditions.

CHAPTER 6

SUMMARY

The chapters in this thesis report the investigation and findings of four areas of research. In Chapter 2, a robust methodological characterization of haboob events based on meteorological and air pollution observations was established and employed for the creation of a library of haboob events, which was necessary for the calculation of dry deposition of air-borne particles.

Between 3 and 20 haboob events occur per year and a somewhat lower number of haboob events occur in years with higher precipitation. The relationship between precipitation and haboob occurrence is complex due to the bimodality of seasonal precipitation as well as the mutual source of haboobs and monsoon precipitation.

The dry deposition flux predicted for Tempe, AZ ranged from a low of 259 kg ha^{-1} in 2010 to a high of 2950 kg ha^{-1} in 2011. The calculated flux is comparable to deposition in other parts of the world. The haboob library and the dry deposition flux are further employed in Chapters 3 and 4.

Chapter 3 reports the calculation of particle dissolution and settling in Tempe Town Lake, which was necessary for the prediction of haboob - induced increases in DOC in Tempe Town Lake. Haboob deposition could be responsible for some of the small changes in the lake, such as DOC, conductivity, and water clarity. The coincidence of haboobs and lake biogeochemical changes was not consistent for every haboob.

Larger changes in lake biogeochemistry (*e.g.*, change by factors of one to seven times) in many, but not all, cases coincided with rain and streamflow into the lake

In Chapter 4, I report the sampling and analysis of PAHs in haboob $PM_{2.5}$. I investigated haboob-induced changes in PAH concentrations and elucidated sources through PAH isomer ratio comparisons. I found that haboobs do alter the PAH concentrations and distributions in Tempe, AZ. PAH isomer ratios suggest $PM_{2.5}$ sources consistent with approximate thunderstorm outflow paths. The increase in PAHs during haboobs appears to be proportional to $PM_{2.5}$ increases and is likely a consequence of transporting PAH-laden $PM_{2.5}$ from surrounding areas.

Field observations have not been able to establish to what extent clouds/fog can process PAHs relative to cloudless conditions. I describe in Chapter 5 the calculation of PAH phase distribution in clouds and fog, which is necessary to predict the processing and lifetimes of PAH present in clouds and fog. With my model I show that PAH processing in clouds and fog results in shorter PAH lifetimes than the lifetimes in cloudless atmospheric conditions. Notwithstanding the low water solubilities of PAHs, the atmospheric aqueous phase cannot be ignored in the analysis of PAH fate in the atmosphere.

6.1 OUTLOOK

This thesis describes advancements in research and understanding of haboobs and PAH processing. Future research can build off these findings. The robust method of single-site haboob identification (Chapter 2) can be employed in other areas surrounding Tempe, AZ as part of the Central Arizona – Phoenix Long-Term Ecological Research (CAP-LTER). Furthermore, the haboob library and deposition database can be employed in future CAP-LTER studies.

The calculation of dry deposition flux (Chapter 2) employs a particle size distribution that is based on literature studies and reasonable assumptions. In future research, the actual mass distribution and the air-concentration of TSP in Tempe could be monitored to for more precise prediction of haboob deposition. This would require alternative sampling techniques not currently employed by the EPA air quality monitoring system. These could include: optical particle counters, Micro-Orifice Uniform Deposit Impactor (MOUDI) samplers, and deposition traps. Commercial optical particle counters boast the ability to estimate the mass of particles with a wide range of diameters (*e.g.*, 0.1 – 1000 μm) but cannot adequately be used to measure particle air-concentrations. An automated TSP sampling device with hourly temporal resolution capable of quantifying the concentrations of particles with diameters from < 0.1 to > 500 μm is not commercially available at the present. MOUDI samplers and deposition traps can be somewhat labor intensive sampling techniques, may not be amenable to sub-hourly and hourly sampling frequencies (the temporal resolution of haboob events) due to sample-size constraints, and can only partially sample the six orders of magnitude range of particle diameters of interest (0.01 – 1000 μm) without producing significant biases.

The advancement of broad-range TSP sampling technologies may not have been of commercial interest in the past since PM_{10} and $PM_{2.5}$ but not $PM_{>10}$ are regulated by the EPA. The short atmospheric lifetimes of $PM_{>10}$ and its aerodynamic exclusion from the recesses of the lungs may have limited past interest in regulating it or routinely sampling it. The development of broader-range TSP samplers may well be of interest to federal funding agencies due to current concerns of extreme weather events as well as concerns for local and global climate changes.

In Chapter 3, haboob deposition consequences on Tempe Town Lake biogeochemistry are predicted in two scenarios: complete particle dissolution and the complete lack of particle dissolution. The timescales of particle dissolution and lake mixing are not known at the present. Theoretical and observational studies could elucidate their actual timescales. However, such efforts may not be warranted since haboobs are not consistently coincident with changes in lake DOC, conductivity, and clarity. Furthermore, the coincident changes which were identified are not as large as many of the extreme-flow event induced changes. Research efforts would, perhaps, be better employed within other components of the urban ecological system of Tempe, such as soils. Funding agencies may desire to prioritize funding to efforts which elucidate phenomena with greater impact on public health and the environment.

There are measurements that have already been performed of other biogeochemical parameters in Tempe Town Lake not considered in Chapter 3, such as daily trace metals data and 2D fluorescence. These databases could be published and compared with the haboob library and deposition database.

In Chapter 4, the observed changes in urban air quality in terms of PAHs in $PM_{2.5}$ during haboobs are reported. This bolsters other research efforts currently underway for other chemical species in $PM_{2.5}$ as well as the results already reported in Aurelie Marcotte's PhD thesis (2015). Chapter 4 contributes greatly to the understanding of haboob redistribution of one of the EPA priority compounds.

In Chapter 5, the lifetimes of PAHs in clouds and fog are calculated to be shorter than when clouds and fog are absent. This has historically been challenging to observe in the field due to limitations of sample size and detection limits. Herckes *et al*. (2016)

reported that fogs have lower liquid water content than in past decades in the central valley of California, the location of many literature fog studies, which has further limited sample sizes. While PAHs are a priority pollutant and while clouds and fog are an important part of the atmosphere, it seems at the present that very little field research of fog and cloud chemistry is being funded by the National Science Foundation. Therefore, Chapter 5 is a significant contribution to the understanding of PAH processing in the atmosphere but may not be readily validated in the field in the near future.

To conclude, I mention lightheartedly that clouds remain somewhat of a "gray" area in the atmosphere (in terms of understood processes and climatic impact) and that "sky is the limit" in atmospheric biogeochemical research (although that may sound somewhat insulting and narrow sighted to oceanic, crustal, and space scientists).

REFERENCES

ADEQ (Arizona Department of Environmental Quality). (2015). ADEQ Air Quality Division: Natural and Exceptional Events. Retrieved December 2, 2015 from https://www.azdeq.gov/environ/air/plan/nee.html

Alaee, M., Whittal, R. M., & Strachan, W. M. J. (1996). The effect of water temperature and composition on Henry's law constant for various PAH's. *Chemosphere*, *32*, 1153–1164. http://doi.org/10.1016/0045-6535(96)00031-8

Alam, M. S., Delgado-Saborit, J. M., Stark, C., & Harrison, R. M. (2013). Using atmospheric measurements of PAH and quinone compounds at roadside and urban background sites to assess sources and reactivity. *Atmospheric Environment*, *77*, 24–35. http://doi.org/10.1016/j.atmosenv.2013.04.068

Albinet, A., Leoz-Garziandia, E., Budzinski, H., & ViIlenave, E. (2007). Polycyclic aromatic hydrocarbons (PAHs), nitrated PAHs and oxygenated PAHs in ambient air of the Marseilles area (South of France): Concentrations and sources. *Science of The Total Environment*, *384*, 280–292. http://doi.org/10.1016/j.scitotenv.2007.04.028

Atkinson, R. (1989). Kinetics and Mechanisms of the Gas-Phase Reactions of the Hydroxyl Radical with Organic Compounds. *Journal of Physical and Chemical Reference Data, Monogram 1*. 1–246. Retrieved March 11, 2016, from http://www.nist.gov/data/PDFfiles/jpcrdM1.pdf

Atkinson, R. (1991). Kinetics and Mechanisms of the Gas-Phase Reactions of the NO3 Radical with Organic Compounds. *Journal of Physical and Chemical Reference Data*, *20*, 459–507. http://doi.org/10.1063/1.555887

Atkinson, R., & Aschmann, S. M. (1987). Kinetics of the gas-phase reactions of alkylnaphthalenes with O_3, N_2O_5 and OH radicals at 298 ± 2 K. *Atmospheric Environment (1967)*, *21*, 2323–2326. http://doi.org/10.1016/0004-6981(87)90367-2

Atkinson, R., & Aschmann, S. M. (1988). Kinetics of the reactions of acenaphthene and acenaphthylene and structurally-related aromatic compounds with OH and NO_3 radicals, N_2O_5 and O_3 at 296 ± 2 K. *International Journal of Chemical Kinetics*, *20*, 513–539. http://doi.org/10.1002/kin.550200703

Atkinson, R., Arey, J., Zielinska, B., & Aschmann, S. M. (1987). Kinetics and Products of the Gas-Phase Reactions of OH Radicals and N_2O_5 with Naphthalene and Biphenyl. *Environmental Science & Technology*, *21*, 1014–1022. http://doi.org/10.1021/es50001a017

Atkinson, R., Arey, J., Zielinska, B., & Aschmann, S. M. (1990). Kinetics and nitro-products of the gas-phase OH and NO_3 radical-initiated reactions of naphthalene-d_8, Fluoranthene-d_{10}, and pyrene. *International Journal of Chemical Kinetics*, *22*, 999–1014. http://doi.org/10.1002/kin.550220910

Atkinson, R., Aschmann, S. M., & Pitts, J. N. (1984). Kinetics of the reactions of naphthalene and biphenyl with hydroxyl radicals and with ozone at 294 .+-. 1 K. *Environmental Science & Technology*, *18*, 110–113. http://doi.org/10.1021/es00120a012

ATSDR (Agency for Toxic Substances & Disease Registry). (1995). Toxicological Profile for Polycyclic Aromatic Hydrocarbons (PAHs). Centers for Disease Control and Prevention, U.S. Department of Health and Human Services, Public Health Service. Atlanta, GA. Retrieved June 27, 2016, from http://www.atsdr.cdc.gov/toxprofiles/tp69.pdf

Ball, B. A., & Alvarez-Guevara, J. (2015). The nutrient plasticity of moss-dominated crust in the urbanized Sonoran Desert. *Plant and Soil*, *389*, 225–235. http://doi.org/10.1007/s11104-014-2355-7

Bamford, H. A., Poster, Di. L., & Baker, J. E. (1999). Temperature dependence of Henry's law constants of thirteen polycyclic aromatic hydrocarbons between 4°C AND 31°C. *Environmental Toxicology and Chemistry*, *18*, 1905–1912. http://doi.org/10.1002/etc.5620180906

Banerjee, S., Yalkowsky, S. H., & Valvani, C. (1980). Water solubility and octanol/water partition coefficients of organics. Limitations of the solubility-partition coefficient correlation. *Environmental Science & Technology*, *14*, 1227–1229. http://doi.org/10.1021/es60170a013

Barry, M., Chiu, C.-A., & Westerhoff, P. (2016). Severe Weather Effects on Water Quality in Central Arizona. *American Water Works Association*, *108*, E221–E231. http://doi.org/10.5942/jawwa.2016.108.0027

Bateman, H. L., Stromberg, J. C., Banville, M. J., Makings, E., Scott, B. D., Suchy, A., & Wolkis, D. (2015). Novel water sources restore plant and animal communities along an urban river. *Ecohydrology*, *8*, 1936–592. http://doi.org/10.1002/eco.1560

Bidleman, T. F. (1988). Atmospheric processes– wet and dry deposition of organic compounds are controlled by their vapor-particle partitioning. *Environmental Science & Technology*, *22*, 361–367. http://doi.org/10.1021/es00169a002

Bond, T. C., Streets, D. G., Yarber, K. F., Nelson, S. M., Woo, J.-H., & Klimont, Z. (2004). A technology-based global inventory of black and organic carbon emissions from combustion. *Journal of Geophysical Research: Atmospheres*, *109*, D14203. http://doi.org/10.1029/2003JD003697

Box, M. A., Radhi, M., & Box, G. P. (2010). The great Sydney dust event: Size-resolved chemical composition and comparison. 17th National Conference of the Australian Meteorological and Oceanographic Society. *IOP Conference Series: Earth and Environmental Science*, *11*, 12015. http://doi.org/10.1088/1755-1315/11/1/012015

Brazel, A. J. (1989). Dust and Climate in the American Southwest. In M. Leinen & M. Sarnthein (Eds.), *Paleoclimatology and Paleometeorology: Modern and Past Patterns of Global Atmospheric Transport* (Vol. 282, pp. 65–96). Dordrecht: Springer Netherlands. Retrieved from http://dx.doi.org/10.1007/978-94-009-0995-3_3 ISBN: 978-94-009-0995-3

Brazel, A. J., & Nickling, W. G. (1986). The relationship of weather types to dust storm generation in Arizona (1965–1980). *Journal of Climatology*, *6*, 255–275. http://doi.org/10.1002/joc.3370060303

Cahill, T. M. (2013). Annual cycle of size-resolved organic aerosol characterization in an urbanized desert environment. *Atmospheric Environment*, *71*, 226–233. http://doi.org/10.1016/j.atmosenv.2013.02.004

Calvert, J. G., Atkinson, R., Becker, K. H., Kamens, R. M., Seinfeld, J. H., Wallington, T. H., & Yarwood, G. (2002). *The Mechanisms of Atmospheric Oxidation of the Aromatic Hydrocarbons*. Oxford University Press. New York, New York, 134–195.

Capel, P. D., Gunde, R., Zuercher, F., & Giger, W. (1990). Carbon speciation and surface tension of fog. *Environmental Science & Technology*, *24*, 722–727. http://doi.org/10.1021/es00075a017

Capel, P. D., Leuenberger, C., & Giger, W. (1991). Hydrophobic organic chemicals in urban fog. *Atmospheric Environment*, *25*, 1335–1346. http://doi.org/10.1016/0960-1686(91)90244-2

Chemicalize.org (2015). ChemAxon, Cambridge, MA. Retrieved May 18, 2015, from http://www.chemicalize.org/structure/#!mol=CCCCCCCCO

Chemicalize.org (2016a). ChemAxon, Cambridge, MA. Retrieved February 25, 2016, from http://www.chemicalize.org/structure/#!mol=benzo(a)pyrene

Chemicalize.org (2016b). ChemAxon, Cambridge, MA. Retrieved February 25, 2016, from http://www.chemicalize.org/structure/#!mol=dibenzo(a%2Ch)anthracene

Chemicalize.org (2016c). ChemAxon, Cambridge, MA. Retrieved February 25, 2016, from http://www.chemicalize.org/structure/#!mol=naphthalene

Chemicalize.org (2016d). ChemAxon, Cambridge, MA. Retrieved February 25, 2016, from http://www.chemicalize.org/structure/#!mol=pyrene

Chen, J., Ehrenhauser, F. S., Liyana-Arachchi, T. P., Hung, F. R., Wornat, M. J., & Valsaraj, K. T. (2011). Adsorption of Gas-Phase Phenanthrene on Atmospheric Water and Ice Films. *Polycyclic Aromatic Compounds*, *31*, 201–226. http://doi.org/10.1080/10406638.2011.585370

Chen, J., Ehrenhauser, F. S., Valsaraj, K. T., & Wornat, M. J. (2006). Uptake and UV-Photooxidation of Gas-Phase PAHs on the Surface of Atmospheric Water Films. 1. Naphthalene. *The Journal of Physical Chemistry A*, *110*, 9161–9168. http://doi.org/10.1021/jp062560b

Chen, W., & Fryrear, D. W. (2002). Sedimentary characteristics of a haboob dust storm. *Atmospheric Research*, *61*, 75–85. http://doi.org/10.1016/S0169-8095(01)00092-8

Chepil, W. S. (1957). Sedimentary characteristics of dust storms; Part III, Composition of suspended dust. *American Journal of Science*, *255*, 206–213. http://doi.org/10.2475/ajs.255.3.206

Chepil, W. S., & Woodruff, N. P. (1957). Sedimentary characteristics of dust storms; Part II, Visibility and dust concentration. *American Journal of Science*, *255*, 104–114. http://doi.org/10.2475/ajs.255.2.104

City of Tempe, AZ. (2015). Town Lake Water Quality. Retrieved November 19, 2015, from http://www.tempe.gov/city-hall/community-development/tempe-town-lake/how-town-lake-works/town-lake-water-quality

City of Tempe, AZ. (2016). Town Lake Fast Facts. Retrieved May 9, 2016, from http://www.tempe.gov/city-hall/community-development/tempe-town-lake/fast-facts-coloring-book-slideshows-and-videos/town-lake-fast-facts

Clark, C. D., De Bruyn, W. J., Ting, J., & Scholle, W. (2007). Solution medium effects on the photochemical degradation of pyrene in water. *Journal of Photochemistry and Photobiology A: Chemistry*, *186*, 342–348. http://doi.org/10.1016/j.jphotochem.2006.09.003

Clements, A. L., Fraser, M. P., Herckes, P., & Solomon, P. A. (2016). Chemical mass balance source apportionment of fine and PM_{10} in the Desert Southwest, USA. *AIMS Environmental Science*, *3*, 115–132. http://doi.org/10.3934/environsci.2016.1.115

Clements, A. L., Fraser, M. P., Upadhyay, N., Herckes, P., Sundblom, M., Lantz, J., & Solomon, P. A. (2013). Characterization of summertime coarse particulate matter in the Desert Southwest-Arizona, USA. *Journal of the Air & Waste Management Association*, *63*, 764–772. http://doi.org/10.1080/10962247.2013.787955

Clements, A. L., Fraser, M. P., Upadhyay, N., Herckes, P., Sundblom, M., Lantz, J., & Solomon, P. A. (2014). Chemical characterization of coarse particulate matter in the Desert Southwest – Pinal County Arizona, USA. *Atmospheric Pollution Research*, *5*, 52–61. http://doi.org/10.5094/APR.2014.007

Collett Jr., J. L., Herckes, P., Youngster, S., & Lee, T. (2008). Processing of atmospheric organic matter by California radiation fogs. *Atmospheric Research*, *87*, 232–241. http://doi.org/10.1016/j.atmosres.2007.11.005

Davis, M. K., Cook, E. M., Collins, S. L., & Hall, S. J. (2015). Top-down vs. bottom-up regulation of herbaceous primary production and composition in an arid, urbanizing ecosystem. *Journal of Arid Environments*, *116*, 103–114. http://doi.org/10.1016/j.jaridenv.2015.01.018

de Maagd, P. G.-J., ten Hulscher, D. T. E. M., van den Heuvel, H., Opperhuizen, A., & Sijm, D. T. H. M. (1998). Physicochemical properties of polycyclic aromatic hydrocarbons: Aqueous solubilities, n-octanol/water partition coefficients, and Henry's law constants. *Environmental Toxicology and Chemistry*, *17*, 251–257. http://doi.org/10.1002/etc.5620170216

De Voogt, P., Van Zijl, G. A., Govers, H., & Brinkman, U. A. T. (1990). Reversed-phase TLC and structure-activity relationships of polycyclic (hetero) aromatic hydrocarbons. *Journal of Planar Chromatography--Modern TLC*, *3*, 24–33.

Delgado-Saborit, J. M., Alam, M. S., Godri Pollitt, K. J., Stark, C., & Harrison, R. M. (2013). Analysis of atmospheric concentrations of quinones and polycyclic aromatic hydrocarbons in vapour and particulate phases. *Atmospheric Environment*, *77*, 974–982. http://doi.org/10.1016/j.atmosenv.2013.05.080

Donaldson, D. J., & Valsaraj, K. T. (2010). Adsorption and Reaction of Trace Gas-Phase Organic Compounds on Atmospheric Water Film Surfaces: A Critical Review. *Environmental Science & Technology*, *44*, 865–873. http://doi.org/10.1021/es902720s

Drees, L. R., Manu, A., & Wilding, L. P. (1993). Characteristics of aeolian dusts in Niger, West Africa. *Geoderma*, *59*, 213–233. http://doi.org/10.1016/0016-7061(93)90070-2

Ehrenhauser, F. S., Khadapkar, K., Wang, Y., Hutchings, J. W., Delhomme, O., Kommalapati, R. R., … Valsaraj, K. T. (2012). Processing of atmospheric polycyclic aromatic hydrocarbons by fog in an urban environment. *Journal of Environmental Monitoring*, *14*, 2566–2579. http://doi.org/10.1039/c2em30336a

Eiguren-Fernandez, A., Miguel, A. H., Froines, J. R., Thurairatnam, S., & Avol, E. L. (2004). Seasonal and Spatial Variation of Polycyclic Aromatic Hydrocarbons in Vapor-Phase and $PM_{2.5}$ in Southern California Urban and Rural Communities. *Aerosol Science and Technology*, *38*, 447–455. http://doi.org/10.1080/02786820490449511

EPA (United States Environmental Protection Agency). (2006). The Treatment of Data Influenced by Exceptional Events; Proposed Rule. *Federal Register*, *71*, 12592–12610.

EPA (United States Environmental Protection Agency). (2007). Treatment of Data Influenced by Exceptional Events; Final Rule. *Federal Register*, *72*, 13560–13581.

EPA (United States Environmental Protection Agency). (2010). National Primary Drinking Water Regulations: Maximum Contaminant Levels and Maximum Residual Disinfectant Levels. *Code of Federal Regulations*, Title 40, Subpart G § 141.60

EPA (United States Environmental Protection Agency). (2013). National Ambient Air Quality Standards for Particulate Matter: Final Rule, *Federal Register*, *78*, 3085–3287. Retrieved December 1, 2015, from http://www.gpo.gov/fdsys/pkg/FR-2013-01-15/pdf/2012-30946.pdf

EPA (United States Environmental Protection Agency). (2014a). Table 1. Dose Response Assessment Tables. Retrieved January 19, 2015, from www2.epa.gov/sites/production/files/2014-05/documents/table1.pdf

EPA (United States Environmental Protection Agency). (2014b). 126 Priority Pollutants, Appendix A to Part 423. *Code of Federal Regulations*, Title 40, Vol 29.

EPA (United States Environmental Protection Agency). (2015a). Overview of the Clean Air Act and Air Pollution: Evolution of the Clean Air Act. Retrieved June 24, 2016, from https://www.epa.gov/clean-air-act-overview/evolution-clean-air-act

EPA (United States Environmental Protection Agency). (2015b). AirData: Query AirData. Retrieved July 2, 2015, from https://aqs.epa.gov/api

EPISuite. (2015). EPISuite v 4.11 Estimation Programs Interface Suite™ for Microsoft® Windows. United States Environmental Protection Agency: Washington, DC.

Erel, Y., Pehkonen, S. O., & Hoffmann, M. R. (1993). Redox chemistry of iron in fog and stratus clouds. *Journal of Geophysical Research: Atmospheres*, *98*, 18423–18434. http://doi.org/10.1029/93JD01575

Ervens, B., Wang, Y., Eagar, J. D., Leaitch, W. R., Macdonald, A. M., Valsaraj, K. T., & Herckes, P. (2013). Dissolved organic carbon (DOC) and select aldehydes in cloud and fog water: the role of the aqueous phase in impacting trace gas budgets. *Atmospheric Chemistry and Physics*, *13*, 5117–5135. http://doi.org/10.5194/acp-13-5117-2013

Fasnacht, M. P., & Blough, N. V. (2002). Aqueous Photodegradation of Polycyclic Aromatic Hydrocarbons. *Environmental Science & Technology*, *36*, 4364–4369. http://doi.org/10.1021/es025603k

Fernández, P., Grimalt, J. O., & Vilanova, R. M. (2002). Atmospheric Gas-Particle Partitioning of Polycyclic Aromatic Hydrocarbons in High Mountain Regions of Europe. *Environmental Science & Technology*, *36*, 1162–1168. http://doi.org/10.1021/es010190t

Finlayson-Pitts, B. J., & Pitts, Jr., J. N. (1999). *Chemistry of the Upper and Lower Atmosphere* (1st ed.). San Diego, CA: Academic Press.

Fioressi, S., & Arce, R. (2005). Photochemical Transformations of Benzo[e]pyrene in Solution and Adsorbed on Silica Gel and Alumina Surfaces. *Environmental Science & Technology*, *39*, 3646–3655. http://doi.org/10.1021/es049192e

Flood Control District of Maricopa County. (2016). ALERT System – Single-Sensor Data. Retrieved June 10, 2016, from http://www.fcd.maricopa.gov/Weather/Rainfall/ALERT/ssdata.aspx

Fraser, M. P., Yue, Z. W., Tropp, R. J., Kohl, S. D., & Chow, J. C. (2002). Molecular composition of organic fine particulate matter in Houston, TX. *Atmospheric Environment*, *36*, 5751–5758. http://doi.org/10.1016/S1352-2310(02)00725-2

Frerichs, H., Tappe, M., & Wagner, H. G. (1990). Comparison of the Reactions of Mono- and Polycyclic Aromatic Hydrocarbons with Oxygen Atoms. *Berichte Der Bunsengesellschaft Für Physikalische Chemie*, *94*, 1404–1407. http://doi.org/10.1002/bbpc.199000043

Gill, P. S., Graedel, T. E., & Weschler, C. J. (1983). Organic films on atmospheric aerosol particles, fog droplets, cloud droplets, raindrops, and snowflakes. *Reviews of Geophysics*, *21*, 903–920. http://doi.org/10.1029/RG021i004p00903

Gillette, D. A., Clayton, R. N., Mayeda, T. K., Jackson, M. L., & Sridhar, K. (1978). Tropospheric Aerosols from Some Major Dust Storms of the Southwestern United States. *Journal of Applied Meteorology*, *17*, 832–845. http://doi.org/10.1175/1520-0450(1978)017<0832:TAFSMD>2.0.CO;2

Giraudeau, M., Chavez, A., Toomey, M. B., & McGraw, K. J. (2015). Effects of carotenoid supplementation and oxidative challenges on physiological parameters and carotenoid-based coloration in an urbanization context. *Behavioral Ecology and Sociobiology*, *69*, 957–970. http://doi.org/10.1007/s00265-015-1908-y

Goossens, D., & Offer, Z. Y. (1995). Comparisons of day-time and night-time dust accumulation in a desert region. *Journal of Arid Environments*, *31*, 253–281. http://doi.org/10.1016/S0140-1963(05)80032-1

Goss, K.-U. (1994). Predicting the enrichment of organic compounds in fog caused by adsorption on the water surface. *Atmospheric Environment*, *28*, 3513–3517. http://doi.org/10.1016/1352-2310(94)90008-6

Goudie, A. S. (1983). Dust storms in space and time. *Progress in Physical Geography*, *7*, 502–530. http://doi.org/10.1177/030913338300700402

Goudie, A. S., & Middleton, N. J. (2000). Dust storms in South West Asia. *Acta Universitatis Carolinae*, *XXXV*, 73–83.

Grossman, J. N., Stern, A. P., Kirich, M. L., & Kahan, T. F. (2016). Anthracene and pyrene photolysis kinetics in aqueous, organic, and mixed aqueous-organic phases. *Atmospheric Environment*, *128*, 158–164. http://doi.org/10.1016/j.atmosenv.2015.12.049

Hagen, L., & Woodruff, N., (1973). Air Pollution from Duststorms in the Great Plains. *Atmospheric Environment*, *7*, 323–332. doi: 10.1016/0004-6981(73)90081-4

Hall, S., & Marusenko, Y. (2009). Environmental fate of combustion-derived organic compounds in arid, urban soils in central Arizona-Phoenix. Retrieved February 13, 2014, from https://sustainability.asu.edu/caplter/data/data-catalog/view/knb-lter-cap.557.9/

Hamilton, G. A., & Hartnett, H. E. (2013). Soot black carbon concentration and isotopic composition in soils from an arid urban ecosystem. *Organic Geochemistry*, *59*, 87–94. http://doi.org/10.1016/j.orggeochem.2013.04.003

Hansch, C., Leo, A., & Hoekman, D. H. (1995). *Exploring QSAR.: Hydrophobic, electronic, and steric constants*. American Chemical Society. Washington, DC, 1995; pp 348

Harner, T., & Bidleman, T. F. (1998a). Measurement of Octanol−Air Partition Coefficients for Polycyclic Aromatic Hydrocarbons and Polychlorinated Naphthalenes. *Journal of Chemical & Engineering Data*, *43*, 40–46. http://doi.org/10.1021/je970175x

Harner, T., & Bidleman, T. F. (1998b). Octanol−Air Partition Coefficient for Describing Particle/Gas Partitioning of Aromatic Compounds in Urban Air. *Environmental Science & Technology*, *32*, 1494–1502. http://doi.org/10.1021/es970890r

Hartnett, H. E. To be submitted for publication, 2016.

Helmig, D., & Harger, W. P. (1994). OH radical-initiated gas-phase reaction products of phenanthrene. *Science of The Total Environment*, *148*, 11–21. http://doi.org/10.1016/0048-9697(94)90368-9

Helmig, D., Arey, J., Atkinson, R., Harger, W. P., & McElroy, P. A. (1992). Products of the OH radical-initiated gas-phase reaction of fluorene in the presence of NOx. *Atmospheric Environment, 26A*, 1735–1745. http://doi.org/10.1016/0960-1686(92)90071-R

Herckes, P., Hannigan, M. P., Trenary, L., Lee, T., & Collett Jr., J. L. (2002). Organic compounds in radiation fogs in Davis (California). *Atmospheric Research*, *64*, 99–108. http://doi.org/10.1016/S0169-8095(02)00083-2

Herckes, P., Marcotte, A. R., Wang, Y., & Collett Jr., J. L. (2015). Fog composition in the Central Valley of California over three decades. Sixth International Conference on Fog, Fog Collection and Dew, *Atmospheric Research*, *151*, 20–30. http://doi.org/10.1016/j.atmosres.2014.01.025

Herckes, P., Valsaraj, K. T., & Collett Jr., J. L. (2013). A review of observations of organic matter in fogs and clouds: Origin, processing and fate. *Atmospheric Research*, *132–133*, 434–449. http://doi.org/10.1016/j.atmosres.2013.06.005

Holcombe, T. L., Ley, T., & Gillette, D. A. (1997). Effects of Prior Precipitation and Source Area Characteristics on Threshold Wind Velocities for Blowing Dust Episodes,

Sonoran Desert 1948–78. *Journal of Applied Meteorology*, *36*, 1160–1175. http://doi.org/10.1175/1520-0450(1997)036<1160:EOPPAS>2.0.CO;2

Huffington Post (2011). Phoenix Dust Storm: Arizona Hit With Monstrous 'Haboob' *Huffington Post*, Posted: Jul 6, 2011. Retrieved November 20, 2015, from http://www.huffingtonpost.com/2011/07/06/phoenix-dust-storm-photos-video_n_891157.html

Hulscher, T. E. M. T., Van Der Velde, L. E., & Bruggeman, W. A. (1992). Temperature dependence of henry's law constants for selected chlorobenzenes, polychlorinated biphenyls and polycyclic aromatic hydrocarbons. *Environmental Toxicology and Chemistry*, *11*, 1595–1603. http://doi.org/10.1002/etc.5620111109

Hyers, A. D., & Marcus, M. G. (1981). Land use and desert dust hazards in central Arizona. *Geological Society of America Special Papers*, *186*, 267–280. http://doi.org/10.1130/SPE186-p267

Idso, S. B. (1976). Dust Storms. *Scientific American*, *235*, 108–114. http://doi.org/10.1038/scientificamerican1076-108

Idso, S. B., Ingram, R. S., & Pritchard, J. M. (1972). An American Haboob. *Bulletin of the American Meteorological Society*, *53*, 930–935. http://doi.org/10.1175/1520-0477(1972)053<0930:AAH>2.0.CO;2

Jang, M., & McDow, S. R. (1997). Products of Benz[a]anthracene Photodegradation in the Presence of Known Organic Constituents of Atmospheric Aerosols. *Environmental Science & Technology*, *31*, 1046–1053. http://doi.org/10.1021/es960559s

Jenerette, G. D., & Wu, J. (2001). Analysis and simulation of land-use change in the central Arizona – Phoenix region, USA. *Landscape Ecology*, *16*, 611–626. http://doi.org/10.1023/A:1013170528551

Joseph, P. V. (1982). A tentative model of Andhi. *Mausam*, *33*, 417–422.

Joseph, P. V., Raipal, D. K., & Deka, S. N. (1980). Andhi, the convective dust-storm of northwest India. *Mausam*, *31*, 431–442.

Kahan, T. F., & Donaldson, D. J. (2007). Photolysis of Polycyclic Aromatic Hydrocarbons on Water and Ice Surfaces. *The Journal of Physical Chemistry A*, *111*(7), 1277–1285. http://doi.org/10.1021/jp066660t

Keyte, I. J., Harrison, R. M., & Lammel, G. (2013). Chemical reactivity and long-range transport potential of polycyclic aromatic hydrocarbons – a review. *Chemical Society Reviews*, *42*, 9333–9391. http://doi.org/10.1039/C3CS60147A

Kong, L., & Ferry, J. L. (2003). Effect of Salinity on the Photolysis of Chrysene Adsorbed to a Smectite Clay. *Environmental Science & Technology*, *37*, 4894–4900. http://doi.org/10.1021/es026124o

Kwok, E. S. C., Atkinson, R., & Arey, J. (1997). Kinetics of the gas-phase reactions of indan, indene, fluorene, and 9,10-dihydroanthracene with OH radicals, NO_3 radicals, and O_3. *International Journal of Chemical Kinetics*, *29*, 299–309. http://doi.org/10.1002/(SICI)1097-4601(1997)29:4<299::AID-KIN9>3.0.CO;2-P

Kwok, E. S. C., Harger, W. P., Arey, J., & Atkinson, R. (1994). Reactions of Gas-Phase Phenanthrene under Simulated Atmospheric Conditions. *Environmental Science & Technology*, *28*, 521–527. http://doi.org/10.1021/es00052a027

Lammel, G., Sehili, A. M., Bond, T. C., Feichter, J., & Grassl, H. (2009). Gas/particle partitioning and global distribution of polycyclic aromatic hydrocarbons – A modelling approach. *Chemosphere*, *76*, 98–106. http://doi.org/10.1016/j.chemosphere.2009.02.017

Lane, D. A., Fielder, S. S., Townsend, S. J., Bunce, N. J., Zhu, J., Liu, L., Wiens, B.; & Pond, P. (1996). Atmospheric Photochemistry of Naphthalene: a Practical and Theoretical Approach. *Polycyclic Aromatic Compounds*, *9*, 53–59. http://doi.org/10.1080/10406639608031201

Lawrence, C. R., & Neff, J. C. (2009). The contemporary physical and chemical flux of aeolian dust: A synthesis of direct measurements of dust deposition. *Chemical Geology*, *267*, 46–63. http://doi.org/10.1016/j.chemgeo.2009.02.005

Lee, J., & Lane, D. A. (2010). Formation of oxidized products from the reaction of gaseous phenanthrene with the OH radical in a reaction chamber. *Atmospheric Environment*, *44*, 2469–2477. http://doi.org/10.1016/j.atmosenv.2010.03.008

Lei, H., & Wang, J. X. L. (2014). Observed characteristics of dust storm events over the western United States using meteorological, satellite, and air quality measurements. *Atmospheric Chemistry and Physics*, *14*, 7847–7857. http://doi.org/10.5194/acp-14-7847-2014

Lei, Y. D., & Wania, F. (2004). Is rain or snow a more efficient scavenger of organic chemicals? *Atmospheric Environment*, *38*, 3557–3571. http://doi.org/10.1016/j.atmosenv.2004.03.039

Lei, Y. D., Wania, F., Shiu, W. Y., & Boocock, D. G. B. (2000). HPLC-Based Method for Estimating the Temperature Dependence of n-Octanol−Water Partition Coefficients. *Journal of Chemical & Engineering Data*, *45*, 738–742. http://doi.org/10.1021/je9902488

Letzel, T., Rosenberg, E., Wissiack, R., Grasserbauer, M., & Niessner, R. (1999). Separation and identification of polar degradation products of benzo[a]pyrene with ozone by atmospheric pressure chemical ionization–mass spectrometry after optimized column

chromatographic clean-up. *Journal of Chromatography A*, *855*, 501–514. http://doi.org/10.1016/S0021-9673(99)00716-5

Leuenberger, C., Czuczwa, J., Heyerdahl, E., & Giger, W. (1988). Aliphatic and polycyclic aromatic hydrocarbons in urban rain, snow and fog. *Atmospheric Environment*, *22*, 695–705. http://doi.org/10.1016/0004-6981(88)90007-8

Li, P., Wang, Y., Li, Y., Wang, Z., Zhang, H., Xu, P., & Wang, W. (2010). Characterization of polycyclic aromatic hydrocarbons deposition in $PM_{2.5}$ and cloud/fog water at Mount Taishan (China). *Atmospheric Environment*, *44*, 1996–2003. http://doi.org/10.1016/j.atmosenv.2010.02.031

Li, X., Li, P., Yan, L., Chen, J., Cheng, T., & Xu, S. (2011). Characterization of polycyclic aromatic hydrocarbons in fog–rain events. *Journal of Environmental Monitoring*, *13*, 2988–2993. http://doi.org/10.1039/C1EM10543D

Li, X., Li, W., Middel, A., Harlan, S. L., Brazel, A. J., & Turner II, B. L. (2016). Remote sensing of the surface urban heat island and land architecture in Phoenix, Arizona: Combined effects of land composition and configuration and cadastral–demographic–economic factors. *Remote Sensing of Environment*, *174*, 233–243. http://doi.org/10.1016/j.rse.2015.12.022

Li, X., Myint, S. W., Zhang, Y., Galletti, C., Zhang, X., & Turner II, B. L. (2014). Object-based land-cover classification for metropolitan Phoenix, Arizona, using aerial photography. *International Journal of Applied Earth Observation and Geoinformation*, *33*, 321–330. http://doi.org/10.1016/j.jag.2014.04.018

Liu, G., Tong, Y., Luong, J. H. T., Zhang, H., & Sun, H. (2009). A source study of atmospheric polycyclic aromatic hydrocarbons in Shenzhen, South China. *Environmental Monitoring and Assessment*, *163*, 599–606. http://doi.org/10.1007/s10661-009-0862-4

Lohmann, R., & Lammel, G. (2004). Adsorptive and Absorptive Contributions to the Gas-Particle Partitioning of Polycyclic Aromatic Hydrocarbons: State of Knowledge and Recommended Parametrization for Modeling. *Environmental Science & Technology*, *38*, 3793–3803. http://doi.org/10.1021/es035337q

Ma, J., Sverko, E., Su, Y., Zhang, J., & Gao, H. (2013). Uptake and Mobilization of Organic Chemicals with Clouds: Evidence from a Hail Sample. *Environmental Science & Technology*, *47*, 9715–9721. http://doi.org/10.1021/es401401u

Ma, Y.-G., Lei, Y. D., Xiao, H., Wania, F., & Wang, W.-H. (2010). Critical Review and Recommended Values for the Physical-Chemical Property Data of 15 Polycyclic Aromatic Hydrocarbons at 25 °C. *Journal of Chemical & Engineering Data*, *55*, 819–825. http://doi.org/10.1021/je900477x

Macpherson, T., Nickling, W. G., Gillies, J. A., & Etyemezian, V. (2008). Dust emissions from undisturbed and disturbed supply-limited desert surfaces. *Journal of Geophysical Research: Earth Surface*, *113*, n/a-n/a. http://doi.org/10.1029/2007JF000800

Mahler, B. J., Metre, P. C. V., Crane, J. L., Watts, A. W., Scoggins, M., & Williams, E. S. (2012). Coal-Tar-Based Pavement Sealcoat and PAHs: Implications for the Environment, Human Health, and Stormwater Management. *Environmental Science & Technology*, *46*, 3039–3045. http://doi.org/10.1021/es203699x

Maley, J. (1980). Etudes palynologiques dans le bassin du Tchad et Paléoclimatologie de l'Afrique nord tropicale de 30.000 ans à 1'époque actuelle. Thesis, Université de Montpellier, France, 1980.

Mallakin, A., Dixon, D. G., & Greenberg, B. M. (2000). Pathway of anthracene modification under simulated solar radiation. *Chemosphere*, *40*, 1435–1441. http://doi.org/10.1016/S0045-6535(99)00331-8

Marcotte, A. R. (2015). *Processing of Trace Metals in Atmospheric Particulate Matter* (Doctoral dissertation). Arizona State University, Tempe, AZ.

Maricopa County Assessor's Office. (2016). Maps: Historical Aerial Photography. Single aerial maps for years 1976 and 2013. Retrieved June 3, 2016, from http://gis.maricopa.gov/MapApp/GIO/AerialHistorical/index.html

Marr, L. C., Kirchstetter, T. W., Harley, R. A., Miguel, A. H., Hering, S. V., & Hammond, S. K. (1999). Characterization of Polycyclic Aromatic Hydrocarbons in Motor Vehicle Fuels and Exhaust Emissions. *Environmental Science & Technology*, *33*, 3091–3099. http://doi.org/10.1021/es981227l

Marusenko, Y., Herckes, P., & Hall, S. J. (2011). Distribution of Polycyclic Aromatic Hydrocarbons in Soils of an Arid Urban Ecosystem. *Water, Air, & Soil Pollution*, *219*, 473–487. http://doi.org/10.1007/s11270-010-0721-5

Mathematica. (2015a). Mathematica version 10.2.0.0; function ThermodynamicData["Air", "Viscosity",{"Pressure", "Temperature"}]; Wolfram Research.: Champaign, IL.

Mathematica. (2015b). Mathematica version 10.2.0.0; function ThermodynamicData["Air", "Density",{"Pressure", "Temperature"}]; Wolfram Research.: Champaign, IL.

Mathematica. (2015c). Mathematica version 10.2.0.0; function GeogravityModelData[GeoPosition[{latitude, longitude, elevation}], "Magnitude"]; Wolfram Research.: Champaign, IL.

Mathematica. (2015d). Mathematica version 10.2.0.0; function ThermodynamicData["Water", "Density",{"Temperature", "Pressure"}]; Wolfram Research.: Champaign, IL.

Mathematica. (2015e). Mathematica version 10.2.0.0; function ThermodynamicData["Water", "Viscosity",{"Temperature", "Pressure"}]; Wolfram Research.: Champaign, IL.

McConkey, B. J., Duxbury, C. L., Dixon, D. G., & Greenberg, B. M. (1997). Toxicity of a pah photooxidation product to the bacteria *Photobacterium phosphoreum* and the duckweed *Lemna gibba*: Effects of phenanthrene and its primary photoproduct, phenanthrenequinone. *Environmental Toxicology and Chemistry*, *16*, 892–899. http://doi.org/10.1002/etc.5620160508

McCrackin, M. L., Harms, T. K., Grimm, N. B., Hall, S. J., & Kaye, J. P. (2008). Responses of soil microorganisms to resource availability in urban, desert soils. *Biogeochemistry*, *87*, 143–155. http://doi.org/10.1007/s10533-007-9173-4

McGowan, H. A., Sturman, A. P., & Owens, I. F. (1996). Aeolian dust transport and deposition by foehn winds in an alpine environment, Lake Tekapo, New Zealand. *Geomorphology*, *15*, 135–146. http://doi.org/10.1016/0169-555X(95)00123-M

McLean, B. J. (2007). *Geochemical consequences of management on water resources in central Arizona* (Master's thesis). Arizona State University, Tempe, AZ.

McTainsh, G. H. (1980). Harmattan dust deposition in northern Nigeria. *Nature*, *286*, 587–588. http://doi.org/10.1038/286587a0

Membery, D.A., (1985). A gravity wave haboob?. *Weather*, *40*, 214–221. doi: 10.1002/j.1477-8696.1985.tb06877.x

MesoWest. (2015). Department of Atmospheric Sciences, University of Utah. Retrieved July 2, 2015 from http://mesowest.utah.edu/cgi-bin/droman/download_ndb.cgi

Mihele, C. M., Wiebe, H. A., & Lane, D. A. (2002). Particle Formation and Gas/Particle Partition Measurements of the Products of the Naphthalene-OH Radical Reaction in a Smog Chamber. *Polycyclic Aromatic Compounds*, *22*, 729–736. http://doi.org/10.1080/10406630290103889

Miller, E. R. (1934). Meteorology of the dust fall of November 12-13, 1933. *Journal of Sedimentary Research*, *4*, 78–81. http://doi.org/10.1306/D4268EBE-2B26-11D7-8648000102C1865D

Miller, J. S., & Olejnik, D. (2001). Photolysis of polycyclic aromatic hydrocarbons in water. *Water Research*, *35*, 233–243. http://doi.org/10.1016/S0043-1354(00)00230-X

Miller, S. D., Kuciauskas, A. P., Liu, M., Ji, Q., Reid, J. S., Breed, D., Walker, A. L., & Mandoos, A. A. (2008). Haboob dust storms of the southern Arabian Peninsula. *Journal of Geophysical Research, 113*. http://doi.org/10.1029/2007JD008550

Møberg, J. P., Esu, I. E., & Malgwi, W. B. (1991). Characteristics and constituent composition of Harmattan dust falling in Northern Nigeria. *Geoderma, 48*, 73–81. http://doi.org/10.1016/0016-7061(91)90007-G

Moza, P. N., Hustert, K., & Kettrup, A. (1999). Photooxidation of naphthalene and phenanthrene in hexane as an oil film on water. *Chemosphere, 39*, 569–574. http://doi.org/10.1016/S0045-6535(99)00122-8

Nickling, W. G., & Brazel, A. J. (1984). Temporal and spatial characteristics of Arizona dust storms (1965–1980). *Journal of Climatology, 4*, 645–660. http://doi.org/10.1002/joc.3370040608

Niu, J., Chen, J., Martens, D., Quan, X., Yang, F., Kettrup, A., & Schramm, K.-W. (2003). Photolysis of polycyclic aromatic hydrocarbons adsorbed on spruce [Picea abies (L.) Karst.] needles under sunlight irradiation. *Environmental Pollution, 123*, 39–45. http://doi.org/10.1016/S0269-7491(02)00362-7

NOAA (U.S. National Oceanic and Atmospheric Administration). (2015). National Centers for Environmental Information: Quality Controlled Local Climatological Data, version 2.5.10. Retrieved July 2, 2015, from http://www.ncdc.noaa.gov/qclcd/QCLCD?prior=N

NWS (U.S. National Weather Service). (2016). NWS Phoenix: Monsoon Awareness Week: June 12th - 17th, 2016. Retrieved June 15, 2016, from http://www.wrh.noaa.gov/psr/pns/2016/June/MonsoonAwarenessWeek.php

O'Hara, S. L., Clarke, M. L., & Elatrash, M. S. (2006). Field measurements of desert dust deposition in Libya. *Atmospheric Environment, 40*, 3881–3897. http://doi.org/10.1016/j.atmosenv.2006.02.020

O'Loingsigh, T., McTainsh, G. H., Tews, E. K., Strong, C. L., Leys, J. F., Shinkfield, P., & Tapper, N. J. (2014). The Dust Storm Index (DSI): A method for monitoring broadscale wind erosion using meteorological records. *Aeolian Research, 12*, 29–40. http://doi.org/10.1016/j.aeolia.2013.10.004

Odabasi, M., Cetin, E., & Sofuoglu, A. (2006). Determination of octanol–air partition coefficients and supercooled liquid vapor pressures of PAHs as a function of temperature: Application to gas–particle partitioning in an urban atmosphere. *Atmospheric Environment, 40*, 6615–6625. http://doi.org/10.1016/j.atmosenv.2006.05.051

Orgill, M. M., & Sehmel, G. A. (1976). Frequency and diurnal variation of dust storms in the contiguous U.S.A. *Atmospheric Environment, 10*, 813–825. http://doi.org/10.1016/0004-6981(76)90136-0

OSHA (Occupational Safety and Health Administration). (2016). Toxic and Hazardous Substances. Occupational safety and Health Standards. *Code of Federal Regulations*, 29 B XVII §1910.1002.

Pearlman, R. S., Yalkowsky, S. H., & Banerjee, S. (1984). Water Solubilities of Polynuclear Aromatic and Heteroaromatic Compounds. *Journal of Physical and Chemical Reference Data*, *13*, 555–562. http://doi.org/10.1063/1.555712

Péwé, T. L., Péwé, E. A., Péwé, R. H., Journaux, A., & Slatt, R. M. (1981). Desert Dust: Characteristics and rates of deposition in central Arizona. *Geological Society of America Special Papers*, *186*, 169–190. http://doi.org/10.1130/SPE186-p169

Pierlot, C., & Aubry, J.-M. (1997). First evidence of the formation of 5,8-endoperoxide from the oxidation of 1,4-disubstituted naphthalene by singlet oxygen. *Chemical Communications*, *n/a*, 2289–2290. http://doi.org/10.1039/A705716D

Plata, D. L., Sharpless, C. M., & Reddy, C. M. (2008). Photochemical Degradation of Polycyclic Aromatic Hydrocarbons in Oil Films. *Environmental Science & Technology*, *42*, 2432–2438. http://doi.org/10.1021/es702384f

Pratesi, P., Villa, L., Ferri, V., De Micheli, C., Grana, E., Grieco, C., Silipo, C., & Vittoria, A. (1979). *II Farmacopia*, *34*, 580. Referenced in: Hansch, C.; Leo, A.; Hoekman, D. *Exploring QSAR Hydrophobic*, electronic, *and steric constants*. American Chemical Society: Washington, DC, 1995; pp 348.

Raja, S., & Valsaraj, K. T. (2006). On the reactive uptake of gaseous PAH molecules by micron-sized atmospheric water droplets. *Atmospheric Research*, *81*, 277–292. http://doi.org/10.1016/j.atmosres.2006.01.004

Raja, S., Raghunathan, R., Yu, X.-Y., Lee, T., Chen, J., Kommalapati, R. R., Murugesan, K.; Shen, X.; Qingzhong, Y.; Valsaraj, K. T.; & Collett Jr., J. L. (2008). Fog chemistry in the Texas–Louisiana Gulf Coast corridor. *Atmospheric Environment*, *42*, 2048–2061. http://doi.org/10.1016/j.atmosenv.2007.12.004

Raman, A., Arellano Jr., A. F., & Brost, J. J. (2014). Revisiting haboobs in the southwestern United States: An observational case study of the 5 July 2011 Phoenix dust storm. *Atmospheric Environment*, *89*, 179–188. http://doi.org/10.1016/j.atmosenv.2014.02.026

Ravindra, K., Sokhi, R., & Van Grieken, R. (2008). Atmospheric polycyclic aromatic hydrocarbons: Source attribution, emission factors and regulation. *Atmospheric Environment*, *42*, 2895–2921. http://doi.org/10.1016/j.atmosenv.2007.12.010

Reheis, M. C. (2006). A 16-year record of eolian dust in Southern Nevada and California, USA: Controls on dust generation and accumulation. *Journal of Arid Environments*, *67*, 487–520. http://doi.org/10.1016/j.jaridenv.2006.03.006

Reyes-Rodríguez, G. J., Gioda, A., Mayol-Bracero, O. L., & Collett Jr., J. L. (2009). Organic carbon, total nitrogen, and water-soluble ions in clouds from a tropical montane cloud forest in Puerto Rico. *Atmospheric Environment*, *43*, 4171–4177. http://doi.org/10.1016/j.atmosenv.2009.05.049

Reza, J., & Trejo, A. (2004). Temperature dependence of the infinite dilution activity coefficient and Henry's law constant of polycyclic aromatic hydrocarbons in water. *Chemosphere*, *56*, 537–547. http://doi.org/10.1016/j.chemosphere.2004.04.020

Roberts, A., & Knippertz, P. (2012). Haboobs: convectively generated dust storms in West Africa. *Weather*, *67*, 311–316. http://doi.org/10.1002/wea.1968

Rogge, W. F., Hildemann, L. M., Mazurek, M. A., Cass, G. R., & Simoneit, B. R. T. (1993a). Sources of fine organic aerosol. 2. Noncatalyst and catalyst-equipped automobiles and heavy-duty diesel trucks. *Environmental Science & Technology*, *27*, 636–651. http://doi.org/10.1021/es00041a007

Rogge, W. F., Mazurek, M. A., Hildemann, L. M., Cass, G. R., & Simoneit, B. R. T. (1993b). Quantification of urban organic aerosols at a molecular level: Identification, abundance and seasonal variation. *Atmospheric Environment*, *27*, 1309–1330. doi:10.1016/0960-1686(93)90257-Y

Sahu, S. K., & Pandit, G. G. (2003). Estimation of Octanol-Water Partition Coefficients for Polycylic Aromatic Hydrocarbons Using Reverse-Phase HPLC. *Journal of Liquid Chromatography & Related Technologies*, *26*, 135–146. http://doi.org/10.1081/JLC-120017158

Sanches, S., Leitão, C., Penetra, A., Cardoso, V. V., Ferreira, E., Benoliel, M. J., Barreto Crespo, M. T., & Pereira, V. J. (2011). Direct photolysis of polycyclic aromatic hydrocarbons in drinking water sources. *Journal of Hazardous Materials*, *192*, 1458–1465. http://doi.org/10.1016/j.jhazmat.2011.06.065

Sander, R. (2015). Compilation of Henry's law constants (version 4.0) for water as solvent. *Atmospheric Chemistry and Physics*, *15*, 4399–4981. http://doi.org/10.5194/acp-15-4399-2015

Sauret, N., Wortham, H., Strekowski, R., Herckes, P., Nieto, L. I. (2009). Comparison of annual dry and wet deposition fluxes of selected pesticides in Strasbourg, France. *Environmental Pollution*, *157*, 303–312. http://doi.org/10.1016/j.envpol.2008.06.034

Seinfeld, J. H., Pandis, S. N. (2006). *Atmospheric Chemistry and Physics: From Air Pollution to Climate Change*, (2nd ed.). Hoboken, New Jersey: Wiley. pp. 400–422. ISBN: 978-0-471-72018-8

Shahpoury, P., Lammel, G., Holubová Šmejkalová, A., Klánová, J., Přibylová, P., & Váňa, M. (2015). Polycyclic aromatic hydrocarbons, polychlorinated biphenyls, and chlorinated pesticides in background air in central Europe – investigating parameters

affecting wet scavenging of polycyclic aromatic hydrocarbons. *Atmospheric Chemistry and Physics*, *15*, 1795–1805. http://doi.org/10.5194/acp-15-1795-2015

Shikula, N. K. (1981). Prediction of dust storms from meteorological observations in the South Ukraine, U.S.S.R. *Geological Society of America Special Papers*, *186*, 261–266. http://doi.org/10.1130/SPE186-p261

Sigman, M. E., Chevis, E. A., Brown, A., Barbas, J. T., Dabestani, R., & Burch, E. L. (1996). Enhanced photoreactivity of acenaphthylene in water: a product and mechanism study. *Journal of Photochemistry and Photobiology A: Chemistry*, *94*, 149–155. http://doi.org/10.1016/1010-6030(95)04099-4

Singer, A., Ganor, E., Dultz, S., & Fischer, W. (2003). Dust deposition over the Dead Sea. *Journal of Arid Environments*, *53*, 41–59. http://doi.org/10.1006/jare.2002.1023

Škrdlíková, L., Landlová, L., Klánová, J., & Lammel, G. (2011). Wet deposition and scavenging efficiency of gaseous and particulate phase polycyclic aromatic compounds at a central European suburban site. *Atmospheric Environment*, *45*, 4305–4312. http://doi.org/10.1016/j.atmosenv.2011.04.072

Sorooshian, A., Wonaschütz, A., Jarjour, E. G., Hashimoto, B. I., Schichtel, B. A., & Betterton, E. A. (2011). An aerosol climatology for a rapidly growing arid region (southern Arizona): Major aerosol species and remotely sensed aerosol properties. *Journal of Geophysical Research: Atmospheres*, *116*. http://doi.org/10.1029/2011JD016197

Straub, K. M., Meehan, T., Burlingame, A. L., & Calvin, M. (1977). Identification of the major adducts formed by reaction of benzo(a)pyrene diol epoxide with DNA in vitro. *Proceedings of the National Academy of Sciences of the United States of America*, *74*, 5285–5289.

Styler, S. A., Loiseaux, M.-E., & Donaldson, D. J. (2011). Substrate effects in the photoenhanced ozonation of pyrene. *Atmospheric Chemistry and Physics*, *11*, 1243–1253. http://doi.org/10.5194/acp-11-1243-2011

Sutton, L. J. (1931). Haboobs. *Quarterly Journal of the Royal Meteorological Society*, *57*, 143–162. http://doi.org/10.1002/qj.49705723906

U.S. Census Bureau. (2013). Metropolitan and Micropolitan: Population Change for Metropolitan and Micropolitan Statistical Areas in the United States and Puerto Rico (February 2013 Delineations): 2000 to 2010. Retrieved November 24, 2015, from http://www.census.gov/population/www/cen2010/cph-t/cph-t-5.html

U.S. National Water Information System: Web Interface. (2016). Retrieved May 16, 2016, from http://waterdata.usgs.gov/nwis/inventory/

Upadhyay, N., Clements, A. L., Fraser, M. P., Sundblom, M., Solomon, P., & Herckes, P. (2015). Size-Differentiated Chemical Composition of Re-Suspended Soil Dust from the Desert Southwest United States. *Aerosol and Air Quality Research, 15*, 387–398. http://doi.org/10.4209/aaqr.2013.07.0253

Valsaraj, K. T. (2004). Adsorption of polycyclic aromatic hydrocarbons at the air-water interface and its role in atmospheric deposition by fog droplets. *Environmental Toxicology and Chemistry, 23*, 2318–2323. http://doi.org/10.1897/03-321

Valsaraj, K. T. (2009). Trace gas adsorption thermodynamics at the air−water interface: Implications in atmospheric chemistry. *Pure and Applied Chemistry, 81*. http://doi.org/10.1351/PAC-CON-08-07-06

Wang, L., Atkinson, R., & Arey, J. (2007). Formation of 9,10-phenanthrenequinone by atmospheric gas-phase reaction of phenanthrene. *Atmospheric Environment*, *41*, 2025–2035. http://doi.org/10.1016/j.atmosenv.2006.11.008

Wang, L., Wang, X., Xu, O., & Tian, L. (1986). Determination of the n-octanol/water partition coefficients of polycyclic aromatic hydrocarbons and estimation of aqueous solubilities. *Acta Scientiae Circumstantiae*, *6*, 491–497.

Warn, G. F., & Cox, W. H. (1951). A sedimentary study of dust storms in the vicinity of Lubbock, Texas. *American Journal of Science*, *249*, 553–568. http://doi.org/10.2475/ajs.249.8.553

Whitehouse, B. G. (1984). The effects of temperature and salinity on the aqueous solubility of polynuclear aromatic hydrocarbons. *Marine Chemistry*, *14*, 319–332. http://doi.org/10.1016/0304-4203(84)90028-8

WHO (World Health Organization). (2006). Air quality guidelines. Global update 2005. Particulate matter, ozone, nitrogen dioxide and sulfur dioxide. WHO Regional Office for Europe; Copenhagen. ISBN 92-890-2192-6. Retrieved December 22, 2015, from http://www.euro.who.int/__data/assets/pdf_file/0005/78638/E90038.pdf?ua=1

Woo, O. T., Chung, W. K., Wong, K. H., Chow, A. T., & Wong, P. K. (2009). Photocatalytic oxidation of polycyclic aromatic hydrocarbons: Intermediates identification and toxicity testing. *Journal of Hazardous Materials*, *168*, 1192–1199. http://doi.org/10.1016/j.jhazmat.2009.02.170

Xie, Z., Blum, J. D., Utsunomiya, S., Ewing, R. C., Wang, X., & Sun, L. (2007). Summertime carbonaceous aerosols collected in the marine boundary layer of the Arctic Ocean. *Journal of Geophysical Research: Atmospheres*, *112*, n/a-n/a. http://doi.org/10.1029/2006JD007247

Yap, C. L., Gan, S., & Ng, H. K. (2012). Evaluation of solubility of polycyclic aromatic hydrocarbons in ethyl lactate/water versus ethanol/water mixtures for contaminated soil

remediation applications. *Journal of Environmental Sciences*, *24*, 1064–1075. http://doi.org/10.1016/S1001-0742(11)60873-5

Yunker, M. B., Macdonald, R. W., Vingarzan, R., Mitchell, R. H., Goyette, D., & Sylvestre, S. (2002). PAHs in the Fraser River basin: a critical appraisal of PAH ratios as indicators of PAH source and composition. *Organic Geochemistry*, *33*, 489–515. http://doi.org/10.1016/S0146-6380(02)00002-5

Zak, J. A. (1994). *Drop size distributions and related properties of fog for five locations measured from aircraft*. Hampton, VA: National Aeronautics and Space Administration, Langley Research Center.

Zepp, R., & Schlotzhauer, P. (1979). Photoreactivity of selected aromatic hydrocarbons in water, In Jones, P.; Leber, P. (Eds.), *Polynuclear Aromatic Hydrocarbons*, Ann Arbor Science Publishers, Ann Arbor, MI, pp 141–158.

Zhang, Y., & Tao, S. (2009). Global atmospheric emission inventory of polycyclic aromatic hydrocarbons (PAHs) for 2004. *Atmospheric Environment*, *43*, 812–819. http://doi.org/10.1016/j.atmosenv.2008.10.050

APPENDIX A

THE CHARACTERIZATION OF HABOOBS IN TEMPE, AZ

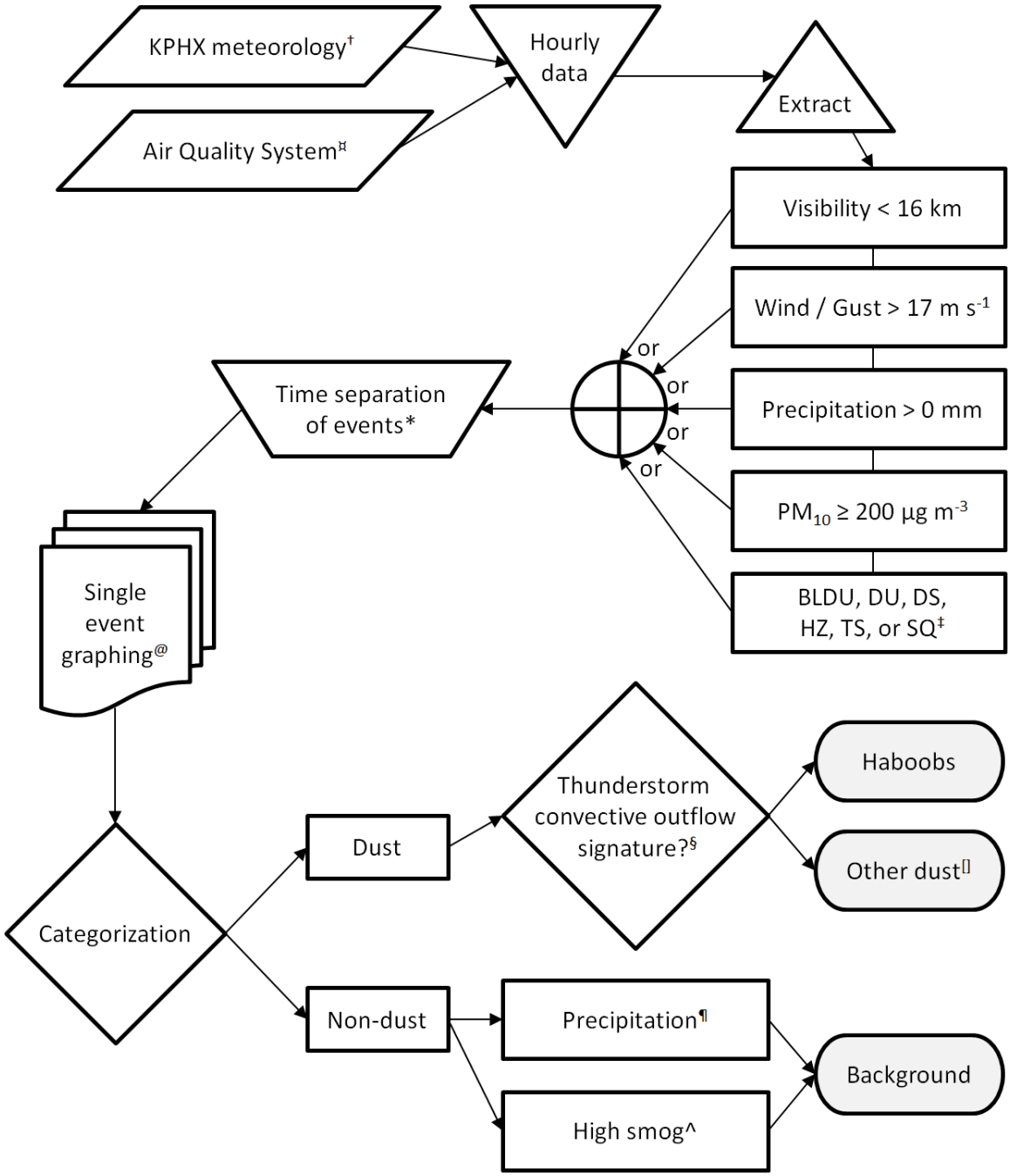

Figure A1. Haboob identification and categorization flowchart. Notes: †, KPHX is the Phoenix Sky Harbor Airport weather station; ¤, U.S. EPA Air Quality System sites 04-013-3002 and 04-013-4005 (CEPH and TE respectively); ‡, weather conditions: BLDU blowing dust, DU widespread dust, DS dust storm, HZ haze, TS thunderstorm, SQ squall;

*, weather appeared to reset to clear, storm-free conditions ≥ 6 hours; @, parallel graphs: wind and gust speeds, wind direction, temperature, relative humidity, pressure, visibility, precipitation, and PM_{10} with a time frame from 24 hours before to 24 hours after the event; §, a temperature and visibility decrease coinciding with an increase in pressure, humidity, PM_{10}, and wind speed; [], high wind signature or haboobs with visibility > 11.3 km (7 mi); ¶, low visibility due to heavy rain, drizzle, mist, fog, or hail; ^, relatively low or zero wind speeds and generally elevated pollutant concentrations (PM_{10}, $PM_{2.5}$, O_3, SO_2, CO, NO_2).

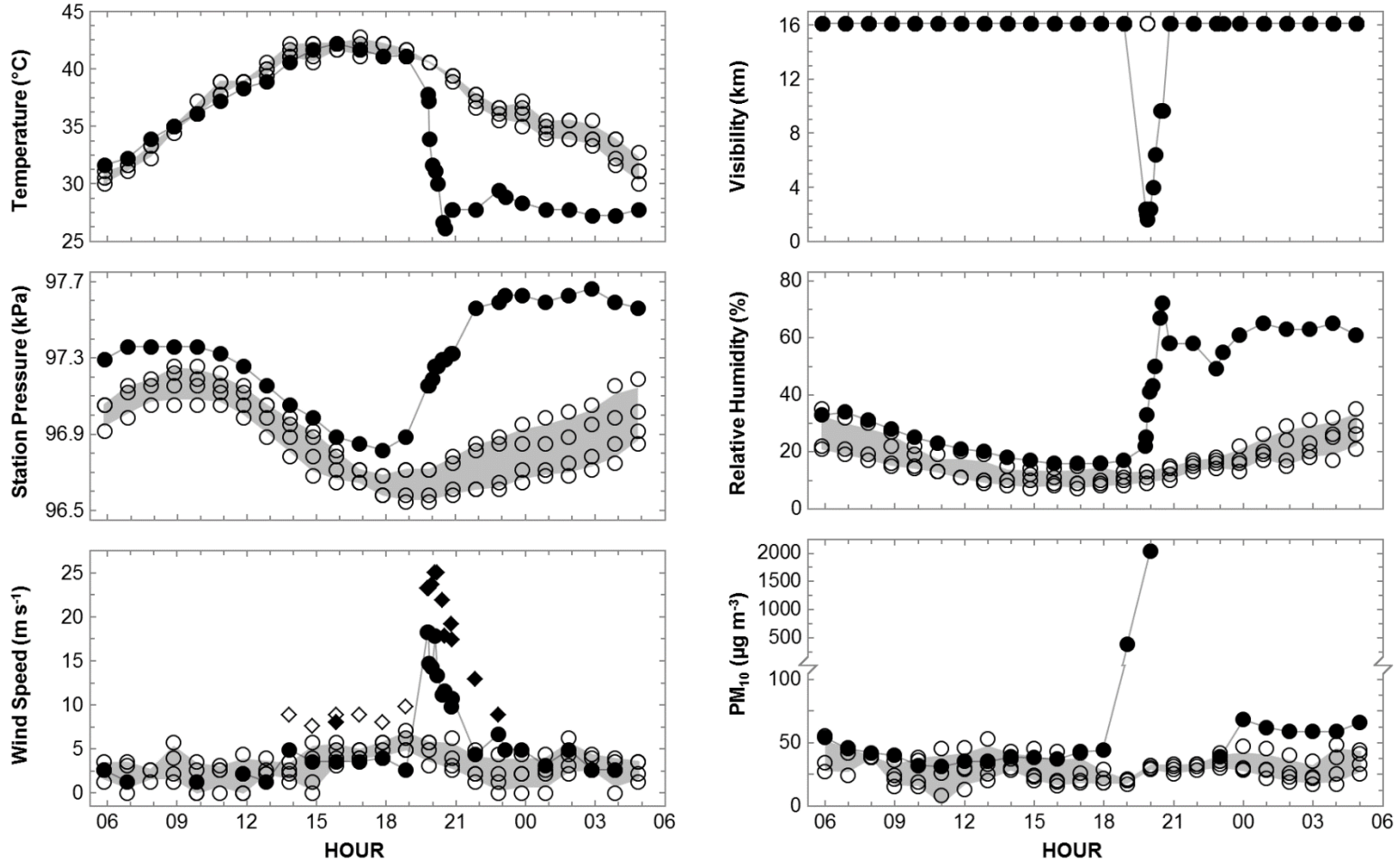

Figure A2. Example of the 3 July, 2014 haboob meteorological and air quality signature (filled circles) compared with the measurements on the 4 preceding days (open circles). The arrival of the convective thunderstorm outflow boundary at KPHX is seen as an abrupt decrease in temperature and visibility, coinciding with abrupt increases in relative humidity, air pressure,

and wind speed. The thin lines connecting the filled circles are intended to help guide the eye. The shaded grey areas indicate the region of the 10^{th} to 90^{th} percentile of the measurements on the 4 days before the haboob. The filled and open diamonds are gust speeds of the haboob day and preceding 4 days respectively. Note the scale break in the PM_{10} plot.

Table A1

List of haboobs in Tempe during the time period 2005 to 2014.

Date time started	Date time ended	Maximum KPHX wind or gust speed (mi h^{-1}) †	Minimum KPHX visibility (mi) †	Maximum CEPH @ PM_{10} (μg m^{-3})	KPHX METAR weather condition code ‡,§	Estimated PM_{10} dry deposition (kg ha^{-1})	Estimated TSP dry deposition (kg ha^{-1})	Ident-ification
2005-05-27 20:00	2005-05-27 23:00	36	3	594	BLDU	0.05	42.4	*
2005-07-17 17:51	2005-07-18 02:00	46	5	296	BLDU	0.05	27.9	*
2005-07-18 22:00	2005-07-19 00:00	77	1.25	482	+TSRA BLDU SQ	0.04	37.5	*
2005-07-22 21:00	2005-07-23 04:51	43	3	319	+RA BLDU	0.03	19.1	*
2005-07-23 18:00	2005-07-24 00:51	47	3	316	BLDU SQ; TS; -RA	0.03	18.9	#
2005-08-02 20:00	2005-08-03 02:51	52	1.75	504	-RA BLDU SQ; +TSRA; TSRA BR	0.04	30.2	*
2005-08-31 18:00	2005-08-31 20:00	32	6	402	TS BLDU; -TSRA	0.03	23.9	*
2006-05-16 16:00	2006-05-16 18:51	30	6	198	BLDU	0.02	12.0	*
2006-06-06 18:00	2006-06-07 01:00	38	0.75	720	HZ BLDU	0.09	43.4	#, ♦
2006-06-24 20:00	2006-06-25 06:00	10	5	549	BLDU	0.12	61.9	*
2006-06-25 16:51	2006-06-25 23:00	54	0.75	343	HZ	0.06	20.9	*
2006-06-30 19:00	2006-06-30 21:12	48	6	299	HZ BLDU; TS	0.02	17.8	*
2006-07-16 21:00	2006-07-17 00:00	25	5	274	TS; BLDU	0.03	16.5	*
2006-07-18 18:00	2006-07-18 22:00	29	2.5	378	BLDU	0.06	44.9	*
2006-07-21 16:00	2006-07-22 02:00	52	6	541	TS HZ; TS BLDU; -TSRA	0.09	55.4	*
2006-08-11 22:00	2006-08-12 03:51	41	1	113	+TSRA BR	0.01	6.8	*
2006-08-21 18:00	2006-08-22 08:51	49	0.75	333	TS HZ; TS BLDU; TSRA	0.04	20.1	*
2007-04-28 15:00	2007-04-28 16:51	51	0.75	732	HZ; BLDU	0.07	78.8	#, ♦
2007-05-08 17:00	2007-05-08 20:00	32	6	152	HZ BLDU	0.02	9.2	#
2007-07-06 18:00	2007-07-07 02:00	39	7	265	BLDU	0.06	16.3	*
2007-07-16 20:00	2007-07-17 00:51	43	1.25	773	HZ BLDU; -TSRA BLDU	0.06	46.0	*
2007-07-18 21:00	2007-07-19 01:00	25	6	736	BLDU	0.07	65.8	*
2007-07-19 22:00	2007-07-20 01:00	55	0.25	3154	BLDU; -RA BLDU; TS BLDU	0.29	303.7	#

Table A1 (continued)

Date time started	Date time ended	Maximum KPHX wind or gust speed (mi h–1) †	Minimum KPHX visibility (mi) †	Maximum CEPH @ PM10 (µg m–3)	KPHX METAR weather condition code ‡,§	Estimated PM10 dry deposition (kg ha–1)	Estimated TSP dry deposition (kg ha–1)	Ident-ification
2007-07-20 23:00	2007-07-21 04:51	15	7	306	VCTS	0.03	18.5	*
2007-08-13 23:00	2007-08-14 03:51	59	3	2422	VCTS BLDU; -RA BLDU; TS BLDU; -TSRA SQ	0.25	265.9	*
2007-08-16 17:00	2007-08-16 23:00	38	5	196	BLDU; HZ BLDU SQ	0.03	11.9	*
2007-08-23 20:00	2007-08-24 01:00	20	2.5	802	BLDU	0.11	67.8	*
2007-08-24 20:00	2007-08-25 08:51	20	5	127	BLDU; VCTS +RA	0.04	8.0	#
2007-08-28 23:30	2007-08-29 02:00	13	5	426	HZ BLDU	0.06	45.7	#
2007-09-05 20:00	2007-09-05 23:00	34	3	475	BLDU	0.05	28.5	*
2008-08-07 20:00	2008-08-08 00:51	53	1.5	532	TS; -TSRA BLDU; +TSRA	0.04	31.7	*
2008-08-14 18:00	2008-08-14 21:51	46	6	118	-TSRA BLDU	0.01	7.1	*
2008-08-28 19:49	2008-08-29 02:51	75	0.25	NA	TS; +RA SQ; +RA FG SQ; +RA BR	NA	NA	#
2008-09-11 18:00	2008-09-11 20:00	51	1.5	1066	HZ BLDU SQ; HZ BLDU	0.06	63.5	*
2009-07-15 21:00	2009-07-15 22:23	40	7	152	SQ; TS	0.01	9.0	*
2009-07-17 18:00	2009-07-18 06:00	40	2.5	849	BLDU	0.24	153.6	*
2009-07-18 18:00	2009-07-19 04:00	29	0.25	165	DS; BLDU	0.06	10.6	*
2009-07-20 18:00	2009-07-20 20:51	55	6	324	TS BLDU; TS	0.03	19.3	*
2009-08-12 21:00	2009-08-13 10:51	28	1	1477	BLDU; +TSRA	0.15	107.4	*
2009-08-21 20:49	2009-08-22 06:51	44	5	289	BLDU	0.05	30.4	*
2009-09-03 20:00	2009-09-03 22:00	37	1.5	1481	BLDU; -TSRA	0.09	88.0	*
2010-07-20 01:51	2010-07-20 04:51	25	5	199	TS HZ	0.02	12.0	*
2010-08-17 17:00	2010-08-17 22:51	43	4	206	-RA	0.02	12.3	*
2010-10-02 17:51	2010-10-02 21:00	43	3	592		0.05	35.4	*
2011-07-03 00:00	2011-07-03 11:00	30	2	1771	BLDU	0.26	174.5	#,&
2011-07-03 17:00	2011-07-03 22:00	36	6	844	HZ BLDU; -TSRA	0.09	50.7	#,&
2011-07-05 19:00	2011-07-06 00:00	53	0.12	3578	+DS; -RA +DS; -RA BLDU	0.30	305.4	#,&, ♦, ◊

Table A1 (continued)

Date time started	Date time ended	Maximum KPHX wind or gust speed (mi h–1) †	Minimum KPHX visibility (mi) †	Maximum CEPH @ PM10 (µg m–3)	KPHX METAR weather condition code ‡,§	Estimated PM10 dry deposition (kg ha–1)	Estimated TSP dry deposition (kg ha–1)	Ident-ification
2011-07-09 20:00	2011-07-10 00:51	41	2	553		0.06	63.2	*
2011-07-10 15:51	2011-07-10 18:00	66	2.5	296	VCTS; -TSRA BLDU	0.02	17.6	#
2011-07-17 22:00	2011-07-18 00:00	20	7	537		0.04	32.0	*
2011-07-18 16:00	2011-07-18 23:00	37	1	2056	HZ BLDU	0.26	248.2	*,&
2011-07-20 22:00	2011-07-21 01:51	26	2.5	2050	BLDU	0.14	122.2	*
2011-07-31 19:51	2011-07-31 23:51	33	7	175	-TSRA	0.02	10.5	#, ♦
2011-08-03 02:41	2011-08-03 06:00	25	1.25	1977	HZ	0.13	117.8	*,&
2011-08-07 21:00	2011-08-08 00:00	14	6	890	HZ	0.08	75.7	*
2011-08-18 18:00	2011-08-18 21:00	39	0.5	4373	DS; BLDU	0.26	284.0	#,&, ♦
2011-08-25 00:00	2011-08-25 11:00	33	1.75	2822	HZ	0.38	284.7	*,&
2011-08-27 18:00	2011-08-28 00:51	32	1	1972	BLDU; HZ	0.25	252.3	*,&
2011-09-02 01:00	2011-09-02 13:00	34	0.75	4392	BLDU; -RA BLDU; DU; -RA	0.37	305.2	*,&
2011-09-09 20:00	2011-09-09 23:00	15	3	875	HZ	0.09	89.5	*
2011-09-10 19:00	2011-09-10 22:00	41	4	283	TS	0.03	17.1	*
2011-09-11 16:51	2011-09-12 01:00	25	1	980		0.16	116.3	#,&
2011-09-12 16:00	2011-09-12 23:00	32	6	928		0.11	83.6	#,&
2011-09-27 18:00	2011-09-27 22:00	30	2.5	563	BLDU	0.07	57.0	*
2012-05-09 16:00	2012-05-09 19:51	54	0.5	425	BLDU; TS DS; -TSRA	0.04	19.6	#, ♦
2012-06-16 17:00	2012-06-17 00:00	32	0.75	990	BLDU	0.10	60.28	#,&
2012-06-26 20:00	2012-06-26 23:00	34	5	846		0.06	61.8	#, ♦
2012-06-27 18:00	2012-06-28 00:51	44	1	4811	BLDU	0.31	296.6	#,&, ♦
2012-07-11 22:00	2012-07-12 02:51	47	1.75	1412	+TSRA	0.13	121.7	#,&
2012-07-15 16:31	2012-07-15 20:51	33	1.25	867	TS; BLDU	0.11	101.1	#
2012-07-21 17:00	2012-07-21 20:51	51	1	912	BLDU SQ; -TSRA	0.07	63.2	#, ♦

Table A1 (continued)

Date time started	Date time ended	Maximum KPHX wind or gust speed (mi h–1) †	Minimum KPHX visibility (mi) †	Maximum CEPH @ PM10 (µg m–3)	KPHX METAR weather condition code ‡,§	Estimated PM10 dry deposition (kg ha–1)	Estimated TSP dry deposition (kg ha–1)	Ident-ification
2012-07-22 16:00	2012-07-22 18:00	30	2.5	188		0.02	10.93	#
2012-07-23 16:00	2012-07-23 17:51	24	1	876		0.03	27.8	#, ♦
2012-07-28 18:00	2012-07-28 21:51	40	6	78	HZ; RA	0.01	9.7	#
2012-07-29 16:55	2012-07-30 03:51	45	2.5	369	VCBLDU; BLDU; -TSRA	0.02	12.6	#
2012-08-11 17:00	2012-08-11 19:00	26	0.75	1224	BLDU	0.11	109.3	#,&
2012-08-13 21:00	2012-08-14 02:51	30	6	604	VCBLDU; TS	0.06	30.4	*
2012-08-14 22:00	2012-08-15 13:00	36	2.5	916	TS BLDU; -TSRA; HZ	0.17	58.0	#,&
2012-08-19 22:51	2012-08-20 01:00	26	7	468		0.05	48.3	*
2012-09-02 20:00	2012-09-03 04:00	23	2	NA	BLDU	0.15	92.8	#
2012-09-03 21:00	2012-09-04 03:49	22	7	NA	TS	0.03	18.2	*
2012-09-06 17:00	2012-09-06 20:00	29	0.75	624	BLDU	0.08	81.4	#,&, ♦
2012-09-10 20:00	2012-09-11 16:51	33	6	338	-RA	0.05	22.9	*
2013-06-30 22:00	2013-07-01 01:00	47	0.75	5251		0.34	362.1	#,&
2013-07-02 03:00	2013-07-02 07:00	39	5	719	-RA	0.07	50.0	#,&
2013-07-12 13:00	2013-07-12 15:51	22	5	250		0.02	15.8	#
2013-08-18 18:00	2013-08-18 23:00	37	6	128		0.02	7.9	#
2013-08-20 19:00	2013-08-20 23:51	36	3	429	HZ; BLDU	0.08	70.9	#
2013-08-26 18:00	2013-08-26 22:00	55	0.25	1697	BLDU; TSRA BLDU	0.11	86.6	#
2013-09-05 21:00	2013-09-06 01:00	11	3	390		0.07	52.1	#
2014-07-03 19:00	2014-07-03 21:51	56	1	2039	DS SQ; -TSRA BLDU	0.11	120.7	#,&
2014-07-13 16:26	2014-07-14 01:51	56	4	301	TSRA	0.03	20.8	#
2014-07-25 17:00	2014-07-26 00:00	46	1.5	840	BLDU	0.15	133.8	#,&
2014-07-26 22:00	2014-07-27 05:00	34	4	396		0.07	45.8	#
2014-08-17 18:00	2014-08-18 03:51	37	7	89	-TSRA	0.03	4.5	*
2014-09-06 18:00	2014-09-06 21:00	38	1.25	1663		0.10	88.6	#,&

Table A1 (continued)

Notes: †, wind / gust speeds and visibility are listed in the units reported by U.S. NOAA in hourly QCLCD (quality controlled local climatological data) which are miles per hour and miles respectively; ‡, KPHX is the Phoenix Sky-Harbor Airport weather station; @, U.S. EPA Air Quality System site 04-013-3002; §, BLDU blowing dust, BR mist, DU widespread dust, DS dust storm, FG fog, HZ haze, RA rain, SQ squall, TS thunderstorm, TSRA thunderstorm with rain, VC in the vicinity; *, haboob identified by meteorological and air quality signature but no photograph was available; #, haboob identified by meteorological signature, air quality signature, and photograph; & haboob documented by ADEQ (2015); ♦, Lei and Wang, 2014; ◊, Raman *et al*., 2014.

APPENDIX B

THE DEPOSITION OF HABOOBS IN TEMPE, ARIZONA

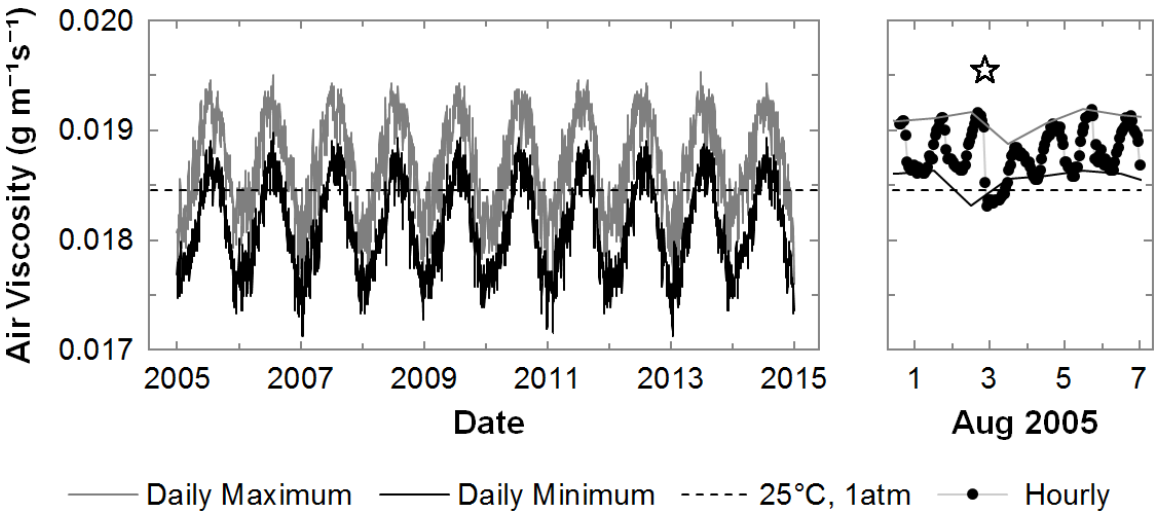

Figure B1. Calculated dynamic air viscosity (η_{air}) at KPHX as a function of dry bulb temperature and station pressure during the time period 2005 to 2014 (right) and during Aug 1 – 6, 2005 (left). Calculations were performed using Mathematica 10 (Mathematica, 2015a). Values of η_{air} had annual and diurnal cycles with maxima in the evening and minima in the morning. η_{air} ranged from 0.0171 to 0.0195 g $m^{-1}s^{-1}$. The star in the right plot indicates the η_{air} decrease associated with a haboob. Hourly markers are omitted from the left figure for clarity.

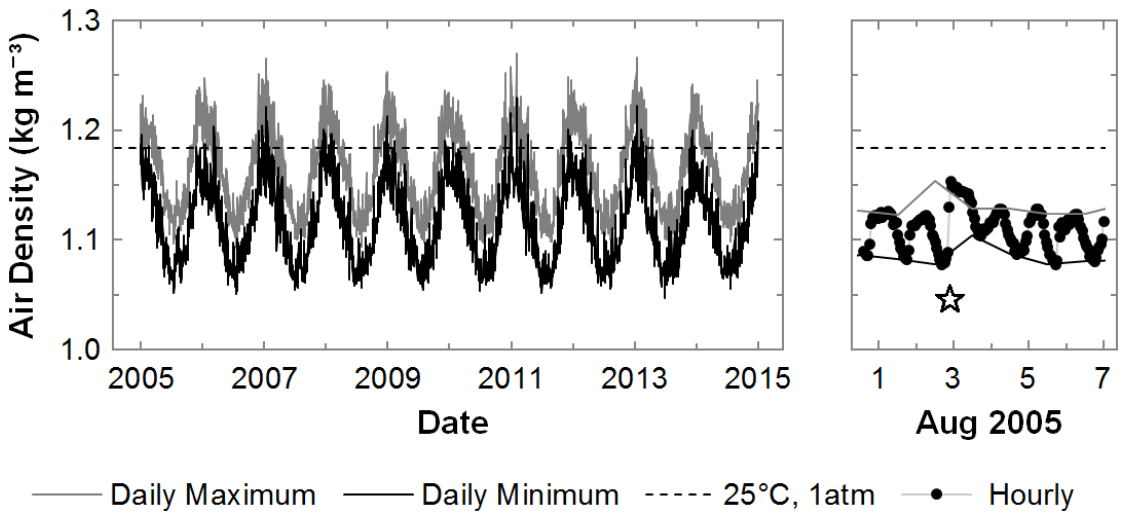

Figure B2. Calculated air density (ρ_{air}) at KPHX as a function of dry bulb temperature and station pressure during the time period 2005 to 2014 (right) and during Aug 1 – 6, 2005 (left). Calculations were performed using Mathematica 10 (Mathematica, 2015b). Values for ρ_{air} had annual and diurnal cycles with maxima in the morning and minima in the evening. ρ_{air} ranged from 1.05 to 1.27 kg m^{-3}. The star in the right plot indicates the ρ_{air} increase associated with a haboob. Hourly markers are omitted from the left figure for clarity.

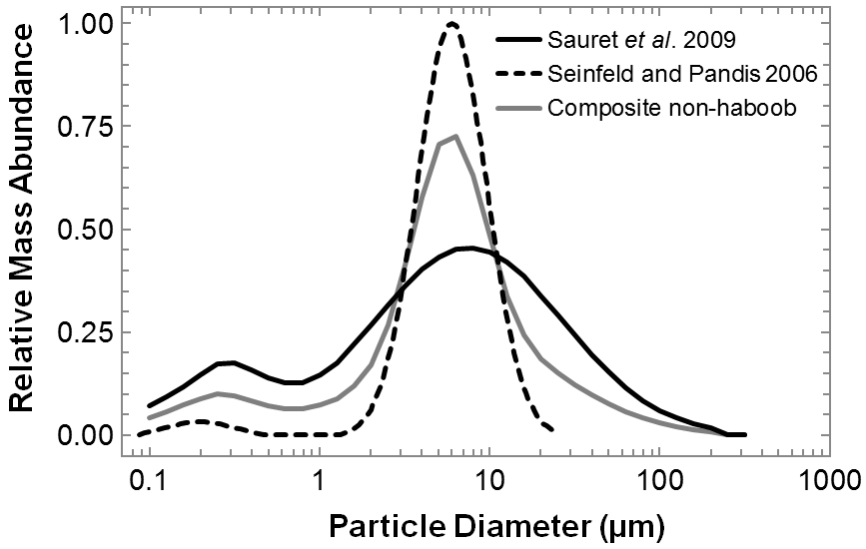

Figure B3. The composite non-haboob PM mass distribution was the average of literature mass distributions (Seinfeld and Pandis, 2006; Sauret *et al*., *2*009). The non-haboob distribution had a $\frac{\mathrm{PM_{10}}}{\mathrm{TSP}}$ mass ratio of 0.78 and a $\frac{\mathrm{PM_{2.5}}}{\mathrm{PM_{10}}}$ mass ratio of 0.24.

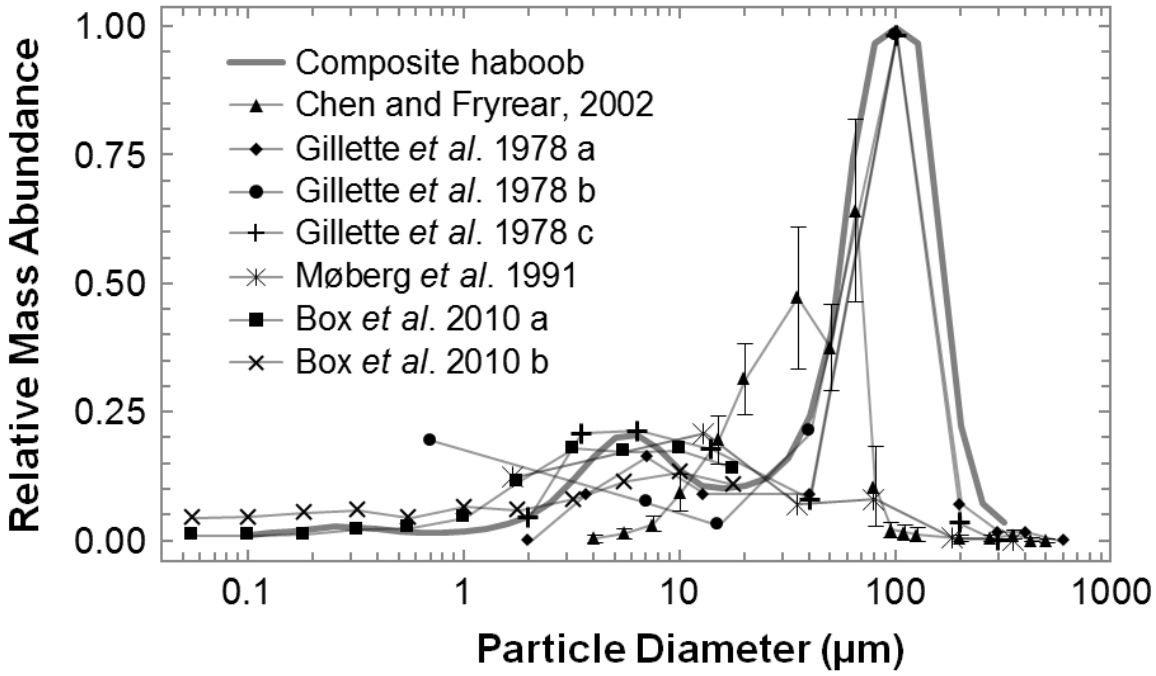

Figure B4. The composite haboob TSP mass distribution was reasonably based on several dust storm distributions in the literature. The composite haboob PM mass distribution was identical to the non-haboob composite distribution for diameters < 10 µm and therefore $\frac{PM_{2.5}}{PM_{10}}$ was the same as well. The haboob composite $\frac{PM_{10}}{TSP}$ mass ratio was 0.20 and its distribution had a large mode around 100 µm. A $\frac{PM_{10}}{TSP}$ mass ratio of 0.06 was estimated from histograms in Chen and Fryrear (2002) using the average of 5 to 20 foot sampler heights. The error bars in the figure above are the standard deviation of the estimated ratios. The mass distributions were estimated from 3 dust storms reported in Gillette *et al*. (Figure 4 and Table 3 therein; 1978) resulting in $\frac{PM_{10}}{TSP}$ mass ratio estimates of 0.18, 0.19, and 0.27. In Box *et al*. (2010), $\frac{PM_{10}}{TSP}$ mass ratios of < 0.85 and < 0.87 were estimated from histograms for two dust storms. These mass ratios are upper bounds since $PM_{>18}$ was not reported due to physical constraints of their sampling equipment.

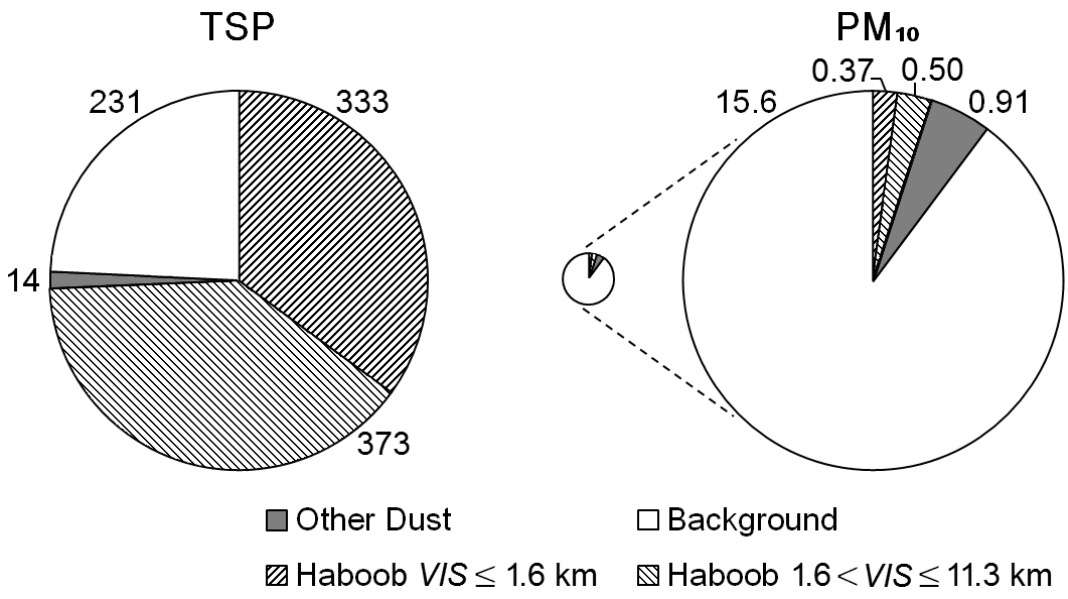

Figure B5. Mean annual dry deposition (kg $ha^{-1}yr^{-1}$) in Tempe for the time period 2005 to 2014. The TSP deposition (left) and the PM_{10} deposition (right) for haboobs, other dust and background time periods. The numbers are the deposition quantities in kg $ha^{-1}yr^{-1}$. The small PM_{10} chart is scaled proportionally to the TSP deposition for comparison. Low visibility haboobs with $VIS \leq 1.6$ km (1 mi) account for one-fourth of the haboobs and deposit 35 % of the total TSP while moderate visibility haboobs with $1.6 < VIS \leq 11.3$ km (1 to 7 mi) account for three-fourths of the haboobs and comprise 39% of TSP deposition. 'Other Dust' is dust events that failed to meet the visibility and meteorological criteria for haboobs. The background includes smog, fog, rain, and fair weather.

APPENDIX C

TEMPE TOWN LAKE CHEMISTRY

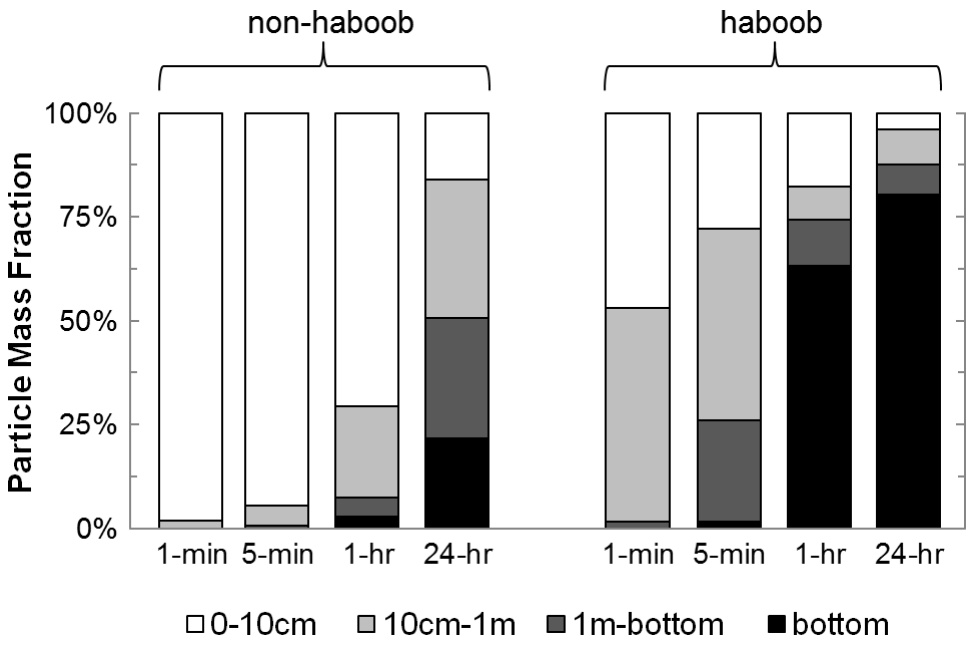

Figure C1. The predicted settling of a non-haboob distribution (left) and a haboob distribution (right) of particles within Tempe Town Lake in a non-dissolution, no-flow scenario, at 10 °C. The shaded bars indicate the percent of overall particle mass contained in three depth layers or on the lake bottom. In less than 24 hours, 50% of the mass in a non-haboob particle distribution will settle below 1 m depth. In 1 minute, 53% of the mass in a haboob particle distribution settles 10 cm or more and during 1 hour, 63% reaches the lake bottom. The values for η_{water} and ρ_{water} employed in the calculations were 0.001306 kg m^{-1} s^{-1} and 999.7 kg m^{-3} respectively (Mathematica, 2015b, 2015c).

APPENDIX D

DISTRIBUTION OF PAHS IN CLOUDS AND FOG

Table D1

Summary of PAH Partition Ratios at 25 °C

Name of PAH / Oxy–PAH	Abbreviation	Molar Mass [Da]	Reference log K_{OW}	Reference log K_{OA}	Reference H [M atm^{-1}]	H^* [M atm^{-1}]
PAH						
naphthalene	NAP	128.17	3.33 [a]	5.19 [j]	2.4 [m]	3.0
acenaphthylene	ACY	152.19	3.94 [b]	6.34 [k]	8.0 [n]	10
acenaphthene	ACE	154.21	3.92 [c]	6.52 [k]	5.5 [n]	16
9*H*–fluorene	FLU	166.22	4.18 [b]	6.90 [k]	10 [n]	21
phenanthrene	PHE	178.23	4.57 [a]	7.68 [k]	21 [m]	53
anthracene	ANT	178.23	4.68 [a]	7.71 [k]	18 [m]	44
fluoranthene	FLT	202.25	5.23 [a]	8.76 [k]	52 [n]	140
pyrene	PYR	202.25	4.88 [b]	8.80 [l]	59 [n]	350
acephenanthrylene	ACP	202.25	(4.93) [d]	(8.40) [j]	(120) [o]	120
11*H*–benzo[*a*]fluorene	BAU	216.27	5.68 [e]	(8.36) [j]	38 [n]	38
11*H*–benzo[*b*]fluorene	BBU	216.27	5.77 [e]	(9.57) [j]	(61) [o]	260
benzo[*a*]anthracene	BAA	228.29	5.91 [a]	10.28 [k]	83 [n]	970
chrysene	CHY	228.29	5.81 [a]	10.30 [k]	190 [n]	1.3×10^3
retene	RET	234.33	(6.53) [d]	(8.70) [j]	(9.0) [o]	6.0
benzo[*b*]fluoranthene	BBF	252.31	5.78 [f]	11.34 [k]	1.5×10^3 [p]	1.5×10^4
benzo[*k*]fluoranthene	BKF	252.31	6.11 [a]	11.37 [k]	1.7×10^3 [p]	7.4×10^3
benzo[*a*]pyrene	BAP	252.31	6.13 [a]	11.56 [k]	2.2×10^3 [p]	1.1×10^4
benzo[*e*]pyrene	BEP	252.31	6.44 [f]	(11.35) [j]	(1.2×10^3) [o]	3.3×10^3
indeno[1,2,3–*cd*]pyrene	IND	276.33	6.30 [g]	12.43 [k]	2.8×10^3 [p]	2.2×10^4
dibenz[*a*,*h*]anthracene	DBA	278.35	6.75 [h]	12.59 [k]	(2.0×10^3) [o]	2.8×10^4
benzo[*g*,*h*,*i*]perylene	BGP	276.33	6.22 [a]	12.55 [k]	3.0×10^4 [p]	8.5×10^4

Table D1 (continued)

Name of PAH / Oxy–PAH	Abbreviation	Molar Mass [Da]	Reference log K_{OW}	Reference log K_{OA}	Reference H [M atm^{-1}]	H^* [M atm^{-1}]
Oxy–PAH						
1,4–naphthoquinone	oNAP	158.16	1.71 [b]	(8.80) [j]	(5.1×10^5) [o]	5.1×10^5
2*H*–chromen–2–one [q]	oCOU	146.14	1.39 [b]	(6.78) [j]	(1.4×10^4) [o]	1.0×10^4
4*H*–chromen–4–one [r]	oCRM	146.15	1.38 [b]	(5.86) [j]	(1.2×10^3) [o]	1.2×10^3
1*H*–phenalen–1–one [s]	oPNE	180.21	(3.39) [d]	(8.77) [j]	(9.7×10^3) [o]	9.7×10^3
9*H*–fluoren–9–one	oFLU	180.21	3.58 [b]	(8.14) [j]	(1.5×10^3) [o]	1.5×10^3
acenaphthenequinone	oACE	182.18	1.95 [b]	(8.80) [j]	(2.9×10^5) [o]	2.9×10^5
9(10*H*)–anthrone [t]	oATR	194.23	3.66 [b]	(8.15) [j]	(1.3×10^3) [o]	1.3×10^3
9*H*–xanthen–9–one [u]	oXAN	196.21	3.39 [b]	(8.49) [j]	(5.2×10^3) [o]	5.2×10^3
6*H*–benzo[*c*]chromen–6–one [v]	oDBP	196.21	(1.99) [d]	(5.73) [j]	(224) [o]	224
phenanthrene–1,4–dione	oPHE1	208.22	(2.84) [d]	(10.95) [j]	(5.2×10^6) [o]	5.2×10^6
phenanthrene–9,10–dione	oPHE2	208.22	2.52 [b]	(9.48) [j]	(3.7×10^5) [o]	3.7×10^5
9,10–anthraquinone	oANT	208.22	3.39 [i]	(9.41) [j]	(3.1×10^5) [o]	4.3×10^4
7*H*–benzo[*de*]anthracen–7–one [w]	oBTR	230.27	(4.73) [d]	(10.38) [j]	(1.5×10^4) [o]	1.8×10^4
11*H*–benzo[*a*]fluoren–11–one	oBAU	230.27	(4.73) [d]	(10.30) [j]	(1.5×10^4) [o]	1.5×10^4
11*H*–benzo[*b*]fluoren–11–one	oBBU	230.27	(4.73) [d]	(10.30) [j]	(1.5×10^4) [o]	1.5×10^4
pyrene–1,6–dione	oPYR1	232.24	(3.60) [d]	(12.69) [j]	(5.0×10^7) [o]	5.0×10^7
pyrene–1,8–dione	oPYR2	232.24	(3.60) [d]	(12.69) [j]	(5.0×10^7) [o]	5.0×10^7
aceanthrylene–1,2–dione [x]	oAAN	232.24	(4.15) [d]	(12.01) [j]	(3.0×10^6) [o]	3.0×10^6
benz[*a*]anthracene–7,12–dione	oBAA	258.27	(4.52) [d]	(12.30) [j]	(3.2×10^6) [o]	2.4×10^6
chrysene–1,4–dione	oCHY	258.27	(4.01) [d]	(13.12) [j]	(5.3×10^7) [o]	5.3×10^7
benzo[*a*]pyrene–1,6–dione	oBAP1	282.29	(4.94) [d]	(14.22) [j]	(7.7×10^7) [o]	7.8×10^7
benzo[*a*]pyrene–3,6–dione	oBAP2	282.29	(4.94) [d]	(14.22) [j]	(7.7×10^7) [o]	7.8×10^7
benzo[*a*]pyrene–4,5–dione	oBAP3	282.29	(5.32) [d]	(14.19) [j]	(3.1×10^7) [o]	3.1×10^7
benzo[*a*]pyrene–6,12–dione	oBAP4	282.29	(3.80) [d]	(13.31) [j]	(1.3×10^8) [o]	1.3×10^8
benzo[*e*]pyrene–4,5–dione	oBEP	282.29	(5.32) [d]	(14.19) [j]	(3.1×10^7) [o]	3.1×10^7

Table D1 (continued)

Notes: Estimated values from US EPA EPISuite are in parenthesis. a. de Maagd *et al*., 1998; b. Hansch *et al*., 1995; c. Banerjee *et al*., 1980; d. EPISuite KOWWIN v1.68 estimate; e. Wang *et al*., 1986; f. De Voogt *et al*., 1990; g. Sahu and Pandit, 2003; h. Sangster, 1989; i, Pratesi *et al*., 1979; j. EPISuite KOAWIN v1.10 estimate; k. Odabasi *et al*., 2006; l. Harner and Bidleman, 1998a; m. calculated from Alaee *et al*., 1996; n. Bamford *et al*., 1999; o. EPISuite HENRYWIN v3.20, Bond Method; p. ten Hulscher *et al*., 1992. Trivial names: q. coumarin; r. chromone; s. perinaphthenone; t. anthrone; u. xanthone; v. dibenzopyranone; w. benzanthrone; x. aceanthraquinone.

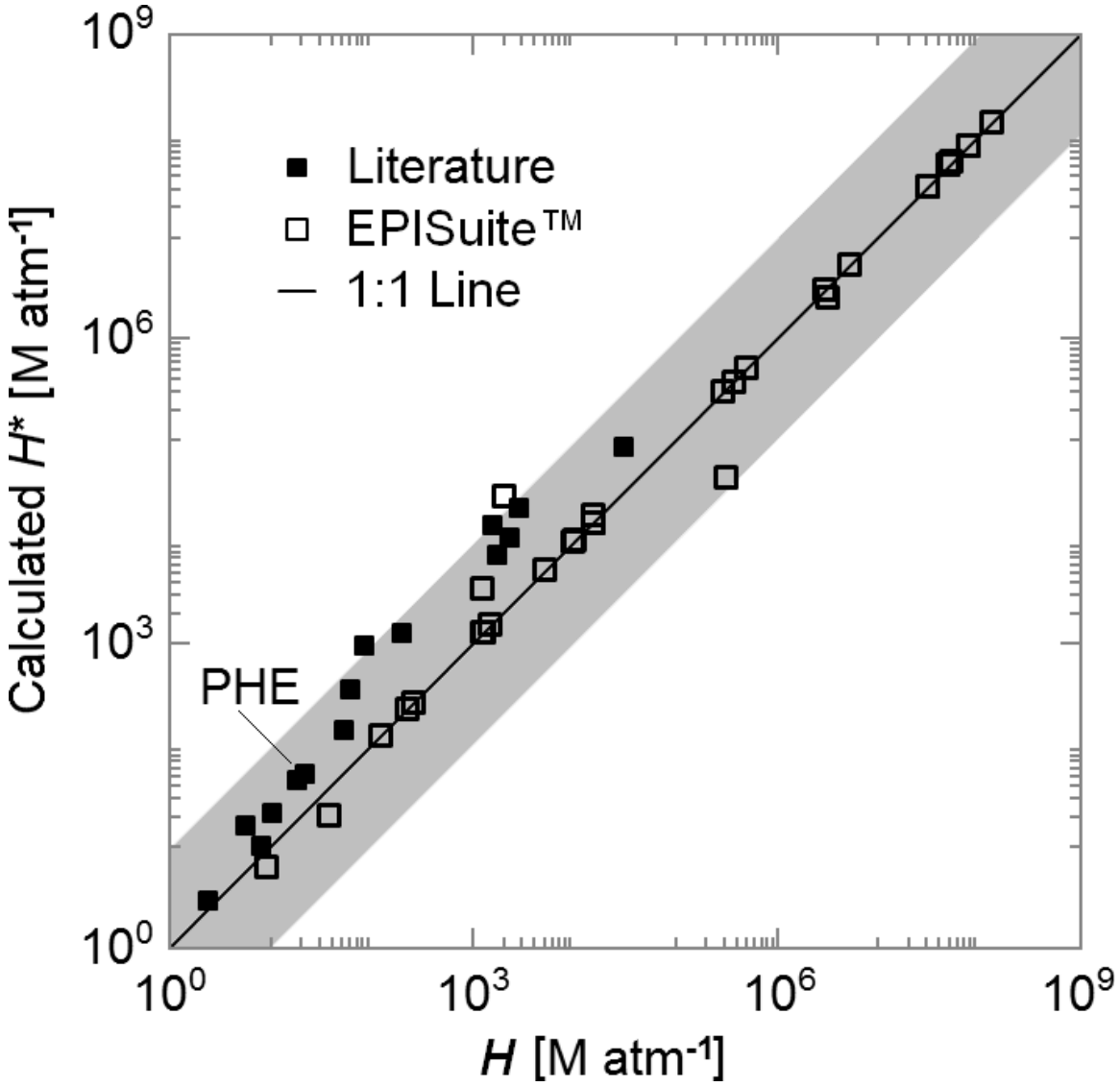

Figure D1. Comparison of ideal Henry's law constants *H* and calculated Henry's law constants *H** at 25 °C. The *H**values calculated with Equation 5.4 were approximately within an order of magnitude (gray area) of the literature *H* (solid square) and EPISuite *H* (open square) values. PAH *H** were generally higher than *H, i.e.*, above the 1:1 line, since Equation 5.4 employs constants measured in octanol saturated water which

increases PAH solubility. Many EPISuite values fall on the 1:1 line with calculated values since EPISuite uses Equation 5.5 to estimate K_{OA} where no literature value exists.

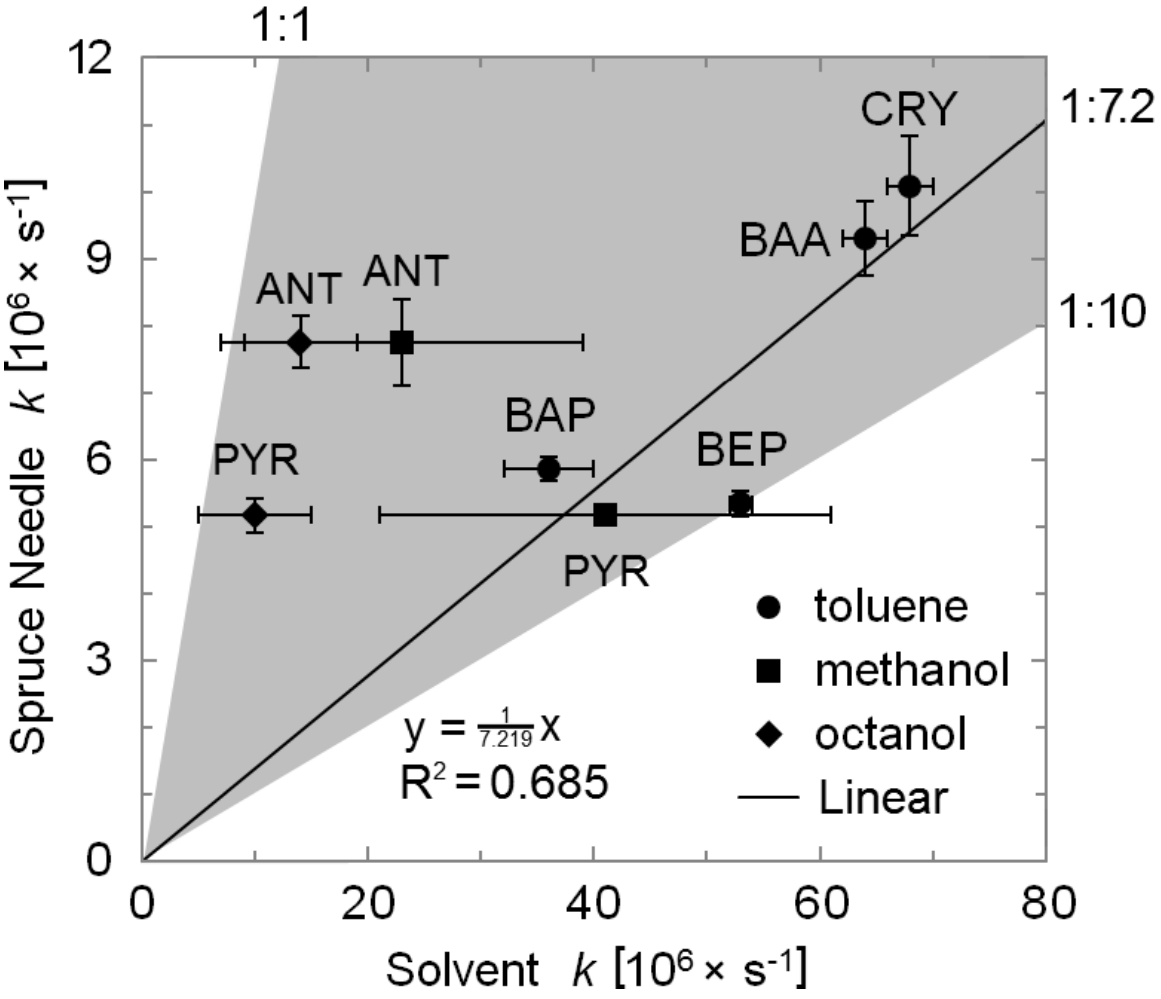

Figure D2. Comparison of the liquid organic phase rates and the 1 / 7.2 relationship for estimating solvent rates based on spruce needle rates. The photooxidation rate in toluene (circle symbols; Plata *et al*., 2008), methanol and 1–octanol (square and diamond symbols respectively; Grossman *et al*., 2016) solvents differs from the photooxidation rate in spruce needles (Niu *et al*., 2003) by less than one order of magnitude (shaded grey area indicates the boundary of 1:1 and 1:10).

Table D2

Summary of Kinetic Rate Constants at 25 °C

	Gas phase [cm^3 $molecule^{-1}$ s^{-1}]				Liquid phase [s^{-1}]	
Name	$k(^{\bullet}OH, g)$	$k(O_3, g)$	$k(O(^3P), g)$	$k(^{\bullet}NO_3, g)$	k(org)	k(aq)
PAH						
NAP	$2.2 \pm 0.7 \times 10^{-11}$ [a]	$< 2 \times 10^{-19}$ [b,f]	1.1×10^{-12} [b]	3.6×10^{-28} [i]		2.7×10^{-6} [q]
ACY	1.09×10^{-10} [b,c]	$\sim 5.5 \times 10^{-16}$ [b,g]		(4.6×10^{-27}) [g,j]	(5.2×10^{-5}) [p]	
ACE	1.0×10^{-10} [b,c]	$< 5 \times 10^{-19}$ [b,g]		(3.8×10^{-28}) [g,j]	(3.1×10^{-5}) [p]	3×10^{-5} [r]
FLU	1.4×10^{-11} [b]	$< 2 \times 10^{-19}$ [b]		(4.9×10^{-28}) [k]	(3.4×10^{-5}) [p]	9×10^{-7} [r]
PHE	$3.1 \pm 0.9 \times 10^{-11}$ [a]	4×10^{-19} [b,h]	1.4×10^{-12} [b]	(2.5×10^{-27}) [h,l]	(1.8×10^{-5}) [p]	9×10^{-6} [r]
ANT	$1.3 \pm 0.4 \times 10^{-11}$ [a]				$2.3 \pm 1.6 \times 10^{-5}$ [s]	$2.3 \pm 2 \times 10^{-4}$ [s]
FLT	$\sim 1.8 \times 10^{-11}$ [b]			5.1×10^{-28} [m]	(5.4×10^{-5}) [p]	5×10^{-6} [r]
PYR	5.0×10^{-11} [d]			1.6×10^{-27} [m]	$4.1 \pm 2.0 \times 10^{-5}$ [s]	$1.8 \pm 0.4 \times 10^{-4}$ [s]
ACP	(1.61×10^{-11}) [e]					
BAU	(4.66×10^{-11}) [e]					
BBU	(4.66×10^{-11}) [e]					
BAA	(5.3×10^{-11}) [b]				$6.4 \pm 0.2 \times 10^{-5}$ [o]	3.3×10^{-4} [q]
CHY	(3.4×10^{-11}) [b]				$6.8 \pm 0.2 \times 10^{-5}$ [o]	4.3×10^{-5} [t]
RET	(4.17×10^{-11}) [e]					
BBF	(1.86×10^{-11}) [e]				(3.0×10^{-5}) [p]	3×10^{-5} [r]
BKF	(5.36×10^{-11}) [e]				(3.2×10^{-5}) [p]	3×10^{-5} [r]
BAP	(9.0×10^{-11}) [b]				$3.6 \pm 0.4 \times 10^{-5}$ [o]	2.1×10^{-3} [r]
BEP	(4.0×10^{-11}) [b]				$5.3 \pm 0.1 \times 10^{-5}$ [o]	
IND	(6.45×10^{-11}) [e]				(3.1×10^{-5}) [p]	
DBA	(4.6×10^{-11}) [b]				(8.8×10^{-5}) [p]	
BGP	(8.69×10^{-11}) [e]				(3.0×10^{-5}) [p]	

Table D2 (continued)

Name	Gas phase [cm^3 $molecule^{-1}$ s^{-1}]				Liquid phase [s^{-1}]	
	$k(^{\bullet}OH, g)$	$k(O_3, g)$	$k(O(^3P), g)$	$k(^{\bullet}NO_3, g)$	$k(org)$	$k(aq)$
Oxy–PAH						
oNAP	3.0×10^{-12} [b]	$< 2 \times 10^{-19}$ [b]		$(< 1.2 \times 10^{-29})$ [b,n]		
oCOU	(1.32×10^{-11}) [e]	(2.10×10^{-17}) [e]				
oCRM	(3.09×10^{-11}) [e]	(8.75×10^{-18}) [e]				
oPNE	(2.39×10^{-11}) [e]	(2.10×10^{-17}) [e]				
oFLU	(6.18×10^{-12}) [e]					
oACE	(8.30×10^{-12}) [e]					
oATR	(9.77×10^{-12}) [e]					
oXAN	(8.97×10^{-12}) [e]					
oDBP	(5.58×10^{-12}) [e]					
oPHE1	(1.06×10^{-11}) [e]	(1.75×10^{-18}) [e]				
oPHE2	(6.18×10^{-12}) [e]					
oANT	(1.50×10^{-12}) [e]					
oBTR	(1.80×10^{-11}) [e]					
oBAU	(1.80×10^{-11}) [e]					
oBBU	(1.80×10^{-11}) [e]					
oPYR1	(2.99×10^{-11}) [e]	(4.20×10^{-17}) [e]				
oPYR2	(2.99×10^{-11}) [e]	(4.20×10^{-17}) [e]				
oAAN	(1.54×10^{-11}) [e]					
oBAA	(9.05×10^{-12}) [e]					
oCHY	(7.25×10^{-12}) [e]	(1.75×10^{-18}) [e]				
oBAP1	(2.31×10^{-11}) [e]	(2.10×10^{-17}) [e]				
oBAP2	(2.31×10^{-11}) [e]	(2.10×10^{-17}) [e]				
oBAP3	(1.92×10^{-11}) [e]					
oBAP4	(3.99×10^{-11}) [e]	(2.52×10^{-16}) [e]				
oBEP	(1.92×10^{-11}) [e]					

Table D2 (continued)

Notes: Estimated and calculated values are in parenthesis. a. Atkinson, 1989; b. calculated rates in Calvert *et al*., 2002 with [$^{\bullet}$OH] = 3×10^6 molecules cm^{-3}, [O_3] = 30 ppb, and [$O(^3P)$] = 200 molecules cm^{-3}; c. Atkinson and Aschmann, 1987; d. Atkinson *et al*., 1987; e. EPISuite AOPWIN v1.92 estimate; f. Atkinson *et al*., 1984; g. Atkinson and Aschmann, 1988; h. Kwok *et al*., 1994; i. Atkinson, 1991; j. calculated with [NO_2] = < 1.2×10^{15} molecules cm^{-3}; k. calculated rate in Kwok *et al*., 1997 with [NO_2] = < 7.2×10^{13} molecules cm^{-3}; l. calculated rate in Kwok *et al*., 1994 with [NO_2] = < 4.8×10^{13} molecules cm^{-3}; m. Atkinson *et al*., 1990; n. calculated rate given in Calvert *et al*., 2002 with [NO_2] = 8×10^{13} molecules cm^{-3}; o. Plata *et al*., 2008; p. estimated from Niu *et al*., 2003; q. Zepp and Schlotzhauer, 1979; r. Fasnacht and Blough, 2002; s. Grossman *et al*., 2016; t. Kong and Ferry, 2003. See Table D1 for abbreviations.

Table D3

Molar oxy–PAH Yields in Gas, Aqueous, and Liquid Organic Phases

Reactant	Molar Conversion, Y_m [Percent]					
Product	Y_m(•OH, g)	Y_m(O_3, g)	Y_m($O(^3P)$, g)	Y_m(aq)	Y_m(org)	Product Comments
NAP						
oNAP [a, b]	(1%)	(1%)	(1%)	(1%)	(1%)	Experimental gas phase •OH product [a, b]
(oCOU) [c]	(0.1%)	(0.1%)	(0.1%)	(0.1%)	(0.1%)	Experimental aqueous non–AR[d] product [c]
(oCRM)	(0.05%)	(0.05%)	(0.05%)	(0.05%)	(0.05%)	Probable product and probable Y_m[e]
ACY						
oACE [f]	(1%)	(1%)	(1%)	0.3–2%[f]	(1%)	Experimental aqueous product and Y_m[f]
(oACE)	(1%)	(1%)	(1%)	(1%)	(1%)	Probable product and probable Y_m[e]
FLU						
oFLU [g]	(1%)	(1%)	(1%)	(1%)	(1%)	Experimental gas phase •OH product [g]
PHE						
oPHE1 [i]	1.36±0.03[i]	(1%)	(1%)	(1%)	(1%)	Experimental gas phase •OH product and Y_m[i]
oPHE2 [h, i, j]	3±3%[h]; 0.98±0.01%[i]	2±1%[h]	(1%)	(1%)	(1%)	Experimental gas phase product [h, i, j] and Y_m[h, i]
oFLU [h, i, j]	0.33±0.02%[i]	(0.05%)	(0.05%)	(0.05%)	(0.05%)	Experimental gas phase [i, j] •OH product and Y_m[h]
oDBP [h, i, j]	(0.05%)	(0.05%)	(0.05%)	(0.05%)	(0.05%)	Experimental gas phase •OH product [h, i, j]
ANT						
oANT [k, l]	(1%)	(1%)	(1%)	0.15±0.02%[k]	(1%)	Experimental aqueous product [k, l] and Y_m[k]
(oATR) [c, l]	(0.05%)	(0.05%)	(0.05%)	(0.05%)	(0.05%)	Experimental aqueous non–AR[d] product [c, l]
(oXAN)	(0.05%)	(0.05%)	(0.05%)	(0.05%)	(0.05%)	Probable product and probable Y_m[e]
FLT						
(oPNE)	(0.1%)	(1%)	(1%)	(0.1%)	(0.1%)	Probable product and probable Y_m[e]
PYR						
(oPYR1)	(0.5%)	(0.5%)	(0.5%)	(0.5%)	(0.5%)	Probable product and probable Y_m[e]
(oPYR2)	(0.5%)	(0.5%)	(0.5%)	(0.5%)	(0.5%)	Probable product and probable Y_m[e]

Table D3 (continued)

Reactant *Product*	Molar Conversion, Y_m [Percent] Y_m(•OH, g)	$Y_m(O_3, g)$	$Y_m(O(^3P), g)$	Y_m(aq)	Y_m(org)	Product Comments
ACP						
(oAAN)	(0.1%)	(0.1%)	(0.1%)	(0.1%)	(0.1%)	Probable product and probable Y_m [e]
BAU						
(oBAU)	(1%)	(1%)	(1%)	(1%)	(1%)	Probable product and probable Y_m [e]
BBU						
(oBBU)	(1%)	(1%)	(1%)	(1%)	(1%)	Probable product and probable Y_m [e]
BAA						
oBAA [m]	(1%)	(1%)	(1%)	(1%)	(1%)	Experimental toluene irradiation product [m]
(oCOU) [c]	(0.1%)	(0.1%)	(0.1%)	(0.1%)	(0.1%)	Experimental aqueous non–AR[d] product [c]
CHY						
oCHY [n]	(1%)	(1%)	(1%)	< 1% [n]	(1%)	Experimental aqueous product and Y_m [n]
BAP						
oBTR[o]	(0.1%)	(0.1%)	(0.1%)	(0.1%)	(0.1%)	Experimental gas phase O_3 product [o]
oBAP1[o]	(0.25%)	(0.25%)	(0.25%)	(0.25%)	(0.25%)	Experimental gas phase O_3 product [o]
oBAP2 [o]	(0.25%)	(0.25%)	(0.25%)	(0.25%)	(0.25%)	Experimental gas phase O_3 product [o]
oBAP3[o,l]	(0.25%)	(0.25%)	(0.25%)	(0.25%)	(0.25%)	Experimental gas phase O_3 product [o]
oBAP4[o]	(0.25%)	(0.25%)	(0.25%)	(0.25%)	(0.25%)	Experimental gas phase O_3 product [o]
BEP						
oBEP [p]	(1%)	(1%)	(1%)	(1%)	(1%)	Experimental acetonitrile irradiation product [p]

Notes: Parentheses indicate probable products and estimated conversion quantities. For products that did not have a literature molar yield, 1% was used for products with native-ring backbone intact while 0.1% was used for ring-rearranged / ring-opened products. The remaining percentage of products has been reported to be monocyclic and acyclic compounds.

Table D3 (continued)

a. Lane *et al*., 1996; b. Mihele *et al*., 2002; c. Woo *et al*., 2009; d. the molar yield, Y_m, was not used for literature that did not employ filters to correct the UV irradiation intensity spectrum to be representative of sunlight at the surface of the Earth (AR); e. reaction not in literature, probable product and probable Y_m; f. calculated from product formed over the total parent lost Sigman *et al*., 1996; g. Helmig *et al*., 1992; h. Wang *et al*., 2007; i. Lee and Lane, 2010; j. Helmig and Harger, 1994; k. Mallakin *et al*., 2000; l. Sanches *et al*., 2011; m. Jang and McDow, 1997; n. Kong and Ferry, 2003; o. Letzel *et al*., 1999; p. Fioressi and Arce, 2005. See Table D1 for the full compound names.

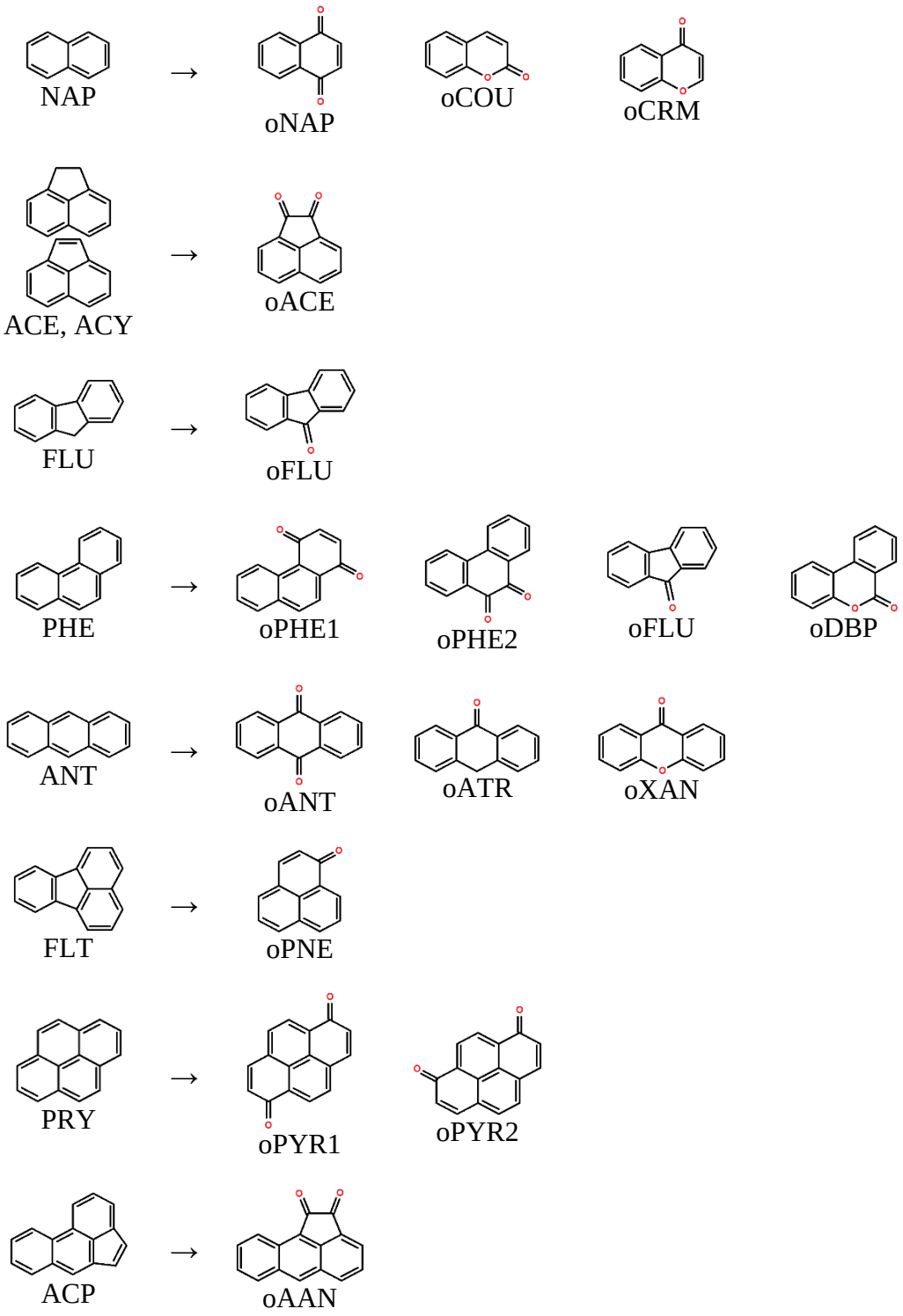

Figure D3a. Molecular structures of PAHs and their oxidation products (oxy–PAHs).

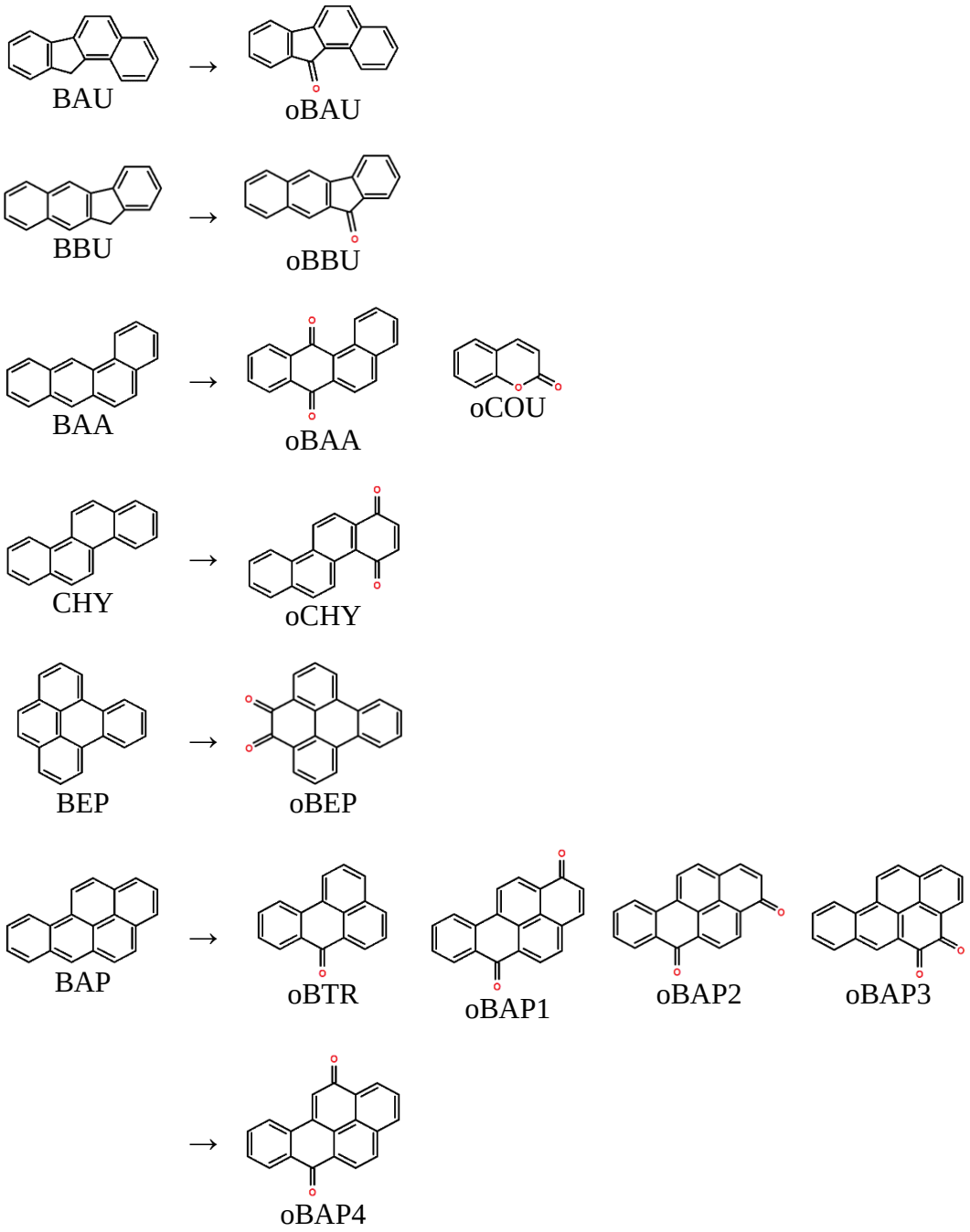

Figure D3b. Molecular structures of PAHs and their oxidation products (oxy–PAHs).

EQUATIONS D1 – D15

Calculation of liquid organic phase volume fraction.

For fog with LWC = 0.3 g m^{-3}, with a TOC of 5 mgC L^{-1} liquid organic phase that is 70% carbon by mass, a liquid organic mass density ρ^{org} = 0.7 g cm^{-3}, and a drop mass density ρ^{aq} = 1 g cm^{-3}, the liquid organic phase volume fraction (ϕ^{org}) is 3×10^{-12} org/air:

$$\phi^{org} = \frac{TOC[mgC\ L_{aq}^{-1}]LWC[g_{aq}\ m_{air}^{-3}](10^{-3}L_{aq}\ cm_{aq}^{-3})(10^{-3}g_{org}\ mg_{org}^{-1})}{0.7[mgC\ mg_{org}^{-1}]\rho^{org}[g_{org}\ cm_{org}^{-3}]\rho^{aq}[g_{aq}\ cm_{aq}^{-3}](10^{6}cm_{org}^{3}\ m_{org}^{-3})} \quad \text{(D1).}$$

Calculation of PAH and oxy–PAH fractions and concentrations in terms of total air volume.

The concentrations of PAHs and oxy–PAHs in Equations 5.1, 5.2, and 5.4 of the main text are in terms of phase volumes, which are different for each phase. In lieu of converting between volume dimensions in every time step, the following equations were developed. The aqueous phase concentration $[PAH]_{aq}$ [mol L_{aq}^{-1}] was converted to c^{aq} [mol m_{air}^{-3}], the concentration in terms of total air volume in Equation D2 where ϕ^{aq} is the aqueous phase volume fraction:

$$c^{aq}[\text{mol } m_{air}^{-3}] = \phi^{aq}[PAH]_{aq} \quad \text{(D2).}$$

The $[PAH]_{org}$ [mol L_{org}^{-1}] were similarly converted to c^{org} [mol m_{air}^{-3}] using Equation D3:

$$c^{org}[\text{mol } m_{air}^{-3}] = \phi^{org}[PAH]_{org} \quad \text{(D3).}$$

The total concentration c_i^{total}[mol m_{air}^{-3}] of a species was calculated (Equation D4) at the end of each time step, *i*-1 (*i.e.*, after reaction during the time step) to become the new concentration of the next time step, *i*.

$$c_i^{total}[\text{mol } m_{air}^{-3}] = c_{i-1}^{g} + c_{i-1}^{aq} + c_{i-1}^{org} \quad \text{(D4).}$$

The species was then re-equilibrated between phases using Equations D5 – D7:

$$c_i^{\mathrm{g}}[\mathrm{mol\ m_{air}^{-3}}] = c_i^{\mathrm{total}} \frac{K_{\mathrm{OW}}}{K_{\mathrm{OW}}+(K_{\mathrm{OA}}\phi^{\mathrm{aq}})+(K_{\mathrm{OW}}K_{\mathrm{OA}}\phi^{\mathrm{org}})} \quad \text{(D5)},$$

$$c_i^{\mathrm{aq}}[\mathrm{mol\ m_{air}^{-3}}] = c_i^{\mathrm{total}} \frac{K_{\mathrm{OA}}\phi^{\mathrm{aq}}}{K_{\mathrm{OW}}+(K_{\mathrm{OA}}\phi^{\mathrm{aq}})+(K_{\mathrm{OW}}K_{\mathrm{OA}}\phi^{\mathrm{org}})} \quad \text{(D6)},$$

$$c_i^{\mathrm{org}}[\mathrm{mol\ m_{air}^{-3}}] = c_i^{\mathrm{total}} \frac{K_{\mathrm{OW}}K_{\mathrm{OA}}\phi^{\mathrm{org}}}{K_{\mathrm{OW}}+(K_{\mathrm{OA}}\phi^{\mathrm{aq}})+(K_{\mathrm{OW}}K_{\mathrm{OA}}\phi^{\mathrm{org}})} \quad \text{(D7)}.$$

The phase fractions were then calculated with Equations D8 – D10. Following that, the reaction of the species was calculated during the new time step, *i*.

$$x_i^{\mathrm{g}}[dimensionless] = c_i^{\mathrm{g}}/c_i^{\mathrm{total}} \quad \text{(D8)}.$$

$$x_i^{\mathrm{aq}}[dimensionless] = c_i^{\mathrm{aq}}/c_i^{\mathrm{total}} \quad \text{(D9)}.$$

$$x_i^{\mathrm{org}}[dimensionless] = c_i^{\mathrm{org}}/c_i^{\mathrm{total}} \quad \text{(D10)}.$$

The calculation of droplet surface film coverage by PAHs and alkyl chain hydrocarbons.

To determine whether the droplets should be modeled with a liquid organic surface film, the fractional surface coverage (θ) of a hypothetical film was calculated with Equations 5.6, 5.7, D11 and D14. The total surface area of PAHs $A^{\mathrm{PAH}}[\mathrm{m^2\ m_{air}^{-3}}]$ assuming they lie flat on the air / water interface (Chen *et al*., 2011) was determined with Equation D11 where $m^{\mathrm{PAH}}[\mathrm{ng\ m_{air}^{-3}}]$ is the mass concentration of PAHs, N_{A} is Avogadro's number $[6.022 \times 10^{23} molecule\ \mathrm{mol^{-1}}]$, and $M^{\mathrm{PAH}}[\mathrm{g\ mol^{-1}}]$ is the molar mass:

$$A^{\mathrm{PAH}}[\mathrm{m^2\ m_{air}^{-3}}] = \frac{m^{\mathrm{PAH}}A\prime^{\mathrm{PAH}}N_{\mathrm{A}}}{M^{\mathrm{PAH}}(10^{18}\mathrm{nm^2\ m^{-2}})(10^{9}\mathrm{ng\ g^{-1}})} \quad \text{(D11)}.$$

$A'^{\mathrm{PAH}}[\mathrm{nm}^2\ molecule^{-1}]$ is the single molecule surface area and corresponded to 0.5000 nm^2 for NAP, 0.7229 nm^2 for PYR, 0.8813 nm^2 for BAP, and 0.9899 nm^2 for DBA (Chemicalize.org, 2016a,b,c,d).

The total surface area $A^{\mathrm{fog}}[\mathrm{m}^2\ \mathrm{m}_{\mathrm{air}}^{-3}]$ of fog droplets was determined to be 0.18 $m^2\ m_{air}^{-3}$ with Equations D12 – D14 using LWC $[0.3\ \mathrm{g}\ \mathrm{m}_{\mathrm{air}}^{-3}]$, ρ^{drop} $[1\mathrm{g}\ \mathrm{cm}^{-3}]$, drop volume $V^{\mathrm{drop}}[\mu\mathrm{m}^3]$, and drop diameter d^{drop} $[10\mu\mathrm{m}]$:

$$A^{\mathrm{fog}}[\mathrm{m}^2\ \mathrm{m}_{\mathrm{air}}^{-3}] = \frac{\mathrm{LWC}\ A^{\mathrm{drop}}}{\rho^{\mathrm{drop}}\ V^{\mathrm{drop}}} \quad \text{(D12)},$$

$$\frac{A^{\mathrm{drop}}}{V^{\mathrm{drop}}} = \frac{6}{d^{\mathrm{drop}}} \quad \text{(D13)},$$

$$A^{\mathrm{fog}}[\mathrm{m}^2\ \mathrm{m}_{\mathrm{air}}^{-3}] = \frac{6\ \mathrm{LWC}}{\rho_{\mathrm{drop}}\ d_{\mathrm{drop}}}\ \frac{(10^{-6}\mathrm{m}^3\ \mathrm{cm}^{-3})}{(10^{-6}\mathrm{m}\ \mu\mathrm{m}^{-1})} \quad \text{(D14)}.$$

A short alkyl chain Van der Waals cross-sectional area $A'^{\mathrm{org}} \approx 0.23\ nm^2$ (*e.g.*, C_7 alkyl chain of 1–octanol cross-sectional area = 0.2282 nm^2; Chemicalize.org, 2015). The total liquid organic surface area $A^{\mathrm{org}}[\mathrm{m}^2\ \mathrm{m}_{\mathrm{air}}^{-3}]$ was determined using as a liquid organic the molar mass of 1–octanol $M^{\mathrm{org}} = M^{1\text{–octanol}}$ $\left[130.23\mathrm{g}_{\mathrm{org}}\ \mathrm{mol}^{-1}\right]$, TOC $\left[5\mathrm{mgC}\ \mathrm{L}_{\mathrm{aq}}^{-1}\right]$ existing entirely as a water-immiscible liquid organic phase, $\mathrm{LWC}\left[0.3\mathrm{g}_{\mathrm{aq}}\ \mathrm{m}_{\mathrm{air}}^{-3}\right]$, drop mass density $\rho^{\mathrm{aq}}\left[1\mathrm{g}_{\mathrm{aq}}\ \mathrm{cm}_{\mathrm{aq}}^{-3}\right]$, and the percent C content of 1–octanol $x^{\mathrm{C}}\left[0.7378\mathrm{mgC}\ \mathrm{mg}_{\mathrm{org}}^{-1}\right]$:

$$A^{\mathrm{org}}[\mathrm{m}^2\ \mathrm{m}_{\mathrm{air}}^{-3}] = \frac{\mathrm{TOC}\ \ \mathrm{LWC}\ \ A'^{\mathrm{org}}\ N_{\mathrm{A}}}{x^{\mathrm{C}}\ \rho^{\mathrm{aq}}\ M^{\mathrm{org}}}\ \frac{(10^{-18}\mathrm{m}^2\ \mathrm{nm}^{-2})}{(10^3\mathrm{mg}_{\mathrm{org}}\ \mathrm{g}_{\mathrm{org}}^{-1})(10^3\mathrm{cm}_{\mathrm{aq}}\ \mathrm{L}_{\mathrm{aq}}^{-3})} \quad \text{(D15)}.$$

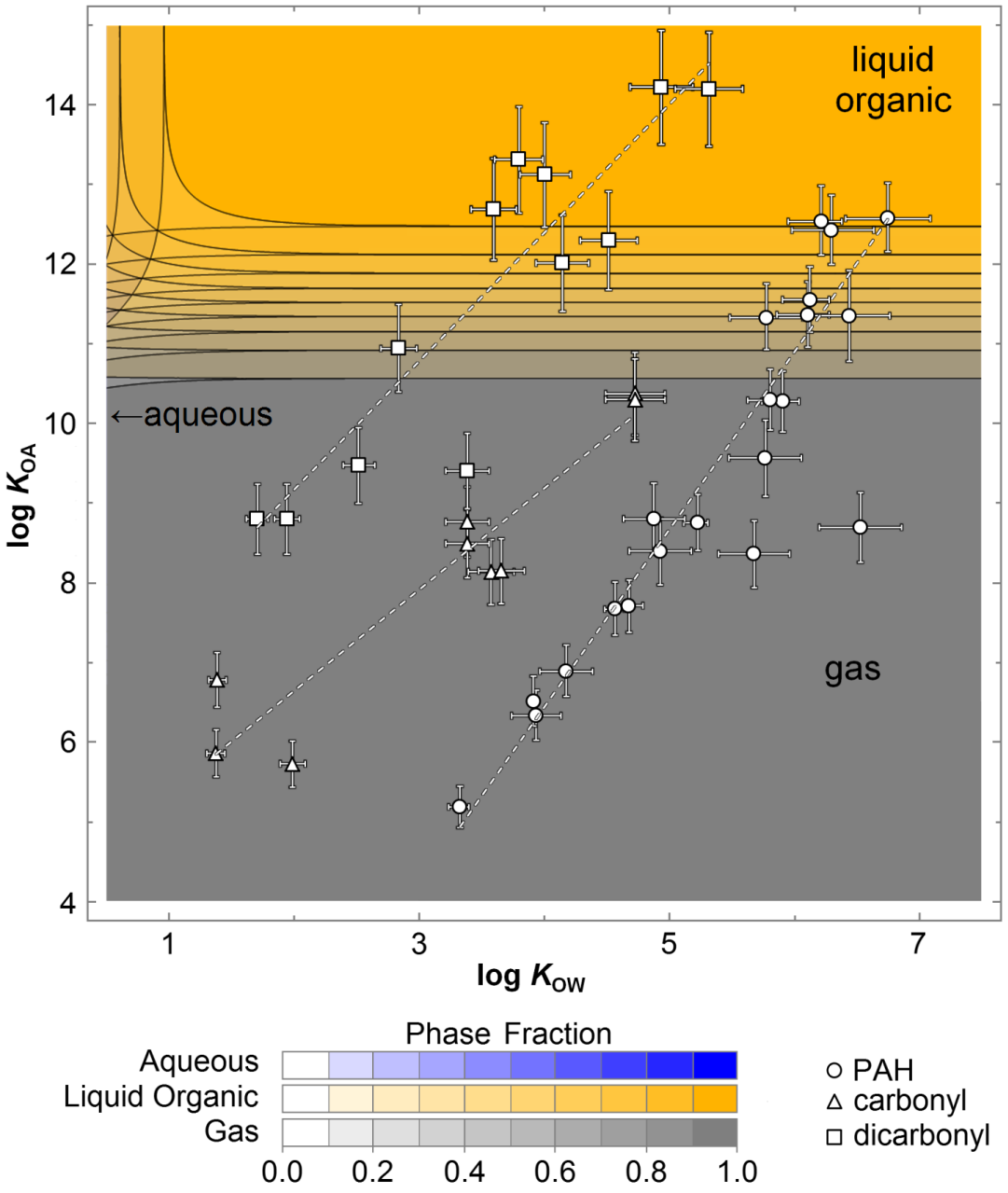

Figure D4. Phase fractions of PAH in a system of air and un-deliquesced liquid organic aerosols. The volume of aqueous phase is 15% as much as the immiscible liquid-organic phase, that is $\phi^{aq} = 4.5 \times 10^{-13}$. Here, the approximate aqueous phase boundary occurs below log $K_{OW} = 1$. All the PAHs and oxy–PAHs would partition between the gas and liquid organic phases according to the magnitude of their K_{OA}. The calculated fraction in the aqueous, liquid organic, and gas phases are in blue, yellow, and greyscale respectively. PAH literature and EPISuite K_{OW} and K_{OA} values are indicated as circle symbols, those of monocarbonyl oxy–PAHs as triangle symbols, and dicarbonyl oxy–PAHs as square symbols. Error bars are literature reported error (95% CI, Odabasi *et al.*, 2006) or 5% if no error was reported.

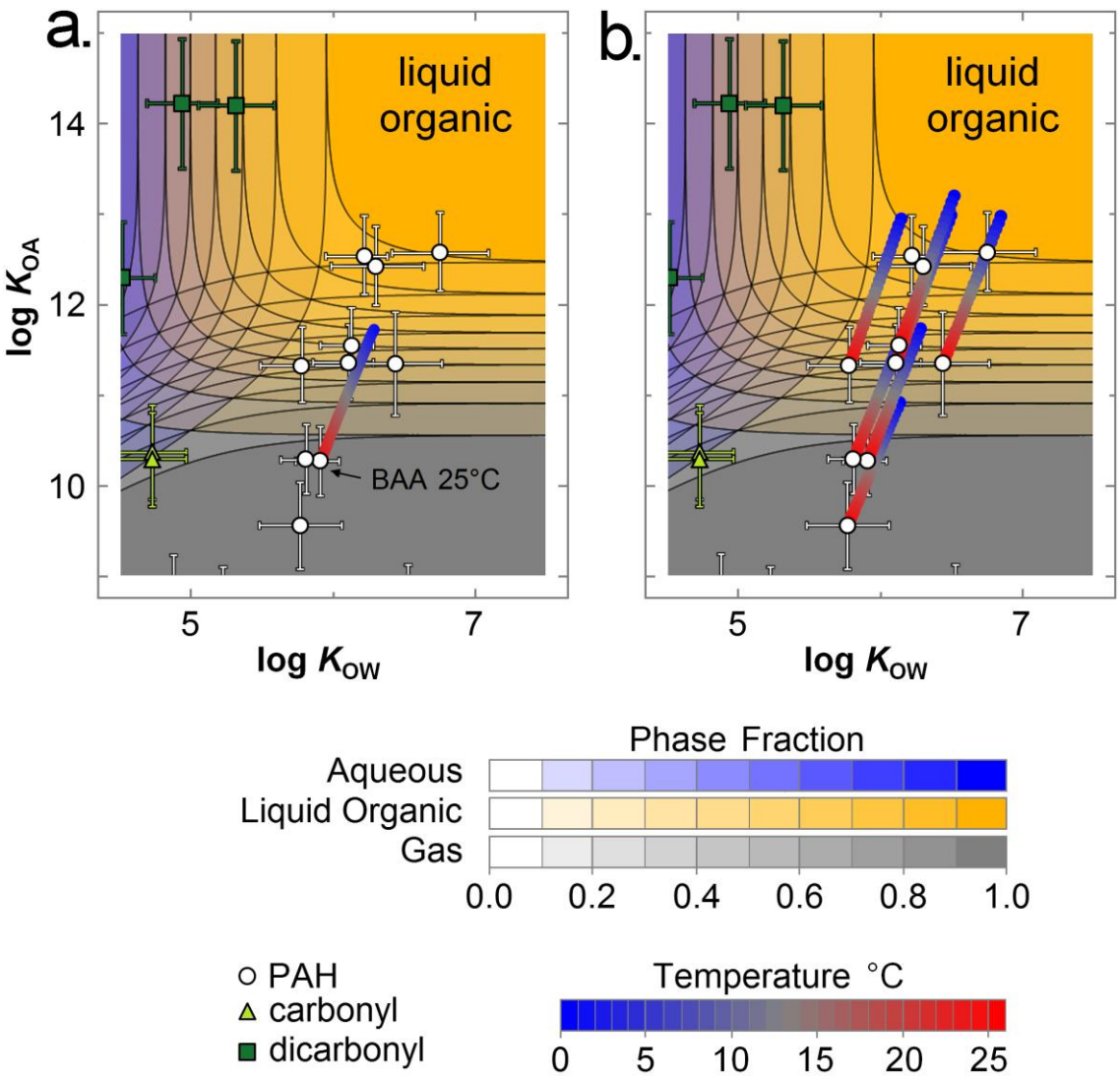

Figure D5. The temperature dependence of K_{OW} and K_{OA} for BAA (panel a) and its influence on x^g; the extrapolated temperature dependence of K_{OW} and K_{OA} for seven PAHs (panel b). The temperature dependent K_{OA} was known for BAA, CHY, BBF, BKF and BAP (Odabasi *et al*., 2006) and temperature dependent K_{OW} was known for BAA (Lei *et al*., 2000). K_{OA} changes for BBU and BEP were estimated from the relative K_{OA} changes for BAA and BAP respectively. The relative changes in K_{OW} for BBU, CHY, BBF, BKF, BAP, and BEP were estimated from BAA. The calculated fraction in the aqueous, liquid organic, and gas phases are in blue, yellow, and greyscale respectively. PAH literature and EPISuite K_{OW} and K_{OA} values are indicated as circle symbols, those of monocarbonyl oxy–PAHs as triangle symbols, and dicarbonyl oxy– PAHs as square symbols. Error bars are literature reported error (95% CI, Odabasi *et al*., 2006) or 5% if no error was reported. As temperature decreases, the partition ratios change which alters the partitioning of PAHs with log K_{OA} 10 to 12 at 25 °C. As an example, BAA is expected have x^g = 0.94 at 25 °C and x^g ~ 0.4 at 1 °C.